EPA-650/2-74-070

July 1974

Environmental Protection Technology Series

THE EFFECTS OF NOZZLE DESIGN AND SAMPLING TECHNIQUES ON AEROSOL MEASUREMENTS

Office of Research and Development
U.S. Environmental Protection Agency
Washington, DC 20460

EPA-650/2-74-070

THE EFFECTS OF NOZZLE DESIGN AND SAMPLING TECHNIQUES ON AEROSOL MEASUREMENTS

by

F. H. Smith

ARO, Incorporated
Arnold Air Force Station, Tennessee 37369

Interagency Agreement No. EPA-IAG-0139(D)
ROAP No. 26AAM
Program Element No. 1AA010

EPA Project Officer: Dr. Kenneth T. Knapp

Chemistry and Physics Laboratory
National Environmental Research Center
Research Triangle Park, North Carolian 27711

Prepared for

OFFICE OF RESEARCH AND DEVELOPMENT
U.S. ENVIRONMENTAL PROTECTION AGENCY
WASHINGTON, D.C. 20460

July 1974

This report has been reviewed by the Environmental Protection Agency and approved for publication. Approval does not signify that the contents necessarily reflect the views and policies of the Agency, nor does mention of trade names or commercial products constitute endorsement or recommendation for use.

CONTENTS

ILLUSTRATIONS

Figure

1.0 INTRODUCTION

The sampling of moving gas streams for accurate determination of particulate content is at best a difficult task. There are several variables existing in a flow of this type which can affect the results of the sampling. Some of these variables are

1. the mean gas velocity and local velocity variations about the mean;

2. the temperature of the gas;

3. the particulate size distribution and concentration in the gas, both of which are time dependent and functions of the duct design in which the gas is flowing;

4. the geometry of the sampling probe, the angle of the probe with respect to the flowing gas, and the extraction rate of the probe.

This investigation was concerned with the evaluation of probe performance as a function of geometry, mean gas velocity, probe angle of attack with respect to the flow, and extraction rate. The performance of the probes was compared using the sampling error determined from the flow parameters based on a zero-error assumption at isokinetic sampling conditions.

Isokinetic, or equal velocity sampling, was accomplished by using a variable speed wind tunnel to obtain the flow field around the probes and then varying the probe extraction velocity by connecting the probes to a controllable vacuum source.

Laser instrumentation was used in this study to confirm the uniformity of the flow in the test section prior to testing the probes. It was also used to measure the flow field adjacent to the probe inlets to determine the isokinetic condition of the probe flow. The use of the laser instrumentation facilitated the effort because the accuracy of conventional aerodynamic measuring instrumentation is susceptible to the same variables as the extraction probes (for example, design, sensitivity to angle of attack, and velocity of the gas streams). Conventional instrumentation also has a perturbing effect on the flow which it is measuring. Since laser instrumentation is perturbationless and insensitive to mechanical calibration errors, it was used to make an accurate evaluation of the probes and also to produce data that were heretofore unobtainable.

2.0 APPARATUS

2.1 WIND TUNNEL

The Environmental Protection Agency (EPA) probes were tested in a small wind tunnel constructed at AEDC (Ref. 1). The tunnel had a 35.6- x 50.8- x 121.19-cm test section with solid walls made of 6.35-mm Plexiglas . The Plexiglas walls allowed undisturbed optical investigation of the flow fields in the vicinity of the probes. The test section floor, or bottom wall, had a 254-mm-diam plate set into it. The probes were mounted on this plate, which was scribed in 5-deg increments to facilitate the accurate alignment of the probes with respect to the tunnel. The tunnel velocities were varied between 3.05 and 30.5 m/sec. The velocity profile in the test section was surveyed with the laser velocimeter (LV) at the selected test velocity before the probe was installed. The survey profiles, shown in Figs. 1, 2, and 3, indicated that there were no large velocity gradients across the test section. An aluminum honeycomb with 9.53-mm hexagonal openings was installed in the bellmouth of the tunnel to break up any gusts or large turbulence formations that might enter.

2.2 LASER VELOCIMETER

This section will briefly cover the principal features of the laser velocimeter so that those unacquainted with the instrument can obtain a working knowledge of it. For a complete development of the principles involved, see Ref. 2.

Basically, the instrument consists of the laser output beam divided into two parallel, equal intensity, coherent, TEM_{OO} beams. These beams are passed through a lens which brings them to a simultaneous cross and focus, forming an ellipsoidal measurement volume of $1/e^2$ relative beam intensity (henceforth referred to as the probe volume) at the region of intersection as shown in Fig. 4. The wavefronts of the two beams interact in this volume and generate interference fringes which are perpendicular to the plane of the beams, parallel to the bisector of the beam angle, and sinusoidal in intensity distribution (see Fig. 5). When a moving particle passes through the probe volume, it scatters light in proportion to the light power in the interference fringes. This scattered light is collected by lenses and focused on a photomultiplier tube, which converts it into an a-c signal with some d-c shift, as shown in the scope trace in Fig. 6.

Data conditioning and processing electronics then determine the period, t, of the a-c component (Ref. 3). Since the distance (δ) between successive interference fringes can be determined from the relationship

$$\delta = \lambda_o/2 \sin(\theta/2) \tag{1}$$

where λ_o is the wavelength of the laser and θ is the angle formed by the two intersecting beams, the rate at which the fringes are cut in the probe volume by a particle having a velocity, V, is

$$f = \frac{V}{\delta} \tag{2}$$

$$V = f\delta \tag{3}$$

Since $t = \frac{1}{f}$,

$$V = \frac{\delta}{t} \tag{4}$$

or

$$V = \frac{\lambda_o}{2t \sin(\theta/2)} \tag{5}$$

There are other considerations which arise in applying the instrument to a particular problem. Some of these are the relationship of the fringe spacing to the size of the particles present, the size of the optical probe volume formed by the beams, the laser power density in this volume, and the value of the velocity-period relationship, which must be compatible with the ranges of the signal-processing electronics. In this investigation a 4880Å argon laser line source was used, and the conversion was determined to be 7.23 m/sec-μsec. Interference fringe spacing, δ, was 7.23 μm, and there were approximately 30 fringes across the width of the ellipsoidal probe volume. The laser power density at the geometric center cross section was 2.25 w/mm^2, which gave a data rate compatible with the acquisition rate of the processing electronics. The LV was mounted on an electrically driven three-component traverse which allowed the accurate positioning of the probe volume throughout the

test section. Each component of the traverse was equipped with a position readout which had a resolution of 787 counts/cm. The traverse and LV installation are shown in Fig. 7.

2.3 EXTRACTION PROBES

The Environmental Protection Agency requested that the following three basic types of extraction probes be evaluated: (1) probes with a 90-deg bend and a square-edge inlet; (2) probes with a 90-deg bend and a sharp-edge inlet of 15 deg; and (3) a vertical, cylindrical probe with a circular opening in the side perpendicular to the axis of the probe. The diameters for each type probe are listed below.

Square-Edge Probes Diam, cm	Sharp-Edge Probes Diam, cm	Side-Opening Probes Diam, cm
1.27	1.27	1.59
5.08	1.91	3.18
	2.54	
	5.08	

The probes were all fabricated locally from 1.24-mm wall thickness stainless steel tubing. The 1.27-cm tubing could be smoothly bent through 90 deg, but the larger sizes buckled in bending and were unsatisfactory. All probes larger than 1.27 cm having 90-deg bends were fabricated by cutting mitered sections from the tubing and heliarc welding them together to form the bend. This fabrication technique was approved by the EPA prior to its use. The drawings of the probes, as received from EPA, are shown in Figs. 8 through 13, together with the modified fabrication drawings for the larger probes. Each of the probes, regardless of its inlet or capture size, initially terminated in a 1.59-cm-diam tube. This tube was used for mounting the probes in the floor plate and for attaching the vacuum line. This technique was found to be satisfactory for all probes tested except the 5.08-cm-diam probes. During testing of these probes it was found that the flow rate was so large that the 1.59-cm tubing choked or reached a sonic velocity, thereby limiting the flow. This was corrected by removing the 1.59-cm tubing and replacing it with 3.18-cm tubing. After this modification no further difficulty was experienced. All of the probes were additionally modified by the installation of internal and external static taps. These taps allowed test conditions to be repeated by using the static pressure difference which

was measured on a precision manometer. The taps were installed on the horizontal centerline of the 90-deg bend probes 1.91 cm behind the leading edge. The taps were installed on the side-opening probes on the vertical centerline at 90 deg to the axis of the opening. They were located at 1.59 and 3.18 cm, respectively, below the center of the opening on the 1.59- and 3.18-cm probes. The taps were stainless steel capillary tubing which was silver soldered to the probes and passed through the wind tunnel floor plate for connection to the manometer. The probes also had positioning rings installed on the 1.59-cm tubing to position them at a constant height above the floorplate. These rings were indexed to the probe centerline and were also used to align the probes with the tunnel floorplate. Figure 14 shows a typical installation of a probe in the wind tunnel.

2.4 EXTRACTION AND SAMPLING SYSTEM

The extraction and particle sampling system used in the test consisted of a filter housing, a vacuum source, and connecting hoses and valves. A schematic drawing of the system is shown in Fig. 15. The filter housing, shown in Fig. 16, was designed to hold three 10.16-cm-diam filters, together with backing screens and seals, and an inlet air flow diffuser which directed the flow uniformly into the three filters. The housing was designed with a 1.59-cm-diam fitting to connect the probes directly. However, due to the choking condition experienced with the 5.08-cm probes, the housing was modified to a 3.18-cm fitting. An adapter was used to connect the 1.59-cm hose to the housing for the smaller probes. The filter housing outlet was connected to the vacuum source with a 5.40-cm vacuum hose, and a 6.35-cm guillotine valve isolated the filter housing from the vacuum source. Coarse vacuum adjustments were made with the 6.35-cm valve, and fine adjustments were made with a 1.91-cm globe valve inbleeding atmospheric air. The vacuum source used on the test consisted of two different vacuum pumps. A 1.42 m^3/min pump was used in testing all probes except the 5.08-cm-diam probe. Figure 17 shows the theoretical isokinetic flow requirements for the probes at different velocities. Due to the extremely large flow rates of the 5.08-cm probes, a pump with increased capacity was sought while testing was being conducted using the smaller one. An 8.50 m^3/min pump was subsequently located and used for the 5.08-cm probes and also for the probe angle-of-attack investigations and the sampling tests.

2.5 PARTICLE INJECTION SYSTEM

2.5.1 Design and Operation

The particulate injection system, shown schematically in Fig. 18, was designed and built using the fluidized bed principle. Air at 0.14 kg/cm^2 was injected into the bottom of the container, thus floating the particulate in the top of the container. A 3.18-mm ejector nozzle in the injection tube, supplied with 3.52-kg/cm^2 air, provided enough suction to draw off the dispersed particulates from the container and eject them at the tunnel bellmouth. An electrically driven stirrer was mounted on the container and stirred the particulates at 10 rpm to eliminate any channeling by the fluidizing air supply. The particulate container was also vibrated to keep the particulate at a uniform level in the container. The solenoid valves, the stirrer, and the vibrator were all connected electrically to an interval timer switch for simultaneous operation.

The additional flow in the wind tunnel resulting from the ejector and the induced air flow with the suspended particulates was calculated using compressible flow theory. The resulting velocity increase at a nominal tunnel velocity of 9.14 m/sec, the worst case, was 0.6 percent, or 0.05 m/sec. This was considered negligible since the uncertainty in the unperturbed velocity profile in the wind tunnel was determined to be greater than this amount.

2.5.2 Particles

The selection of the particles to be used in the sampling portion of the test was based on three considerations: (1) mean particle size, (2) size distribution, and (3) material density. It was desired to select some material that generally had physical characteristics similar to those combustion byproducts found in stack gases. It was also desirable to have a material that was commercially available, nontoxic, and not overly expensive. An inspection of the sizes of air-borne particles (Ref. 4) indicated that the size range from 1 to 50 μ would include a large portion of fly ash, cement dust, pulverized coal, foundry dust, and smelter dust. The apparent densities of this type of material were found to range from 160.2 kg/m^3 for lamp black to 240.3 kg/m^3 for charcoal, with slag and coke included in this range (Ref. 5). After surveying many materials whose characteristics fell into these categories, diatomaceous silica was selected. It is inexpensive and readily available and has an apparent density of 224.3 kg/m^3 (Ref. 6). Samples were sized on a fiber optics particle sizer (Ref. 7), and a

representative of the size distribution is shown in Fig. 19. Statistically, the average linear dimension was 5.53μm, and the average diameter on a volume basis was 10.03μm. These parameters (size and density) were input into an existing computer program to determine the flow-following capabilities of the material. Figure 20 shows the plotted results, which indicate that the diatomaceous silica is capable of following 95 percent of turbulent velocity fluctuations up to a frequency of 42,500 Hertz. This was felt to be a much higher frequency level than would be encountered in the low-speed wind tunnel.

2.6 DATA ACQUISTION INSTRUMENTATION

The data acquisition instrumentation used for the tests consisted of a relatively standard instrument package which is routinely used at AEDC with the laser velocimeter. A block diagram of the system is shown in Fig. 21. The output signal from the 931A photomultiplier (PM) tube was sent to a Tektroniks Model 7623 oscilloscope, where the signal could be displayed and amplified if desired. The signal from the oscilloscope was used to select inputs to the Doppler Data Processor (DDP) (Ref. 3), which subjected the signal to certain logic considerations such as signal-to-noise ratio and periodicity and, upon successful passage of the signal, determined its period. A narrow band filter was used on the signal input to the DDP to reject any noise signals outside of the frequency range of interest. The binary coded decimal (BCD) output of the DDP went to a Hewlett-Packard (HP) 2547A coupler and an HP 2515A scanner, which sequenced inputs of position, date, run number, and period-to-velocity conversion constant, and then transmitted them to a Kennedy Model 1600 Incremental Tape Recorder. The recorder stored the data on magnetic tape for processing by a computer. An HP 5050A line printer was paralleled with the tape recorder so the data could be monitored directly if desired. This instrumentation was rack mounted as a unit and is shown in Fig. 22.

3.0 DATA PROCESSING

The data obtained with the LV consist of a set of values varying about some mean. Each value is obtained in a random time sequence; therefore, it must be treated statistically. In working with such data, it is important to determine when a sufficiently large data sample has been obtained to constitute a statistically valid observation. This determination

allows the acquisition of the data to be discontinued when the data obtained satisfy the restraints that have been placed upon it, thereby saving run time and data processing time. These restraints are the desired accuracy of the mean value and the confidence level or probability of obtaining this accuracy. These factors are related by the expression

$$Z = \frac{\bar{V}[TOL]}{\sigma\bar{V}} \simeq \frac{\bar{V}[TOL]\sqrt{N}}{S} \tag{6}$$

where

Z = number of standard deviations away from the mean velocity

$\bar{V}$ = mean velocity

TOL = tolerance or desired accuracy

N = number of samples

σV = standard deviation of the sample averages $\simeq S/\sqrt{N}$

S = standard deviation = $\left[\frac{\sum_{i=1}^{N} (Vi - \bar{V})^2}{N-1}\right]^{1/2}$

The above expression (6) can be rewritten for N as

$$N = \left[\frac{ZS}{\bar{V}(TOL)}\right]^2 \tag{7}$$

but turbulent intensity (TI) = $S/\bar{V}$; therefore,

$$N = \left[\frac{Z(TI)}{TOL}\right]^2 \tag{8}$$

This expression was solved for several values of Z, TI, and TOL and is shown in Figs. 23 through 25.

When values of the wind tunnel turbulent intensity with the probe installed were determined from data, Figs. 23 through 25 were used to obtain a value of N commensurate with the tolerance and probability function Z. A 90-percent probability of obtaining an average velocity within 1 percent of the actual average velocity was used for the experimental work. This gave values of N between 4 and 60. Since it was necessary to have a constant value of N for compatibility with the computer program, N = 50 was used for all data. A computer program was used to discard any measurements that were more than two standard deviations, 2σ, away from the mean. The remaining data were then recalculated to obtain a new mean and standard deviation. This mean and standard deviation, calculated using the data period, were converted into velocity units using the LV conversion constant. An example of the computer program printout is shown in Fig. 26. The Doppler Data Processor was operated in the 1.5-percent window mode. This caused it to reject all LV input data whose eight-cycle period varied more than 1.5 percent from the five-cycle period. This implies that the data from particles that were accelerating or decelerating by more than 1.5 percent, as they traversed the probe volume, were rejected. It also increased the validity of the data by eliminating any aperiodic electronic noise which might occur in the frequency range of the data.

4.0 PROCEDURE

The sampling probes were installed in the wind tunnel, and velocity surveys were made of the flow field at different conditions of tunnel velocity and extraction rate to determine the extent of the flow disturbances resulting from their presence. These preliminary tests indicated that the disturbances extended transversely approximately 1.5 times the probe inside diameter (I.D.), and axially upstream approximately twice the probe I.D. These values were used as the bounds of the survey area with transverse traverses made at 1/4, 1/2, 1, and 2 probe I.D.'s axially upstream of the probe inlet plane. The axial location of the probe inlet plane was determined with the LV under probe operating conditions of tunnel velocity and extraction prior to the test. This was necessary because the probes deflected slightly under the aerodynamic loads imposed on them during flow.

Measurements were made on each of the four transverse traverses at ±1.5 I.D., ±1.25 I.D., ±1 I.D., ±3/4 I.D., ± the center position on the probe lip, and at five selected

locations across the probe opening. The internal flow area of the probe was divided into three equal areas, and the five measurements were made on the centers of these areas. As shown in Fig. 27, one measurement was made on the probe center, which is the center of area 1, and measurements were made on the centers of areas 2 and 3. The velocities for the three areas were averaged to obtain the mean velocity in the probe.

$$V_{probe} = \frac{V_1 + \frac{V_{2_1} + V_{2_2}}{2} + \frac{V_{3_1} + V_{3_2}}{2}}{3} = \frac{2V_1 + V_{2_1} + V_{2_2} + V_{3_1} + V_{3_2}}{6} \quad (9)$$

The velocities used in this average were from the I.D./4 axial position only, which was the closest approach to the probe inlet that could be made because of the beam angle. All measurements were made in a horizontal plane on the probe centerline. Figure 28 shows the 60 locations at which velocity measurements were made for each condition of extraction rate and velocity. The locations for these measurements were calculated for each probe using the probe I.D. and then converted into count readings for the digital-to-analog position readout panel meters, whose resolution was 787 counts/cm. The velocity profiles in Figs. 30 and 31 are shown as a function of the probe I.D. for convenience in plotting and comparison. The preceding procedure for determining the measurement locations applied only to the 90-deg bend probes at zero angle of attack. The measurement points for the side-opening probes were determined in the same manner, with two exceptions. Instead of the probe inside diameter, the diameter of the probe inlet opening was used as the normalizing parameter, and the probe velocity was calculated using two equal areas instead of three. Two equal areas were also used for the probes at angles of attack of 7.5 and 15 deg because as the probes are yawed the projected frontal area becomes elliptical, with the smaller dimension occurring in the line of measurement. The use of the two areas facilitated the measurements across the smaller distance. The offset distance from the center of the projected ellipsoid to the tunnel centerline was calculated for each probe at 7.5 and 15 deg and was used as the reference around which the transverse measurements were made.

The procedure for setting the extraction flow rate consisted of establishing a flow through the probe and then adjusting it to give a selected static pressure differential across the probe. Since the differential for isokinetic conditions was unknown, differentials above and below the null or zero differential, as well as the zero differential, were set. These points were -12.7mm H_2O differential (static pressure inside probe > static pressure outside probe), 0 differential, and +12.7mm H_2O differential (static pressure inside probe < static pressure outside). Experience showed that because of the steep slope of the curve defined by these points, an additional set point was desirable in the positive differential sector. Therefore, a +25.4-mm H_2O differential point was added to the schedule. This allowed good definition of the curves and more accurate determination of the static pressure differential for isokinetic conditions. The pressure differentials were set on a Meriam Model 34FB2 micromanometer which was directly connected to the static pressure leads from the probes. The effect of the isokinetic condition on the probe flow is shown in Fig. 29. Figure 29a illustrates a less than isokinetic condition in which the flow entering the probe is decelerated; by continuity, a portion of the flow in the projected area of the probe must be rejected to the outside. Figure 29b shows a condition greater than isokinetic in which the probe is capturing flow from outside the projected probe area. It is readily apparent why sampling under either of these conditions should be greatly in error. A true or 100-percent isokinetic condition has the flow streamlines in the projected probe area entering the sampling probe and those outside the area passing the probe with a minimum disturbance of the flow. It is not possible to have a flat probe velocity profile whose magnitude is the same as that of the free stream since there is a boundary layer developing as the flow enters the probe. Because of this, the velocity in the center portion of the probe must be slightly greater than the mean to account for the boundary velocities which are less than the mean velocity.

The procedures used in sampling involved the extraction and sampling system and the particulate injection system. Before a sampling test was conducted, groups of three filters were weighed to the nearest 10^{-4} grams. The filters were identified by group number and placed in plastic bags for protection. Before the filters were installed, the vacuum system was turned on to remove any stray or residual particles that might be in the probe, filter housing, or hoses. The

filters were then installed and the vacuum adjusted to give the desired differential pressure between the probe inside and outside static orifices. As soon as conditions were stable, the particle injection system was energized and operated for sixty seconds. Any change in the probe ΔP due to particle buildup on the filters was corrected by adjusting the probe vacuum during the test interval. When the interval timer turned the injection system off, the vacuum line was closed and the filters were removed from the housing and replaced in their plastic bags. These filters were returned to the chemical lab for reweighing. The weight differential was identified with the probe and test conditions for data reduction.

The standardization and calibration procedures for this test were conducted as follows:

1. The laser velocimeter period-to-velocity constant was determined initially and reverified monthly.

2. The wind tunnel manometer and the probe static pressure differential manometer were disconnected and zeroed prior to each test.

3. The traverse position indication instrumentation was checked before each run and rezeroed and spanned if required. A mechanical scale and pointer on each axis of the traverse was used as a standard for the position indicators.

4. The laser velocimeter alignment with the wind tunnel was verified before each test.

5. The Doppler Data Processor was returned to the laboratory monthly, and the operation of its counter circuits was checked and verified.

5.0 RESULTS

The results of this test are presented in Figs. 30 through 64. These figures represent a condensation of 282 plots of velocity profiles obtained with the LV on the different probes. These plots were not formally published because of their quantity and also because their most pertinent information has been extracted and is presented herein. They are of interest in examining the flow disturbances of specific probes and can be used to develop constant potential fields for specific probes. Figures 30 and 31 are examples

of this for the 1.27-cm square-edge probe. Figure 30 is for a ΔP of 7.11 mm H_2O, $P_{in} > P_{out}$, or less than isokinetic, and Fig. 31 is for a ΔP of 25.4 mm H_2O, $P_{in} < P_{out}$, or greater than isokinetic. These figures illustrate how the flow is drastically accelerated or decelerated, depending on the kinetic condition of the sampling.

The condensed plots used only the traverse data from the I.D./4 axial position, the closest position to the probe. The data are plotted against the arguments of probe ΔP and the percent-isokinetic condition. These plots have grouped the probes by velocity and angle of attack, allowing comparison of the different probe designs at the same conditions. Figure 32, at 9.14 m/sec and zero angle of attack, shows the 90-deg bend probes grouped together and crossing the isokinetic line at ΔP's of 0.76 to 2.54 mm H_2O, $P_{in} < P_{out}$. The 1.27-mm square-edge probe requires the greatest ΔP of the 90-deg bend probes to reach isokinetic flow. However, it is considerably more efficient than the side-opening probes, which have not reached isokinetic flow conditions at a ΔP of 25.4 mm H_2O, $P_{in} < P_{out}$. Figure 33, with the flow also at 9.14 m/sec but with the probes at 7.5 deg angle of attack, shows the probe curves somewhat spread but not greatly deteriorated. Figure 34, for 9.14 m/sec and 15 deg angle of attack, shows the 5.08-cm, 90-deg bend probes operating more efficiently than the other similar probes, whose performance is between 90 and 95 percent isokinetic at a zero ΔP.

Figure 35, zero angle of attack at 15.24 m/sec, shows much steeper curves for the probes although the zero-ΔP crossing of the curves is about the same as that at 9.14 m/sec. This indicates that the kinetic condition, or percent isokinetic, is not as sensitive to changes in ΔP as it was at 9.14 m/sec. The 5.08-cm sharp-edge probe gives the best performance in terms of highest percent isokinetic condition at zero ΔP. At 7.5 deg angle of attack and 15.24 m/sec (Fig. 36), the performance showed an improvement for all the probes except the 1.59-cm side-opening probe, which decreased. In Fig. 37, at 15 deg angle of attack, the performance decreased uniformly for all the probes except for the 5.08-cm ones, which remained relatively the same, and the 3.18-cm side-opening probe, which improved.

The performance curves at 21.34 m/sec, Fig. 38, were much steeper that at 15.24 m/sec, but the ΔP required for isokinetic flow conditions changed very little. At 7.5 deg angle of attack, Fig. 39, there was very little change in the zero ΔP performance with the exception of the 1.27-cm square-edge probe, the 3.18-cm side-opening probe, and the

5.08-cm sharp-edge probe, all of which improved a small amount. Figure 40, 15 deg angle of attack at 21.34 m/sec, showed a general decrease in performance except for the 3.18-cm side-opening probe and the 5.08-cm sharp-edge probe, both of which improved slightly.

These results may be summarized as follows:

1. The probe static pressure differential (ΔP) required to perform isokinetic sampling varies directly as the stream velocity.

2. The static pressure differential required for isokinetic sampling varies inversely as the probe diameter.

3. The square-edge lip design on a probe requires a much greater static pressure differential. This differential varies from a factor of 2 for the 1.27-cm probe to a factor of 5 for the 5.08-cm probe.

4. The side-opening probes require a much greater static pressure differential than the 90-deg bend probes to achieve isokinetic sampling. Since these probes were not designed with the same side opening-to-I.D. ratio, it is not possible to isolate the observed differences in their performance.

The performance of the probes was also presented as a function of percent sampling error plotted versus the probe pressure drop, ΔP, in mm of water. These plots were developed with the premise that at isokinetic sampling conditions there is a zero sampling error. Each plot shows the performance of a single probe at the three test velocities. The plots are arranged by ascending size and lip design; that is, the data on the 1.27-cm-diam square-lip probe are first, and the 5.08-cm-diam sharp-lip data are last. Figures 41 through 48 are the zero angle-of-attack plots, 49 through 56 are the 75-deg angle-of-attack data, and 57 through 64 are the data for an angle of attack of 15 deg. Typically the lower 9.14 m/sec velocity data have sampling errors which are larger per unit change in probe ΔP. As the stream velocity increases, the data become less sensitive to error for a unit change in the probe ΔP. The side-opening probes (Figs. 43 and 46) were so inefficient that isokinetic conditions were not met over the normal range of testing used for the other probes. However, an extension of the curves to the horizontal "zero error" line will give an indication of the probe ΔP required to reach isokinetic conditions for these probes. This is typically true at the three different angles of attack for these probes. The three velocity plots for any probe and

angle-of-attack situation have nearly the same sampling error at a probe "zero" ΔP or null condition. This is typical for all probes except the 5.08-cm square-edge probe at an angle of attack of 7.5 deg, shown in Fig. 55. The 9.14 m/sec data were considerably lower in value than the two other velocities for this case. These data were checked, and nothing was found to invalidate them. This effect did not occur at 15 deg and was not apparent to the extent noted in any of the other data.

6.0 CONCLUSIONS

There are significant errors in extraction probe sampling that are caused by sampling at nonisokinetic conditions. The magnitude of the errors is a function of several variables, the major ones of which were evaluated in this investigation. The effects of the variables on the sampling error are as follows:

1. Velocity: the sampling error is greater for low velocities (9.14 m/sec) than for high velocities (21.3 m/sec) for the same static pressure differential (inside to outside) across the probe.

2. Probe Diameter: the larger probes appeared to be more efficient at all velocities than the smaller probes. The larger (5.08-cm-diam) probes closely approached isokinetic flows at a zero static pressure differential.

3. Probe Shape: the sharp-edge probes in all cases were more efficient than the square-edge probes. The two side-opening probes were much less efficient than the 90-deg bend probes.

4. Angle of Attack: in general the efficiency of the probes decreased with increasing angle of attack. There were some exceptions where the efficiency apparently increased. These cases were few, however, and generally were limited to the 7.5-deg angle-of-attack cases.

7.0 RECOMMENDATIONS

This study has demonstrated techniques that are applicable to a field in which there is limited information available.

These techniques can also be applied to the related problem of where the samples are taken in the duct. The concentration of airborne particulates is directly affected by flow disturbances such as bends, T's, and Y's in the ducting and by the location of the sampling probe. This information can be obtained by electro-optical techniques, and the effect of the variables can be shown in nondimensional form for general sampling application.

The location and size of the static taps on the probes should be standardized. This would allow the use of probes based on the calibration of one sample probe, and would thereby eliminate the need for individual probe calibration.

The sampling probes should be evaluated to determine an optimum, or minimum total pressure loss design. A review of the literature indicates that even simple shapes such as 90-deg bends can be optimized. These techniques are applicable to sampling probes and would result in more efficient probes that would require less suction pressure for isokinetic sampling.

REFERENCES

1. Kroeger, Richard A. "Wind Tunnel Design for Testing V/STOL Aircraft in Transition Flight." AEDC-TR-72-119 (AD 749154), September 1972.

2. Lennert, A. E., Brayton, D. B., Crosswy, F. L., Goethert, W. H., and Kalb, H. T. "Laser Metrology." AGARD Lecture Series No. 49 on Laser Technology in Aerodynamic Measurements, presented from June 14-18, 1971 at the von Karman Institute. Published March 1972.

3. Kalb, H. T., Brayton, D. B., and McClure, J. A. "Laser Velocimetry Data Processing." AEDC-TR-73-116 (AD 766418), September 1973.

4. Sheehy, James P., Achinger, William C., and Simon, Regina A. "Handbook of Air Pollution." U. S. Department of Health, Eduction and Welfare, Robert A. Taft Engineering Center, Cincinnati, Ohio, 05226.

5. McAdams, William H. Heat Transmission. McGraw-Hill Book Company, Inc., New York, 1954. (Third Edition).

6. Kreith, Frank. Principles of Heat Transfer. International Textbook Company, Scranton, PA, 1958.

7. Bentley, H. T. "Fiber Optics Particle-Sizing System." AEDC-TR-73-111 (AD 766647), September 1973.

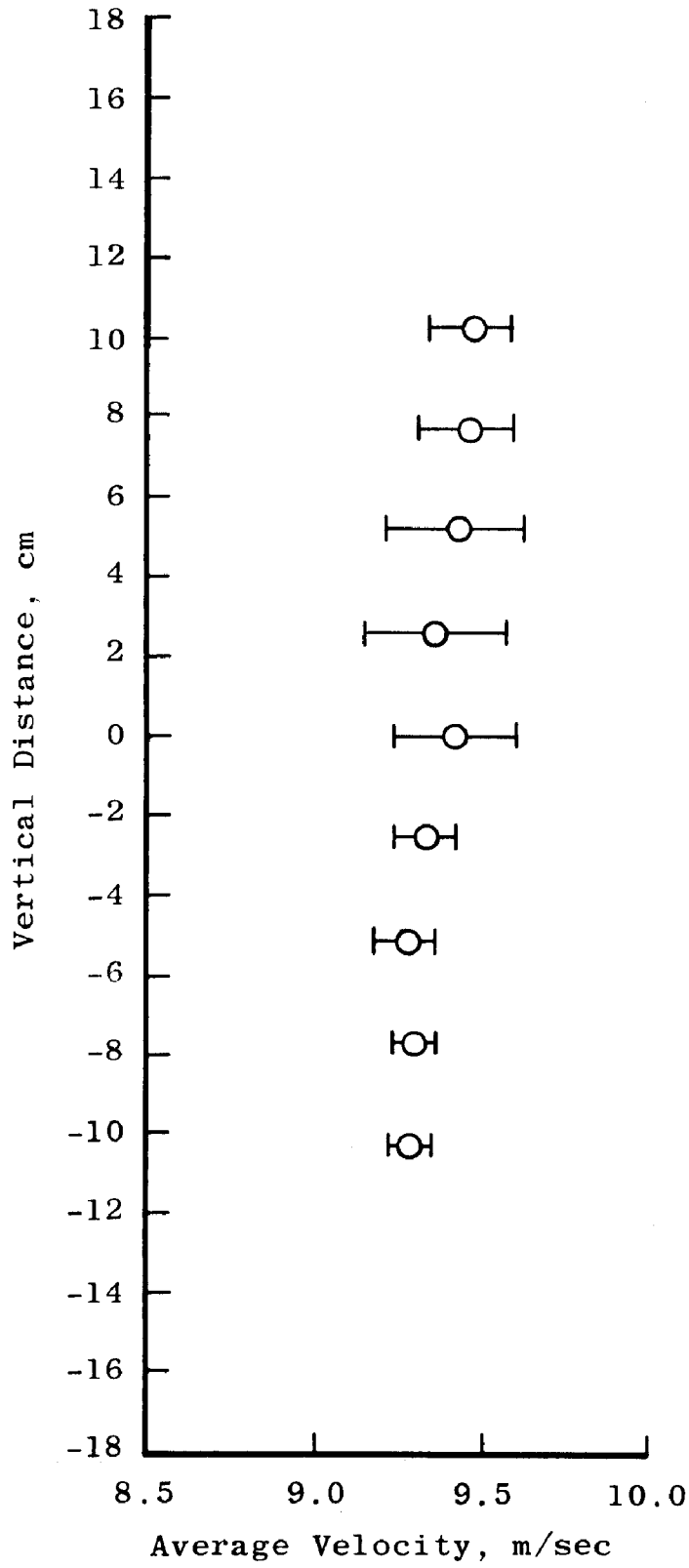

Figure 1. Velocity profile along vertical centerline of wind tunnel at probe mounting location, nominal flow rate = 9.14 m/sec.

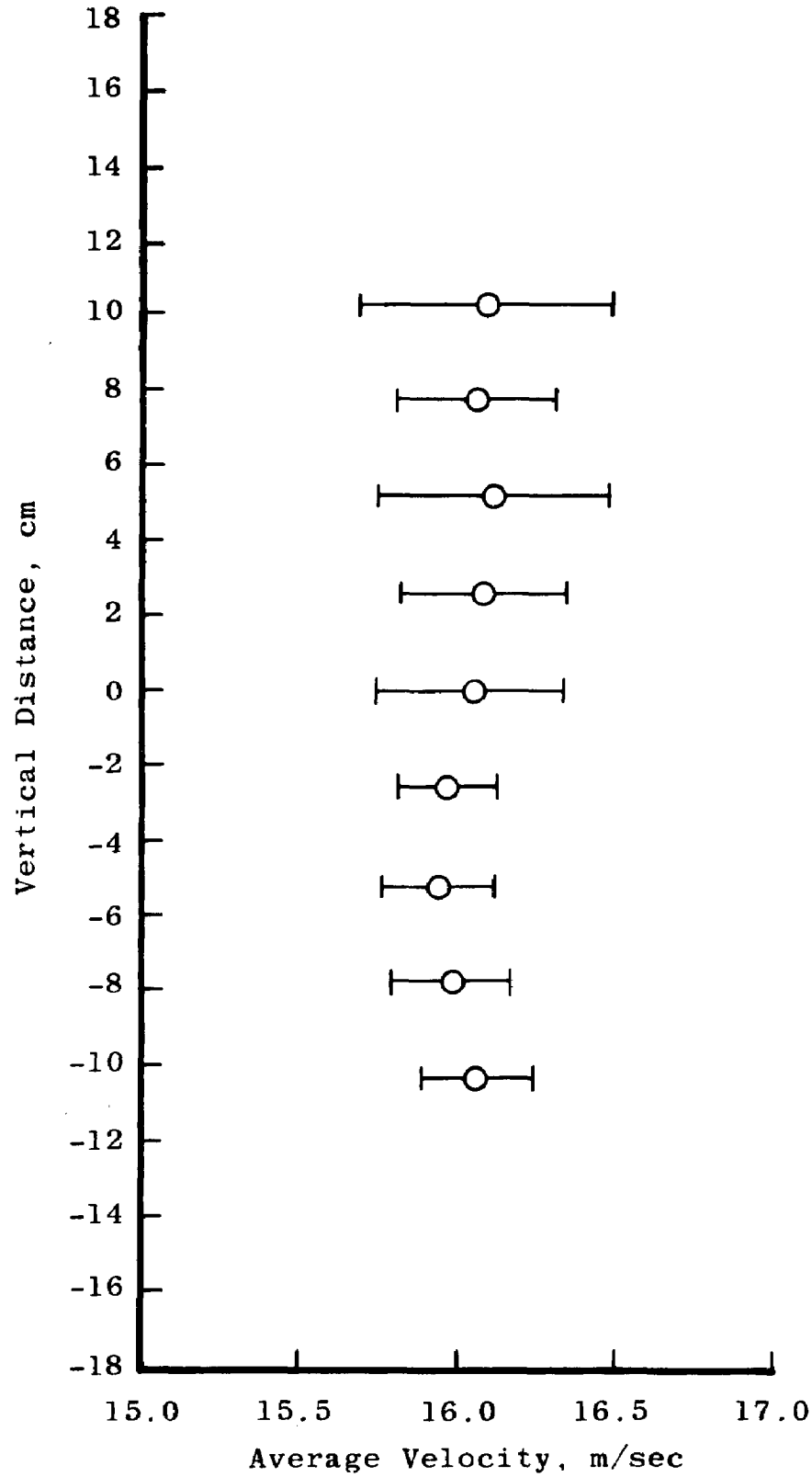

Figure 2. Velocity profile along vertical centerline of wind tunnel at probe mounting location, nominal flow rate = 15.24 m/sec.

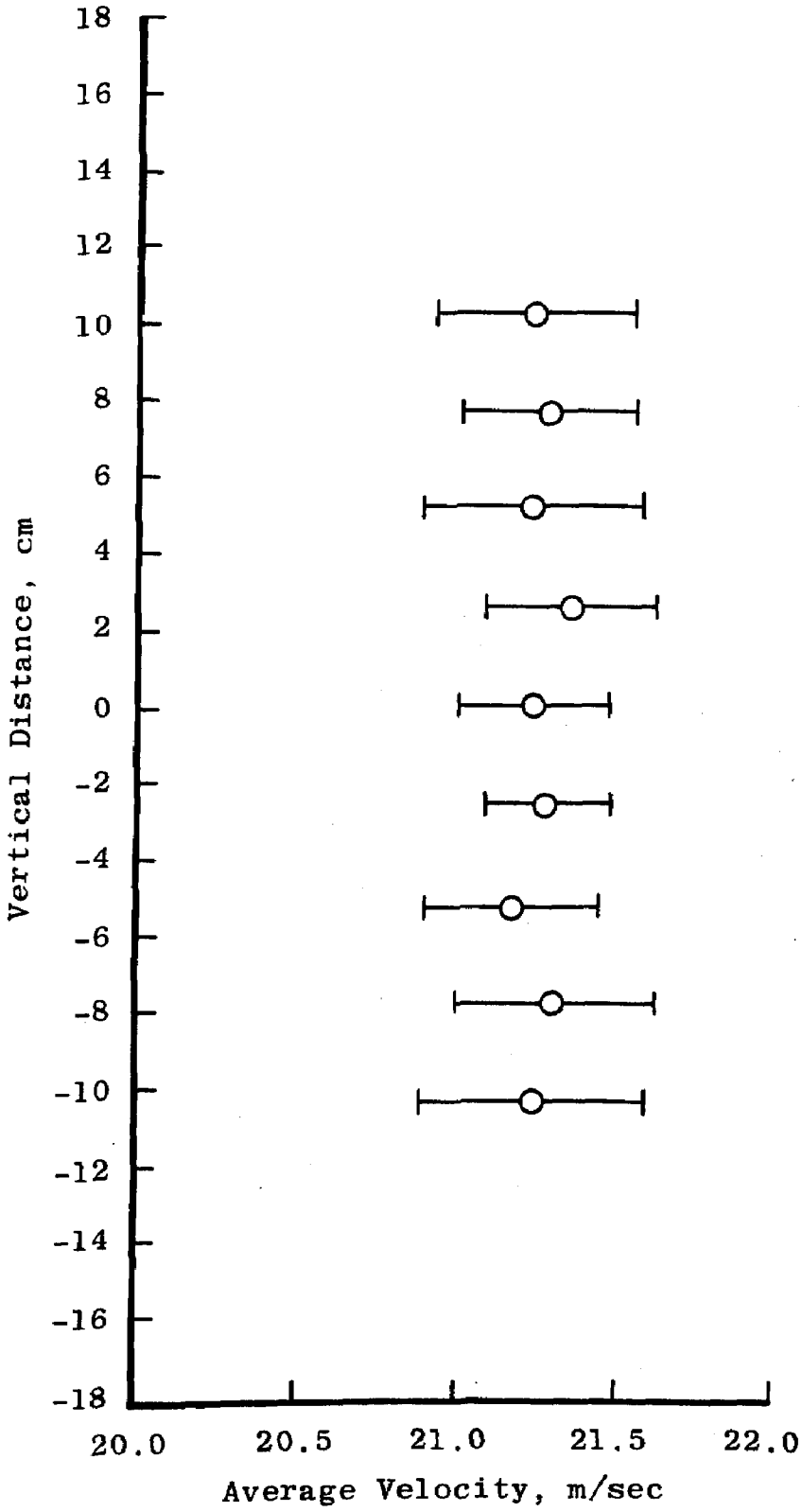

Figure 3. Velocity profile along vertical centerline of wind tunnel at probe mounting location, nominal flow rate = 21.34 m/sec.

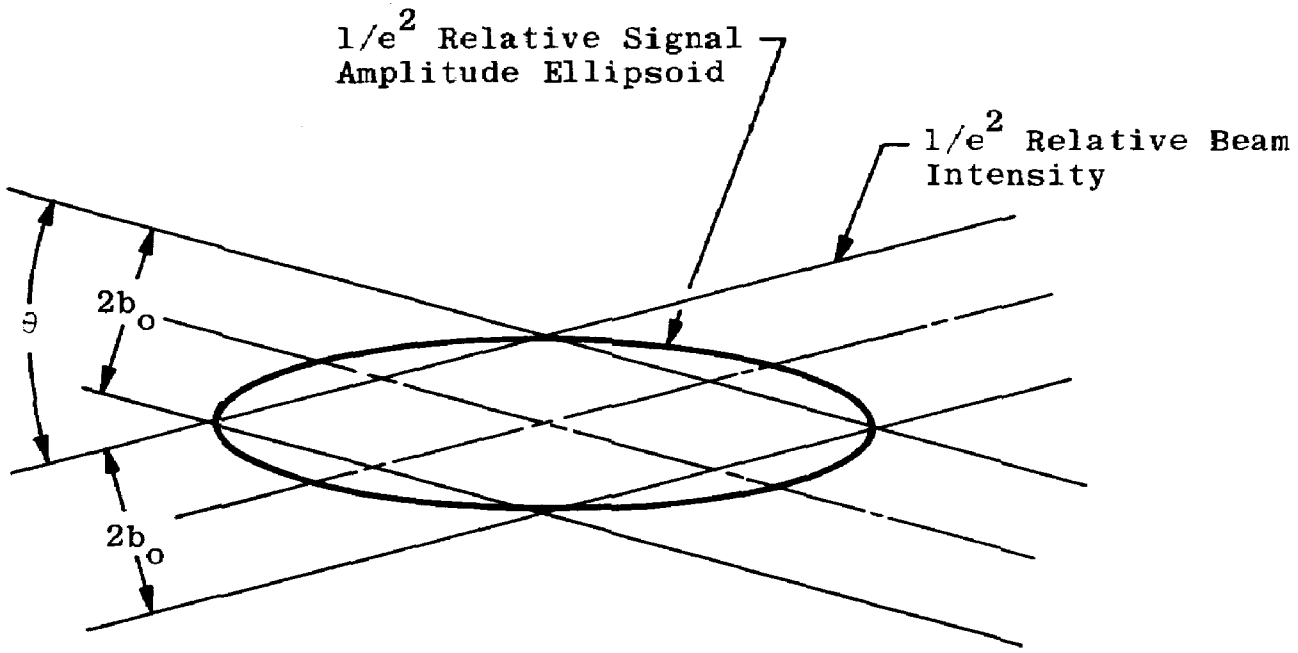

Figure 4. Focal volume ellipsoid.

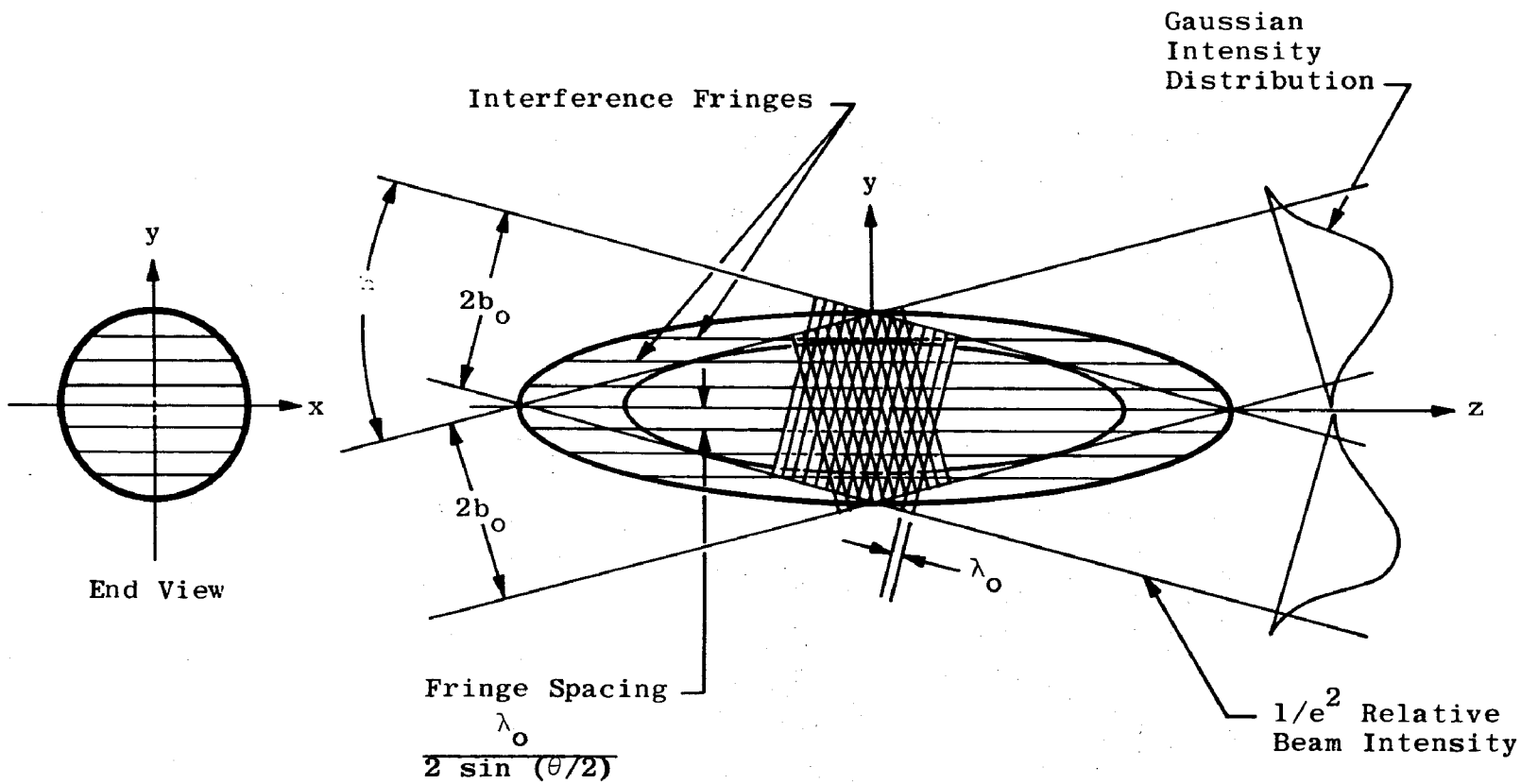

Figure 5. Beam interference fringes.

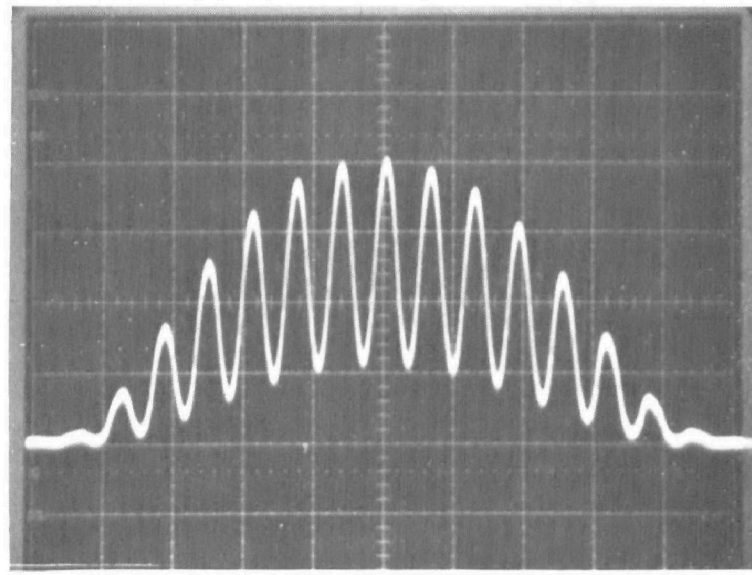

Figure 6. Oscilloscope trace of particle crossing fringes in ellipsoidal volume.

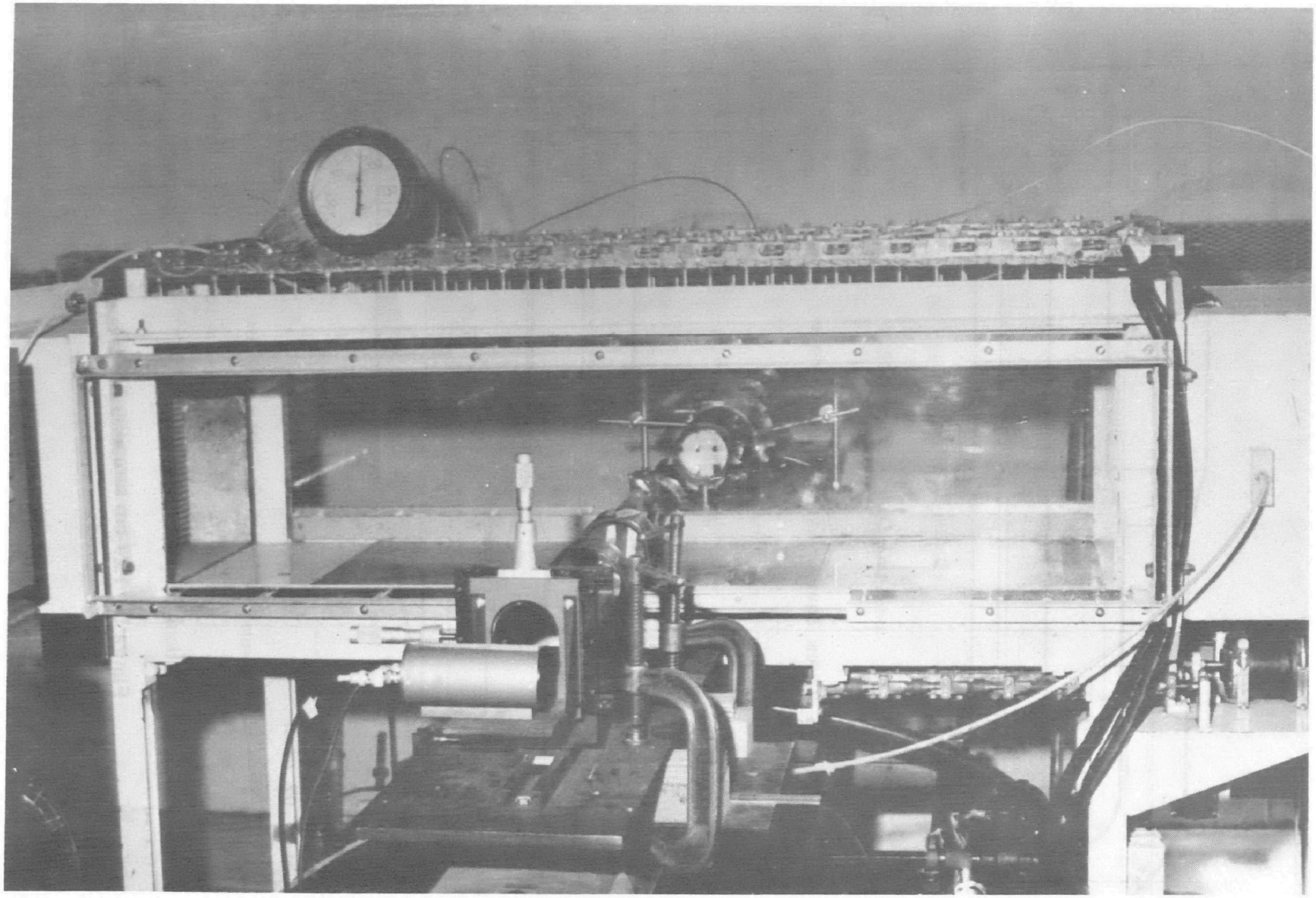

Figure 7. EPA laser velocimeter and traverse installation.

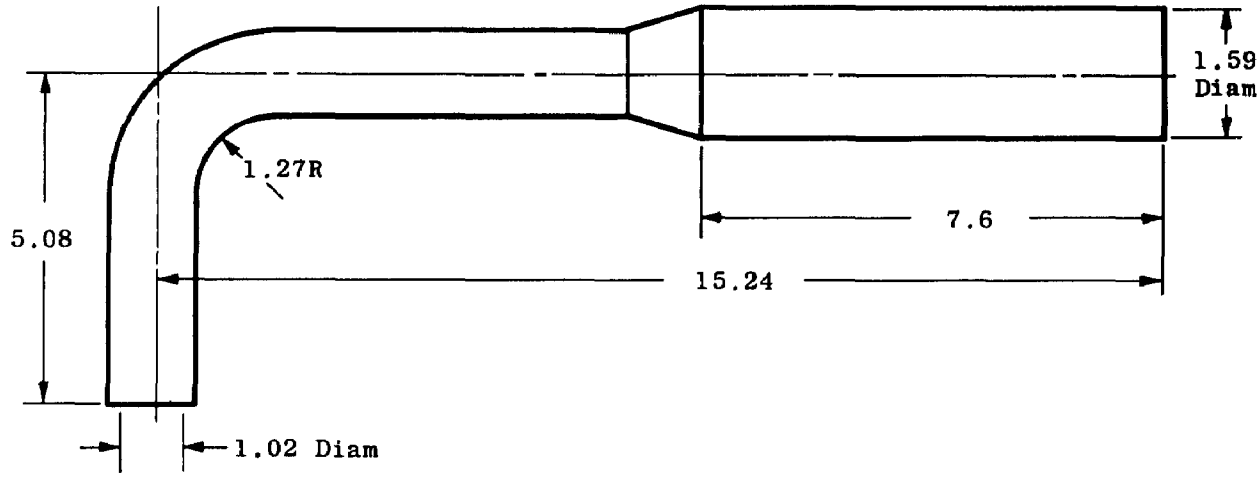

1.27-cm Square-Lip Sampling Probe

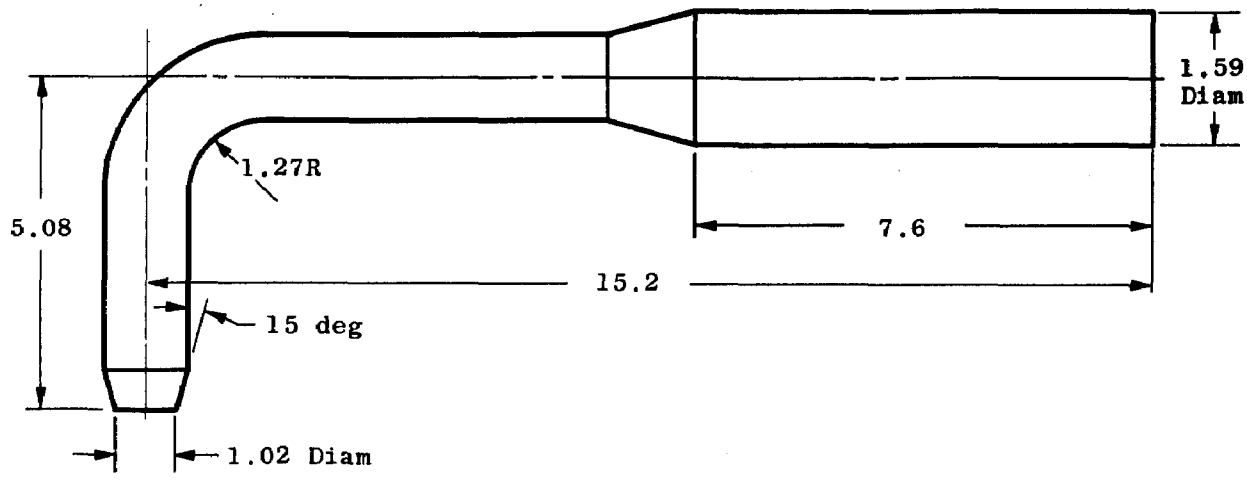

1.27-cm Sharp-Lip Sampling Probe

All Dimensions in Centimeters

Figure 8. 1.27-cm sampling probes.

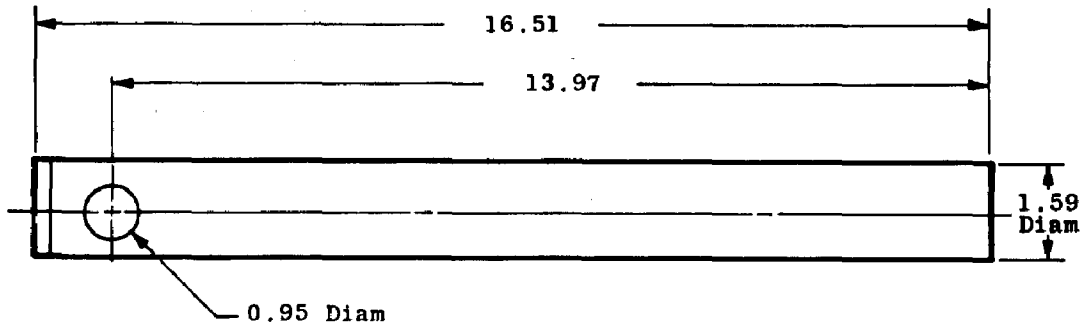

1.59-cm Side-Opening Probe

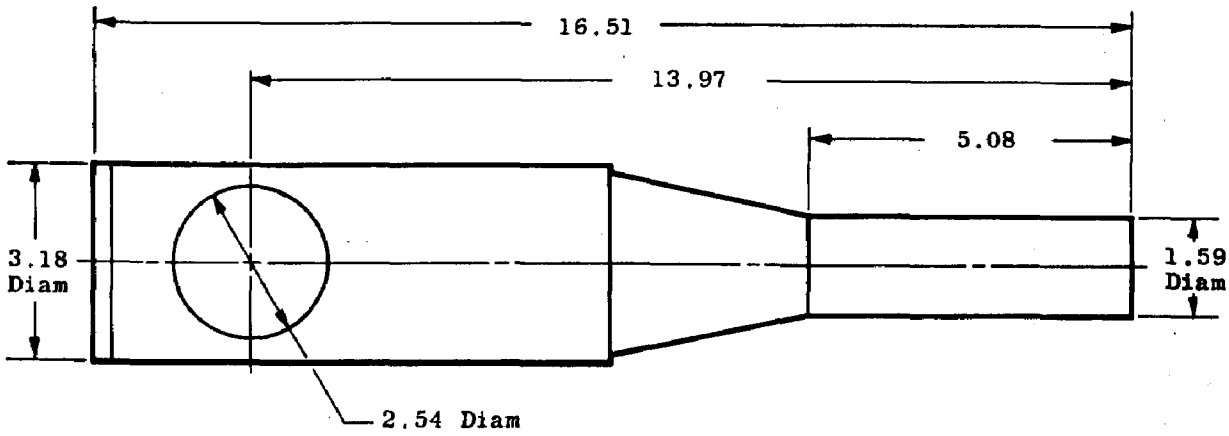

3.18-cm Side-Opening Probe

All Dimensions in Centimeters

Figure 9. EPA side-opening probes.

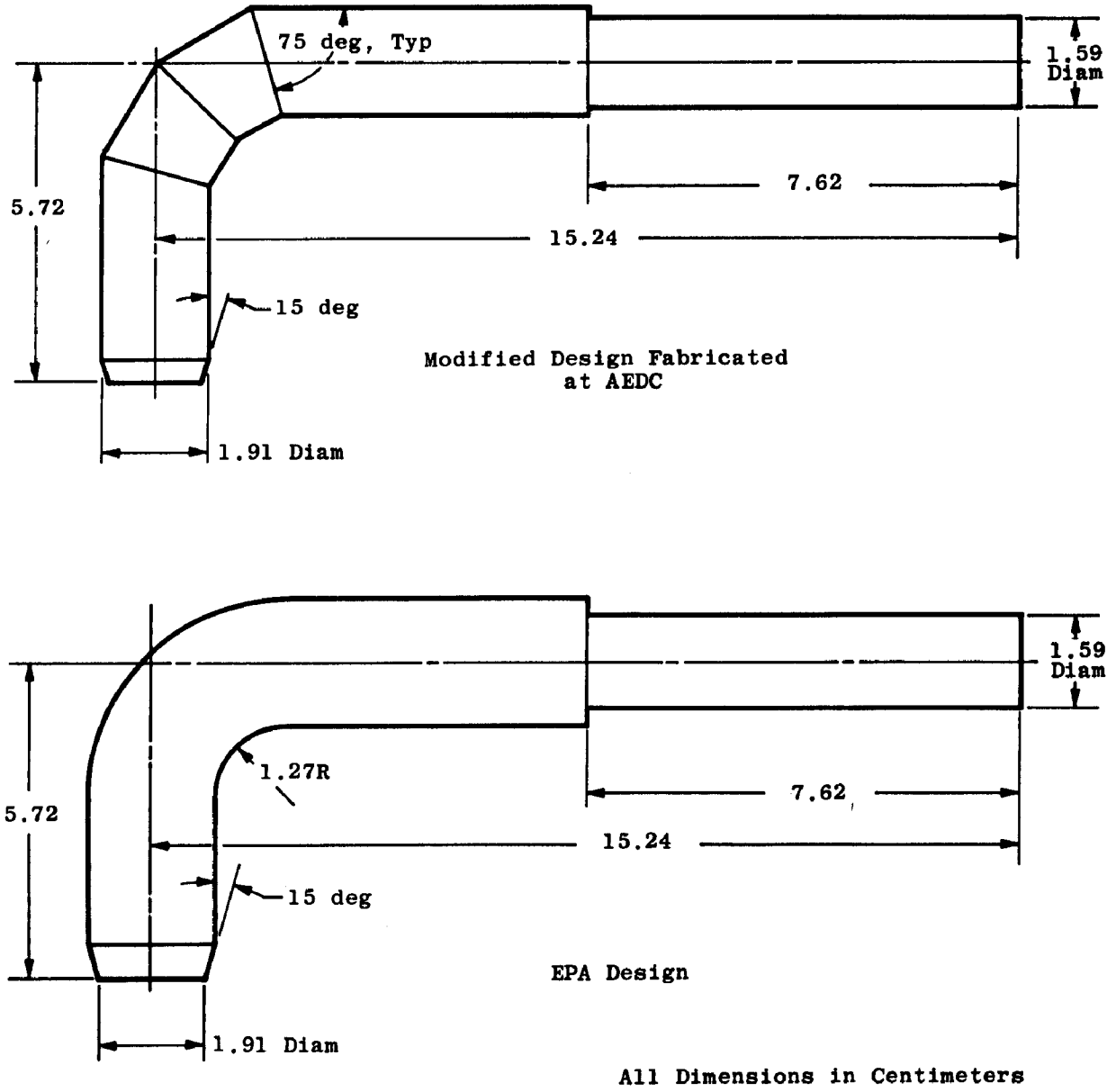

Figure 10. 1.91-cm sampling probes.

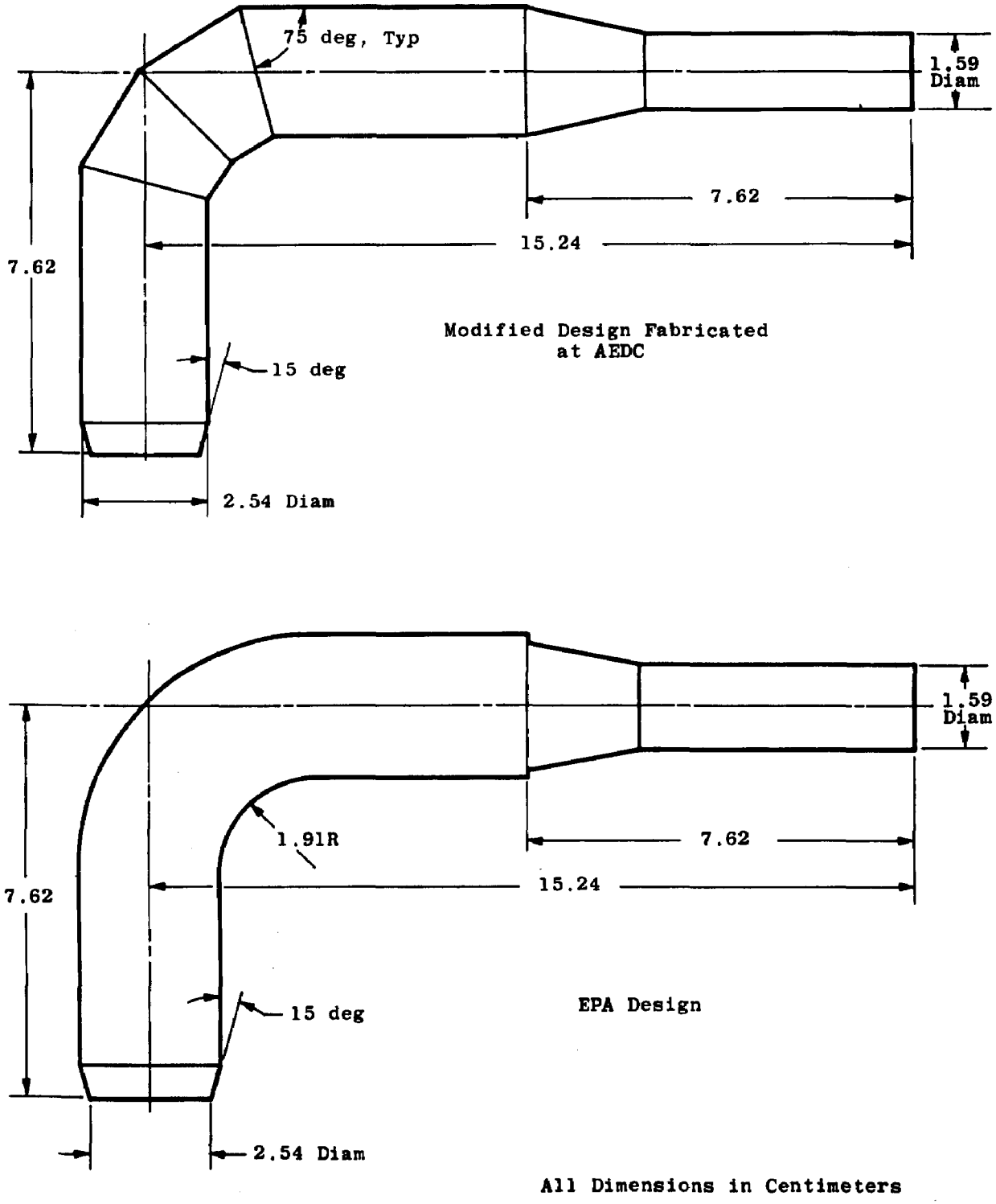

Figure 11. 2.54-cm sampling probes.

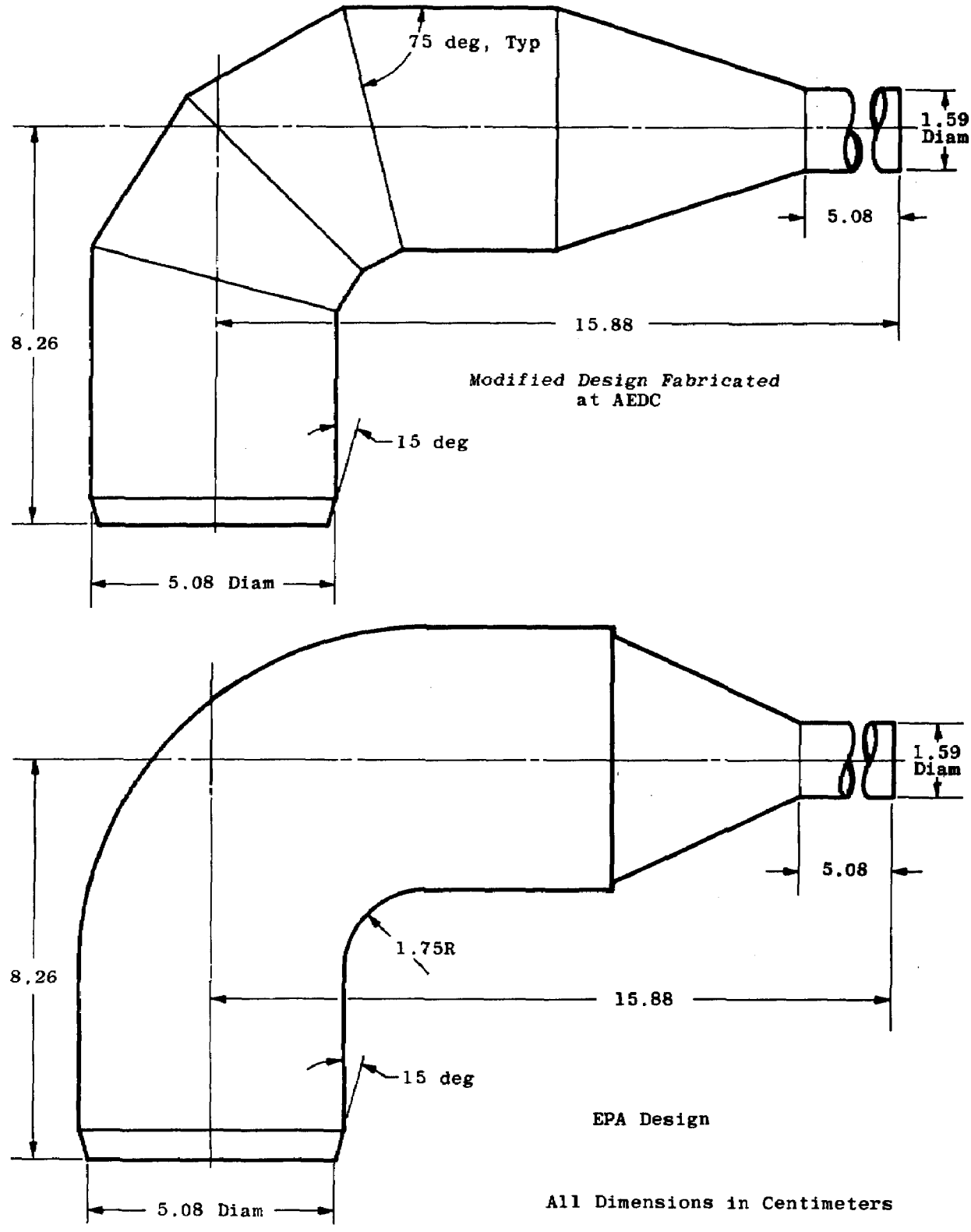

Figure 12. 5.08-cm sampling probe (sharp edge).

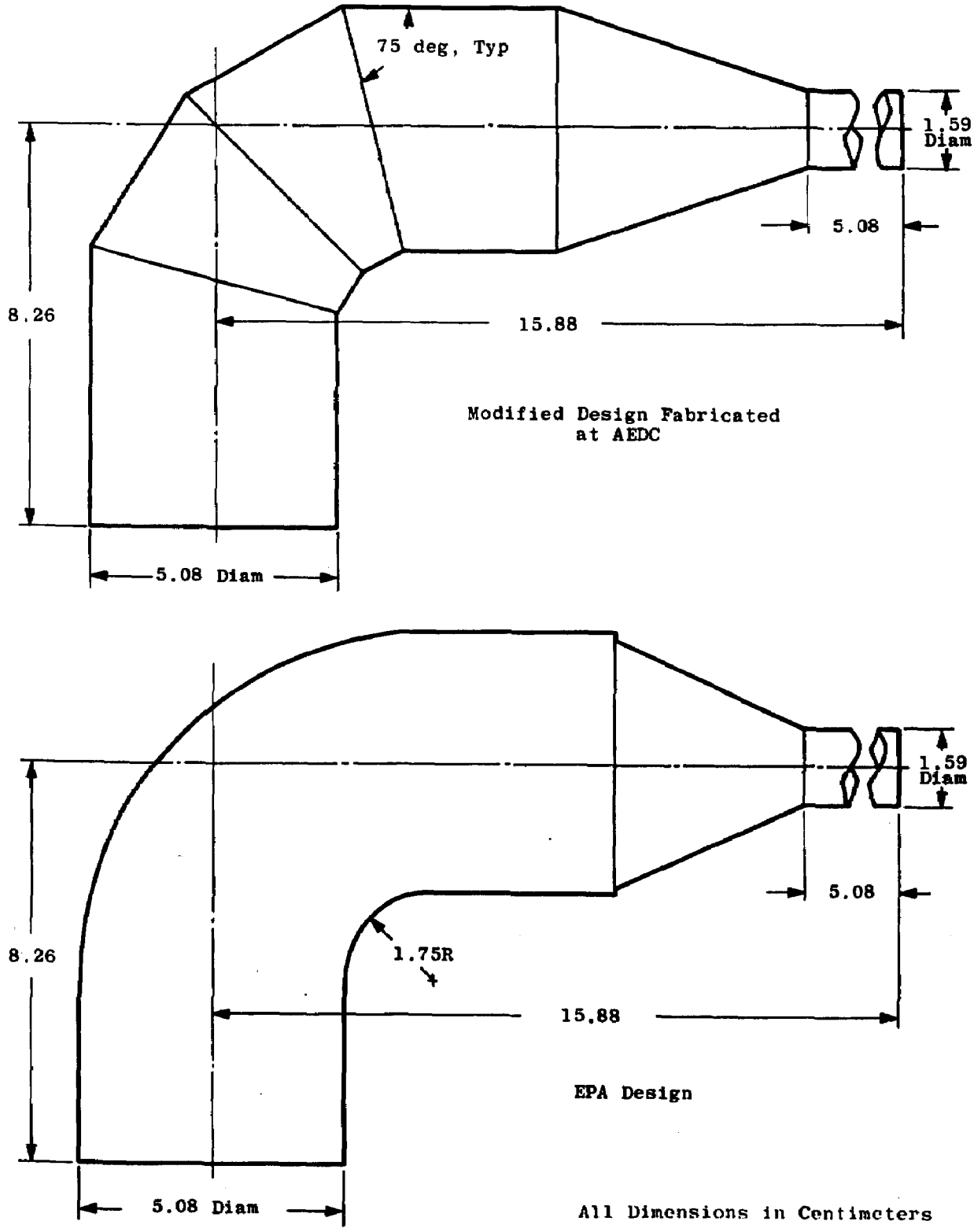

Figure 13. 5.08-cm sampling probe (square-edge).

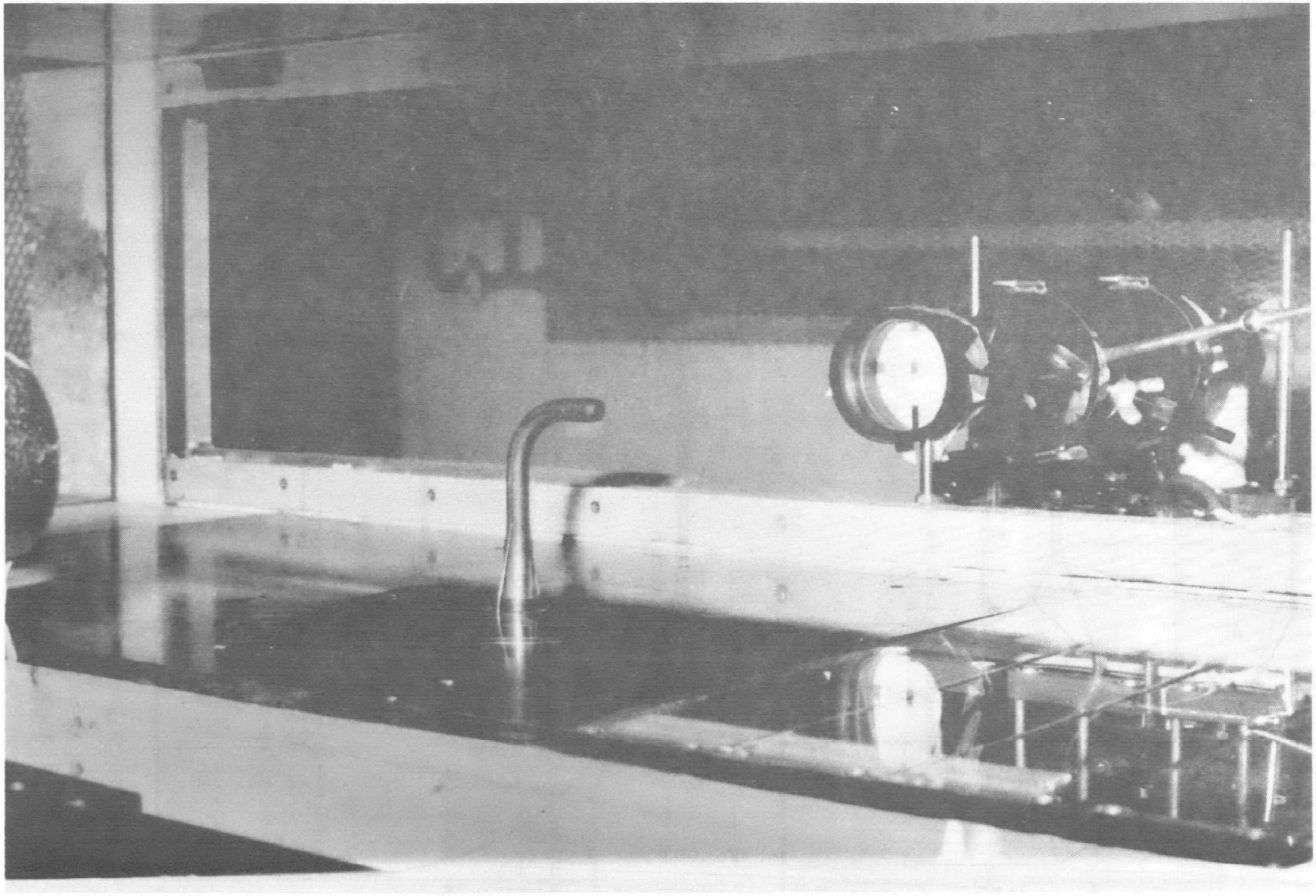

Figure 14. EPA sampling probe mounted in wind tunnel.

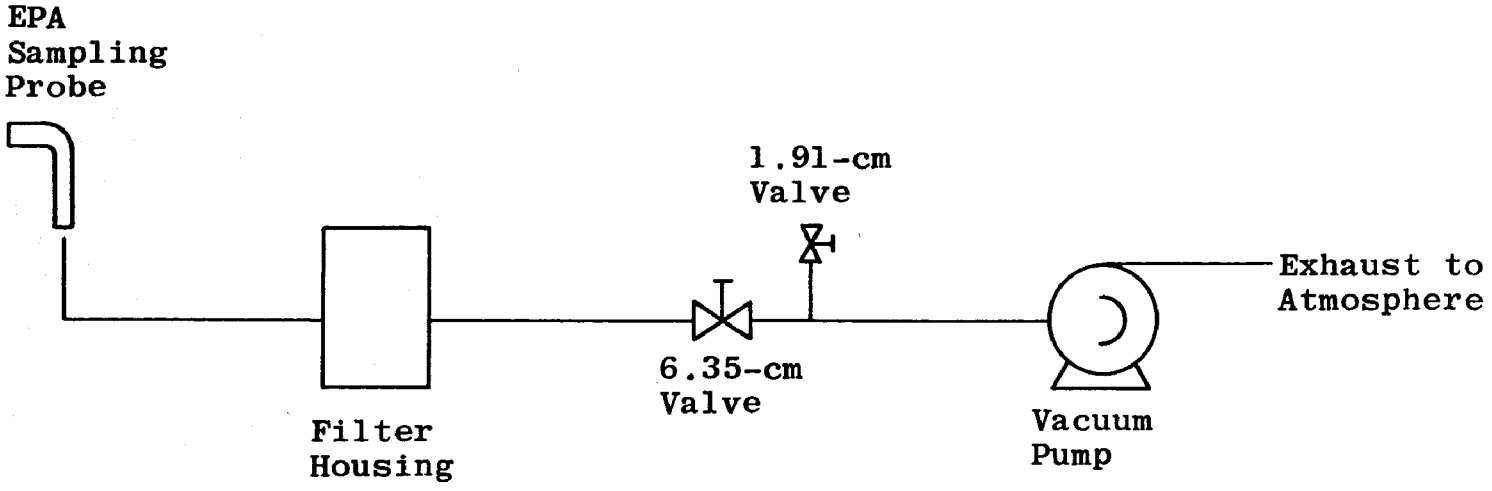

Figure 15. Schematic of extraction and sampling system.

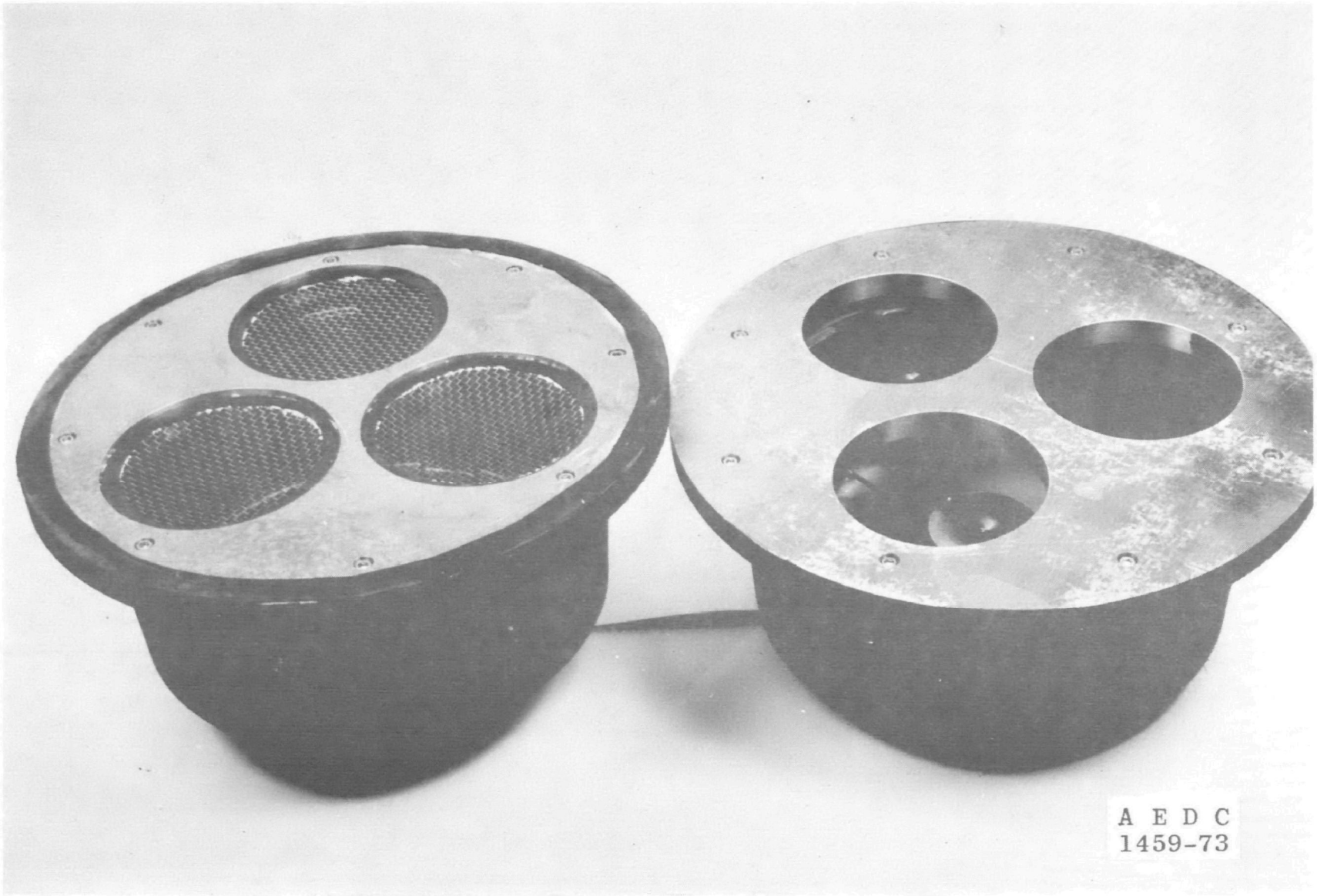

Figure 16. Filter housing.

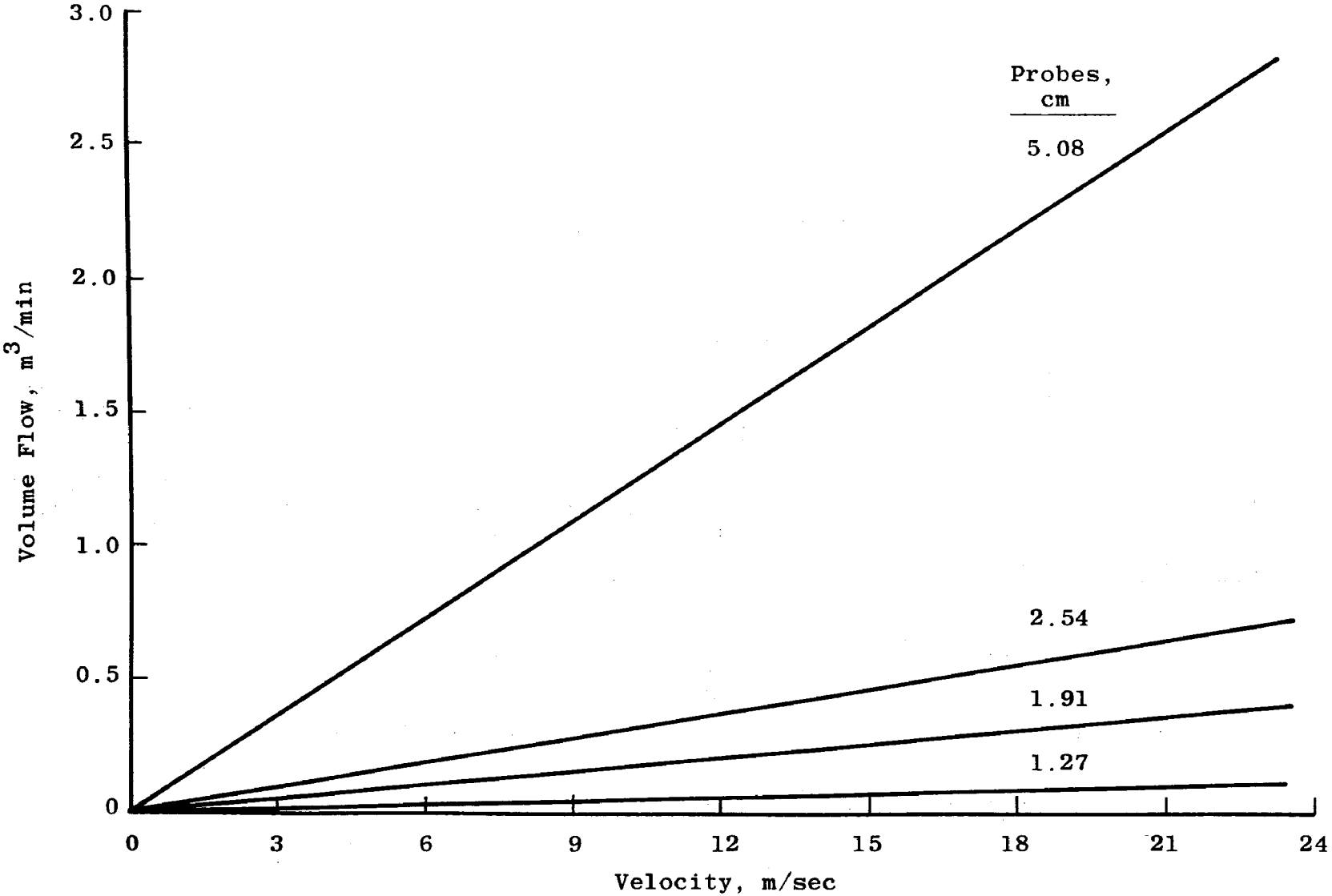

Figure 17. Theoretical isokinetic flow requirements of the EPA sampling probes.

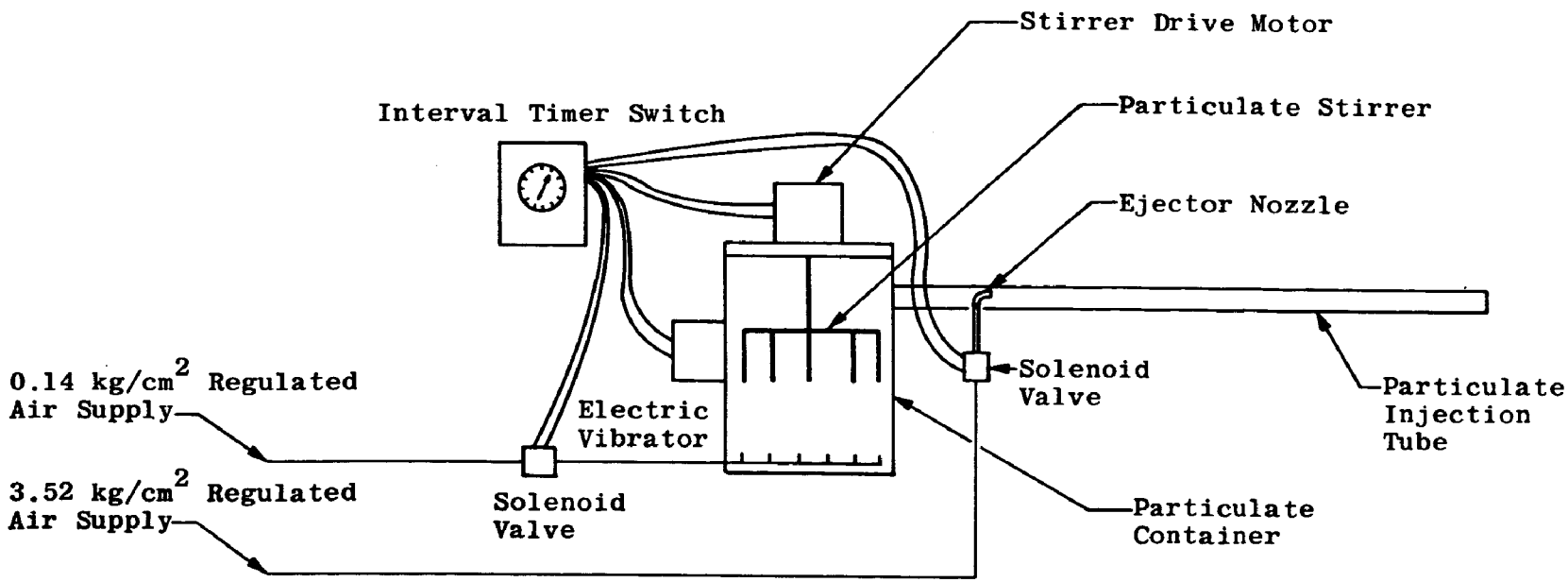

Figure 18. Schematic of particulate injection system.

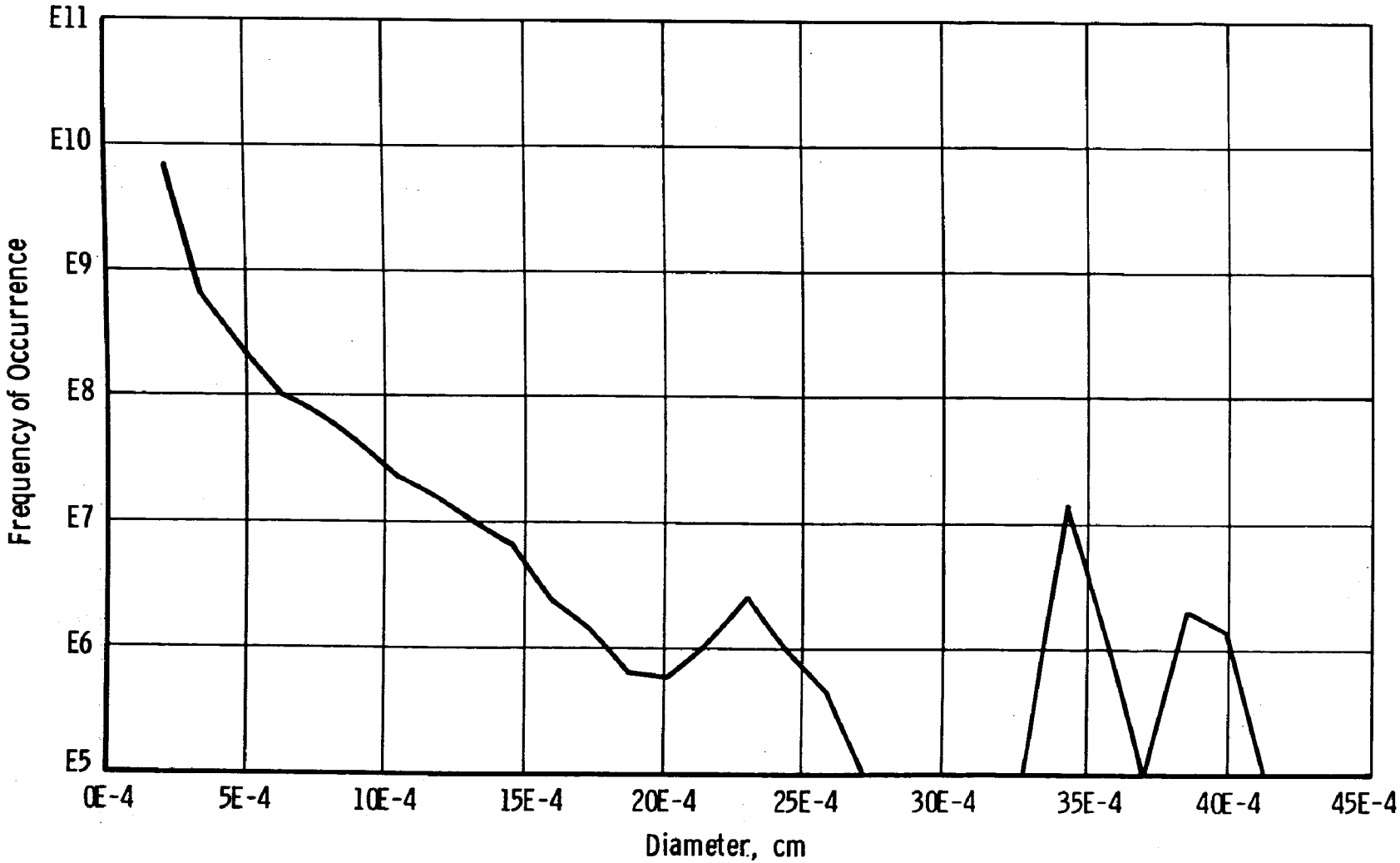

Figure 19. Fiber optics particle sizing of diatomaceous silica.

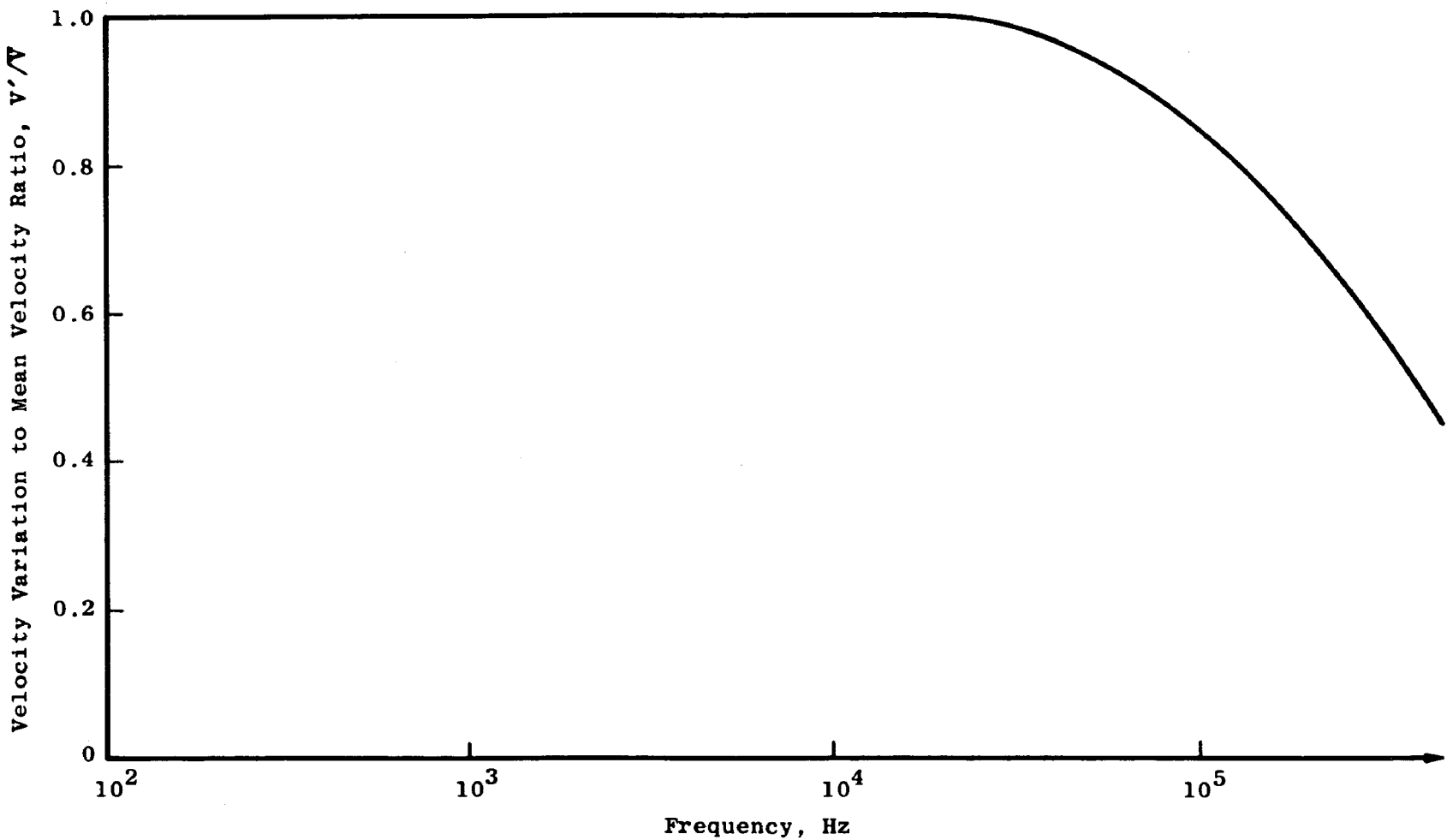

Figure 20. Frequency response of diatomaceous silica.

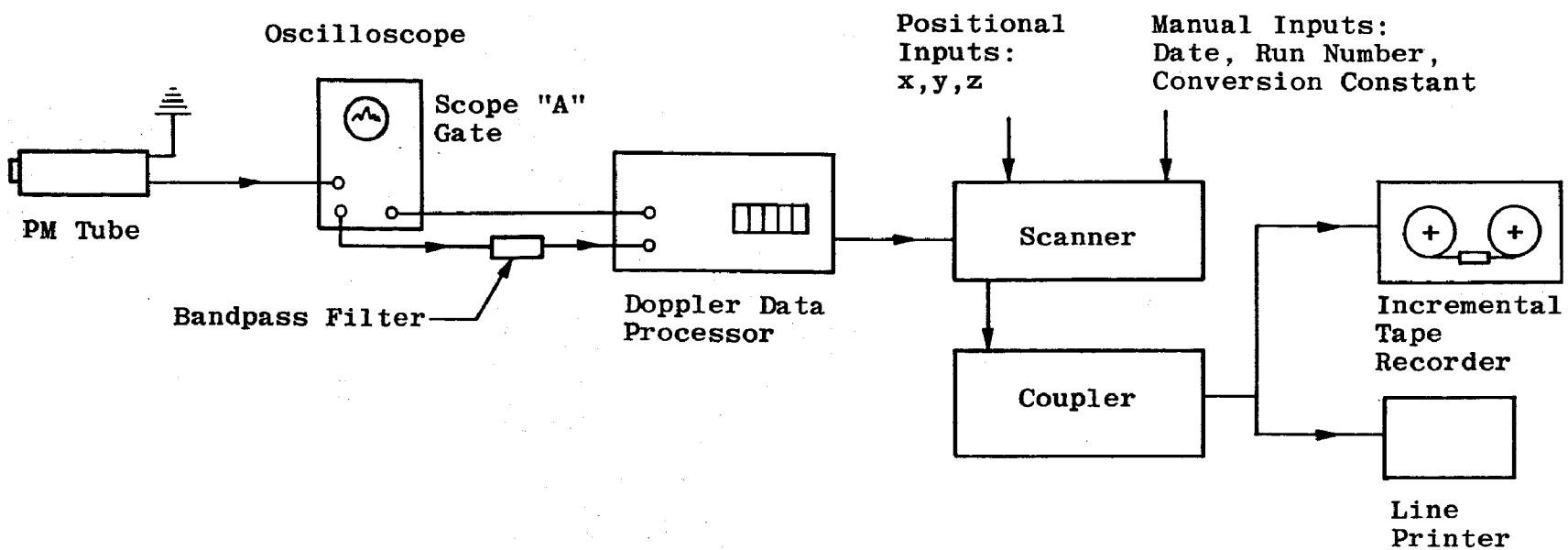

Figure 21. Data acquistion instrumentation.

Figure 22. Laser velocimeter data acquistion and processing instrumentation.

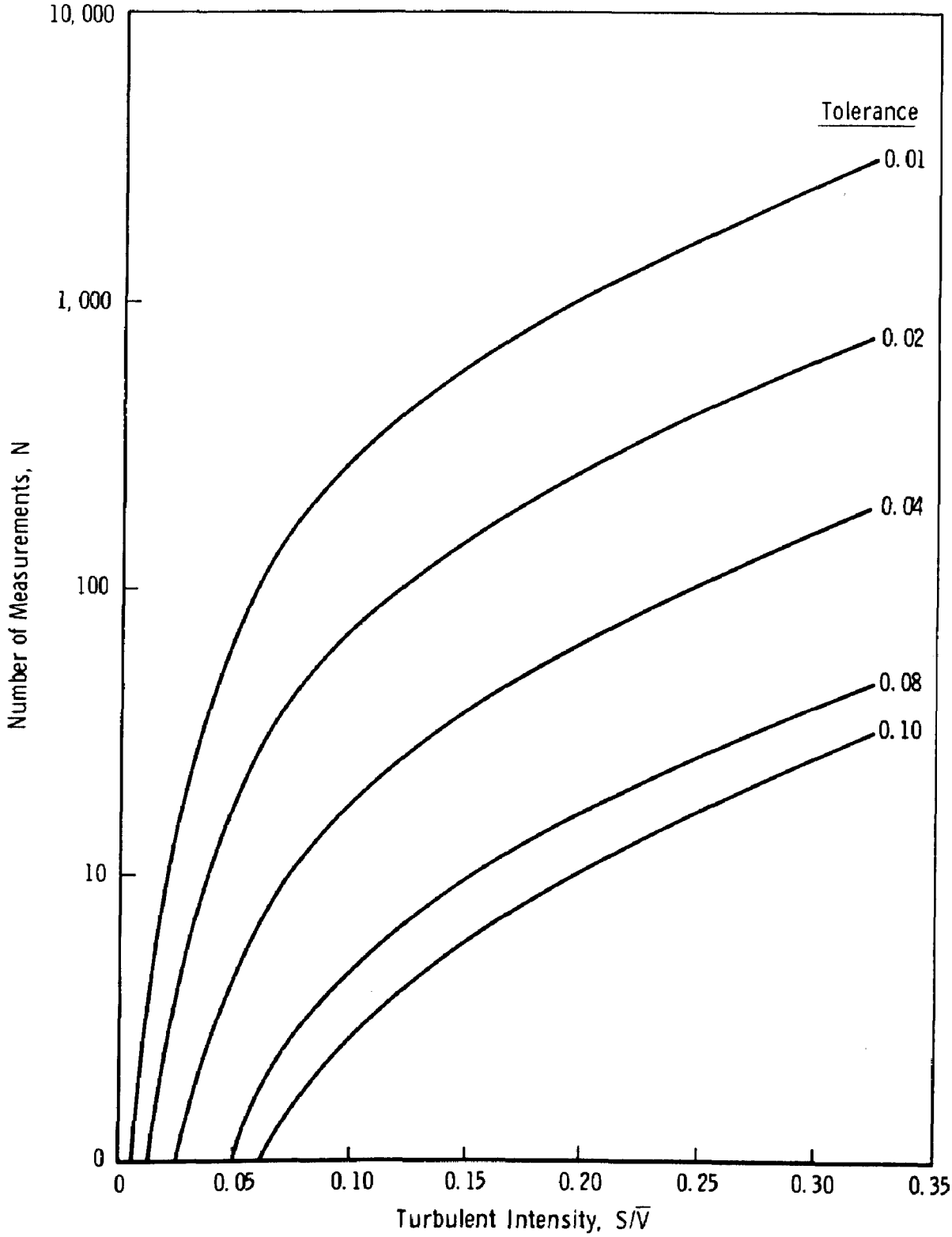

Figure 23. Number of measurements required for a 90-percent probability (Z) of the mean velocity.

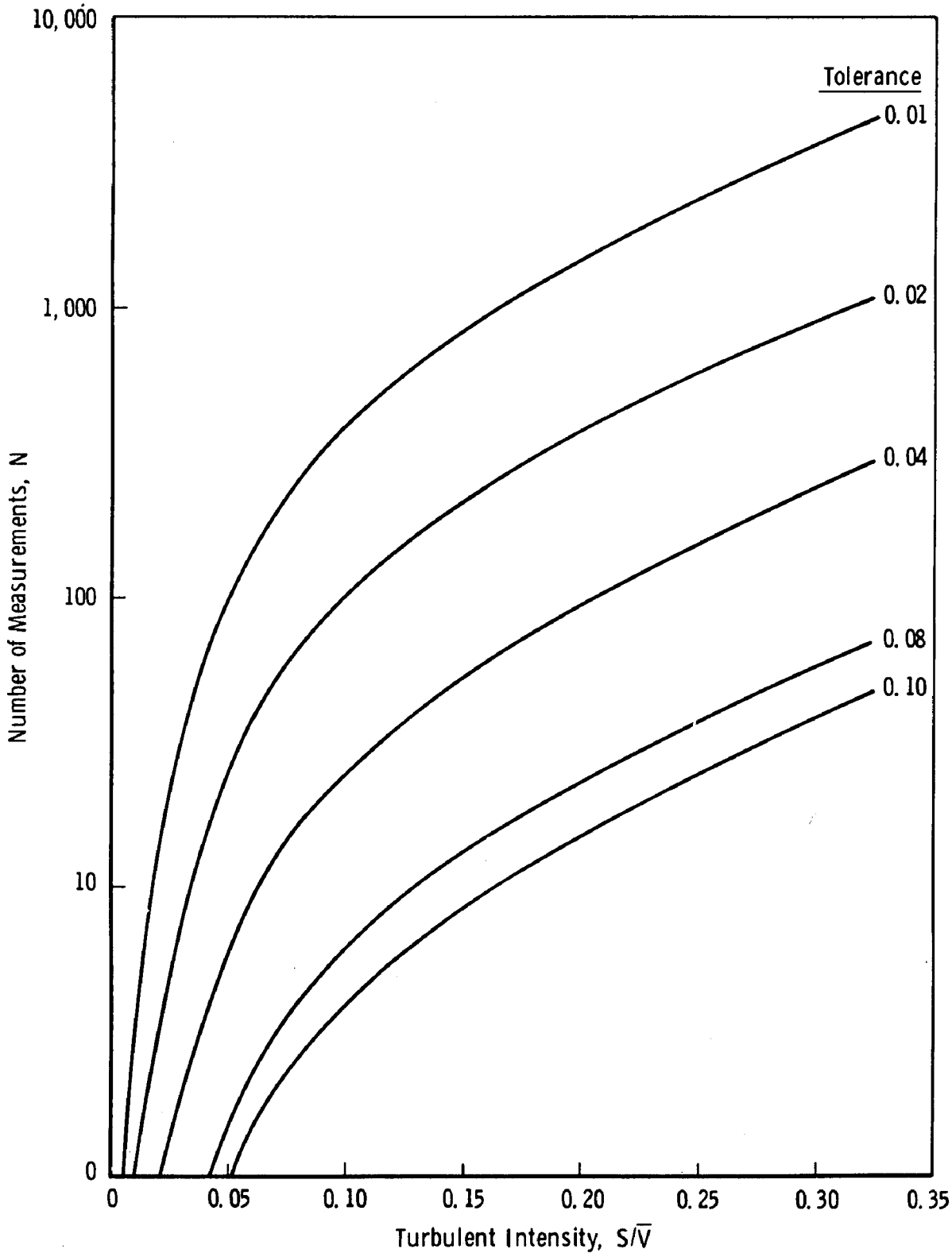

Figure 24. Number of measurements required for a 95-percent probability (Z) of the mean velocity.

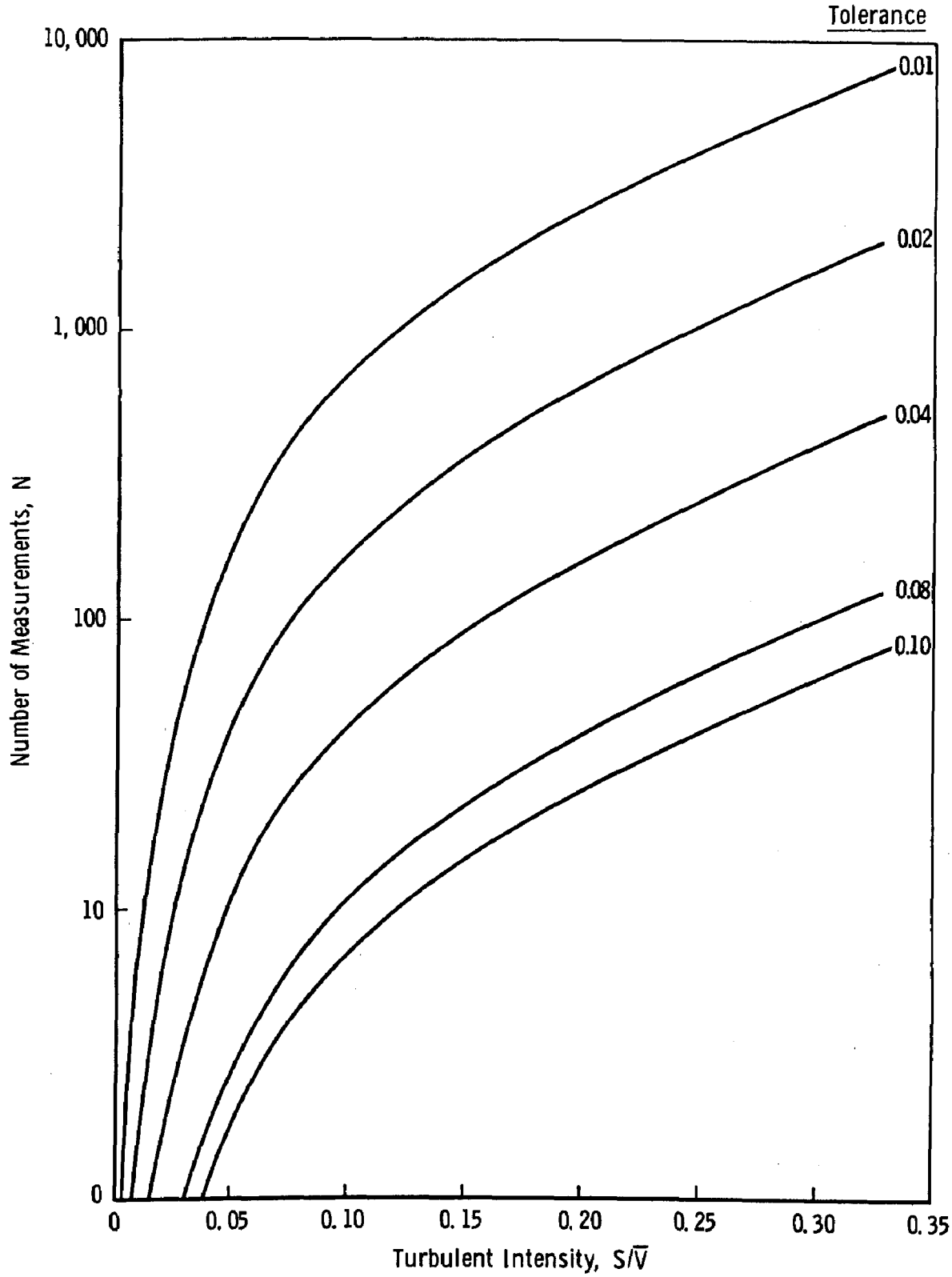

Figure 25. Number of measurements required for a 99-percent probability (Z) of the mean velocity.

```
DATA REDUCTION FOR TECH STAFF LDV DATA

                    RAW DATA PRINT OUT                    TAPE RECORD NUMBER      1

1101  70373  700   3433  700   3347  700   3392  700   3429  700   3318  700   3395  700   3391  700   3336  700   3358
 700   3318  700   3359  700   3452  700   3310  700   3331  700   3374  700   3385  700   3263  700   3308  700   3524
 700   3429  700   3443  700   3302  700   3331  700   3367  700   3363  700   3378  700   3339  700   3379  700   3329
 700   3355  700   3483  700   3355  700   3370  700   3417  700   3290  700   3335  700   3390  700   3191  700   3283
 700   3470  700   3326  700   3433  700   4888  700   3342  700   3473  700   3417  700   3361  700   3309  700   3415
 700   3312 2200    904 3300   3502 4401  23733 5540   8660

RUN NUMBER    1      DATE  7- 3-73        CONVERSION CONSTANT =    23.733 (FT/SEC)/MHZ

POSITION  -  X =    0.45      Y =   -0.75      Z =    4.33

ID =  0.500

VELOCIMETER DATA - PERIOD OF DOPPLER DATA IN MICROSECONDS

     0.3433       0.3347       0.3392       0.3429       0.3318       0.3395       0.3391       0.3336       0.3358       0.3318
     0.3359       0.3452       0.3310       0.3331       0.3374       0.3385       0.3263       0.3308       0.3524       0.3429
     0.3443       0.3302       0.3331       0.3367       0.3363       0.3378       0.3339       0.3379       0.3329       0.3355
     0.3483       0.3355       0.3370       0.3417       0.3290       0.3335       0.3390       0.3191       0.3283       0.3470
     0.3326       0.3433       0.4888       0.3342       0.3473       0.3417       0.3361       0.3309       0.3415       0.3312

 NUMBER OF MEASUREMENTS =  50
PERIOD- AVERAGE =     0.3398MICROSECONDS
                STANDARD DEVIATION =     0.0224MICROSECONDS

VELOCITY  -  AVERAGE =      69.845 FEET/SECOND
                STANDARD DEVIATION =       4.598 FT/SEC =     6.58 PER CENT

VELOCIMETER DATA - PERIOD OF DOPPLER DATA IN MICROSECONDS
CORRECTED TO AVERAGE +/-2.00 STANDARD DEVIATIONS

     0.3433       0.3347       0.3392       0.3429       0.3318       0.3395       0.3391       0.3336       0.3358       0.3318
     0.3359       0.3452       0.3310       0.3331       0.3374       0.3385       0.3263       0.3308       0.3524       0.3429
     0.3443       0.3302       0.3331       0.3367       0.3363       0.3378       0.3339       0.3379       0.3329       0.3355
     0.3483       0.3355       0.3370       0.3417       0.3290       0.3335       0.3390       0.3191       0.3283       0.3470
     0.3326       0.3433       0.0          0.3342       0.3473       0.3417       0.3361       0.3309       0.3415       0.3312

 NUMBER OF MEASUREMENTS =  49
PERIOD- AVERAGE =     0.3368MICROSECONDS
                STANDARD DEVIATION =     0.0062MICROSECONDS

VELOCITY  -  AVERAGE =      70.476 FEET/SECOND
                STANDARD DEVIATION =       1.305 FT/SEC =     1.85 PER CENT
```

Figure 26. EPA data program printout.

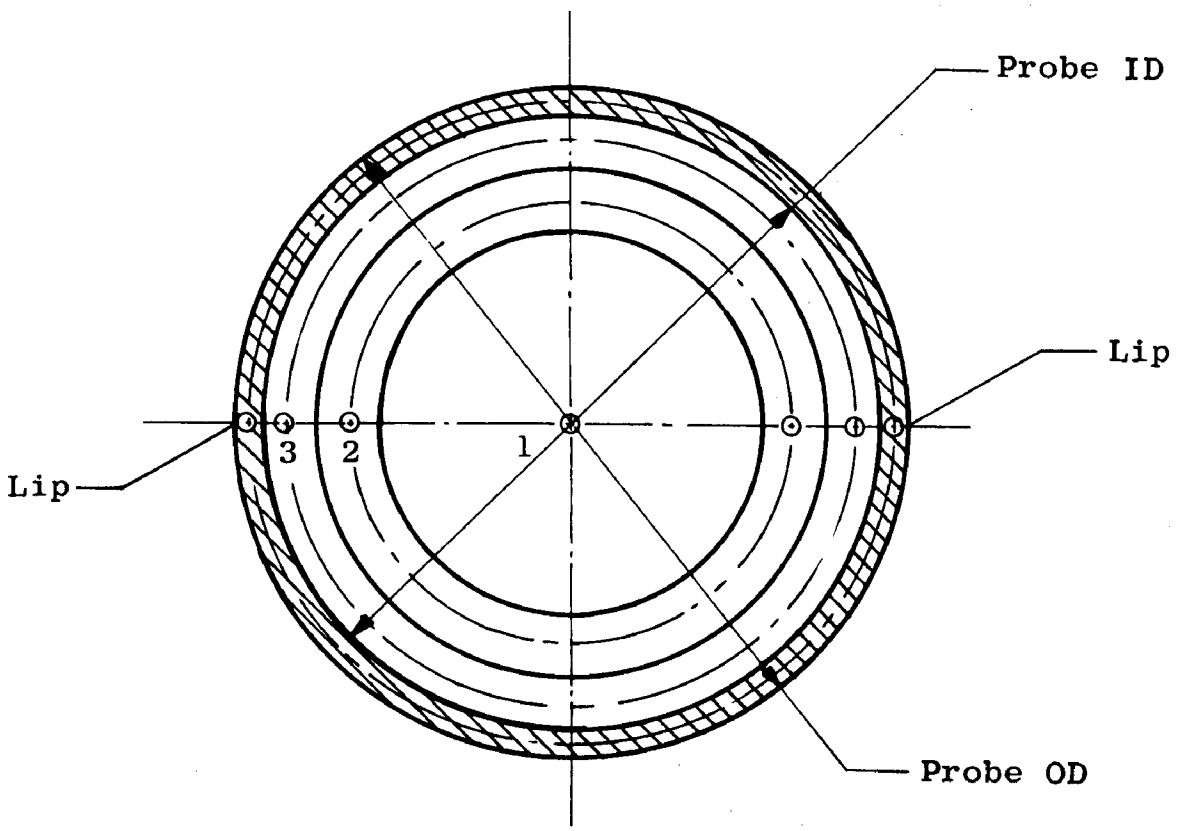

Figure 27. Location of probe equal area measurement points.

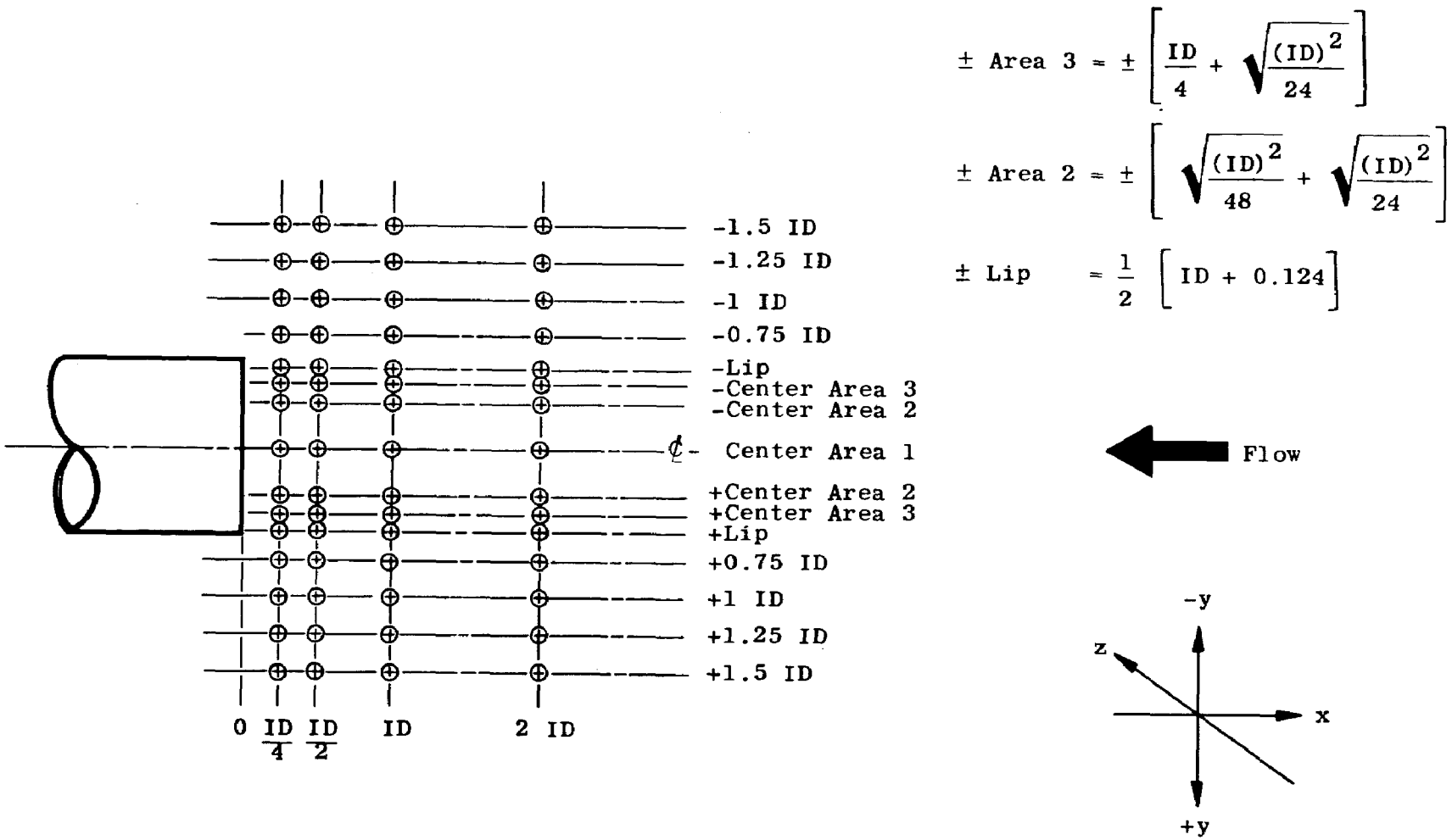

Figure 28. Location of probe velocity measurements for zero angle of attack.

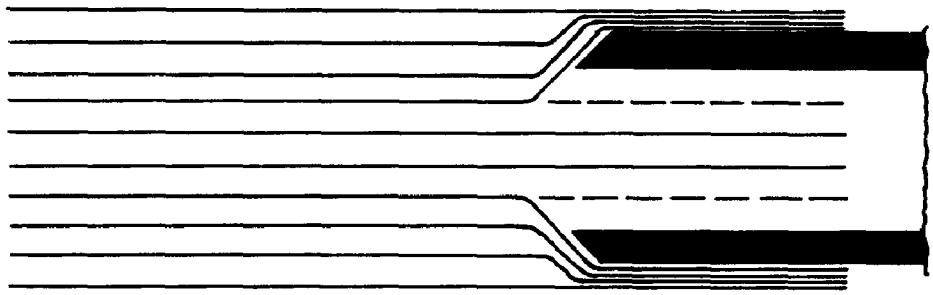

a. Less than isokinetic conditions.

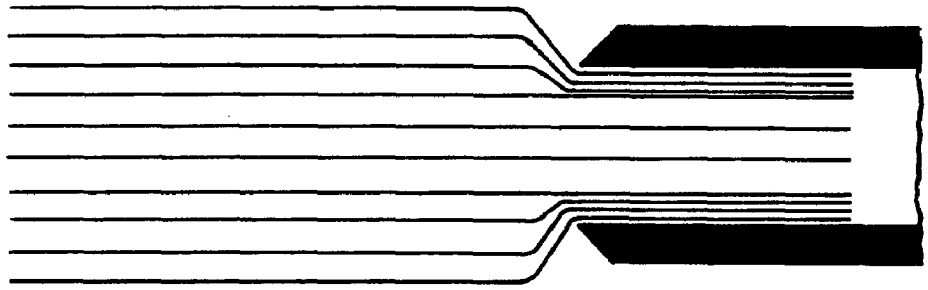

b. Greater than isokinetic conditions

Figure 29. Flow streamlines around a probe.

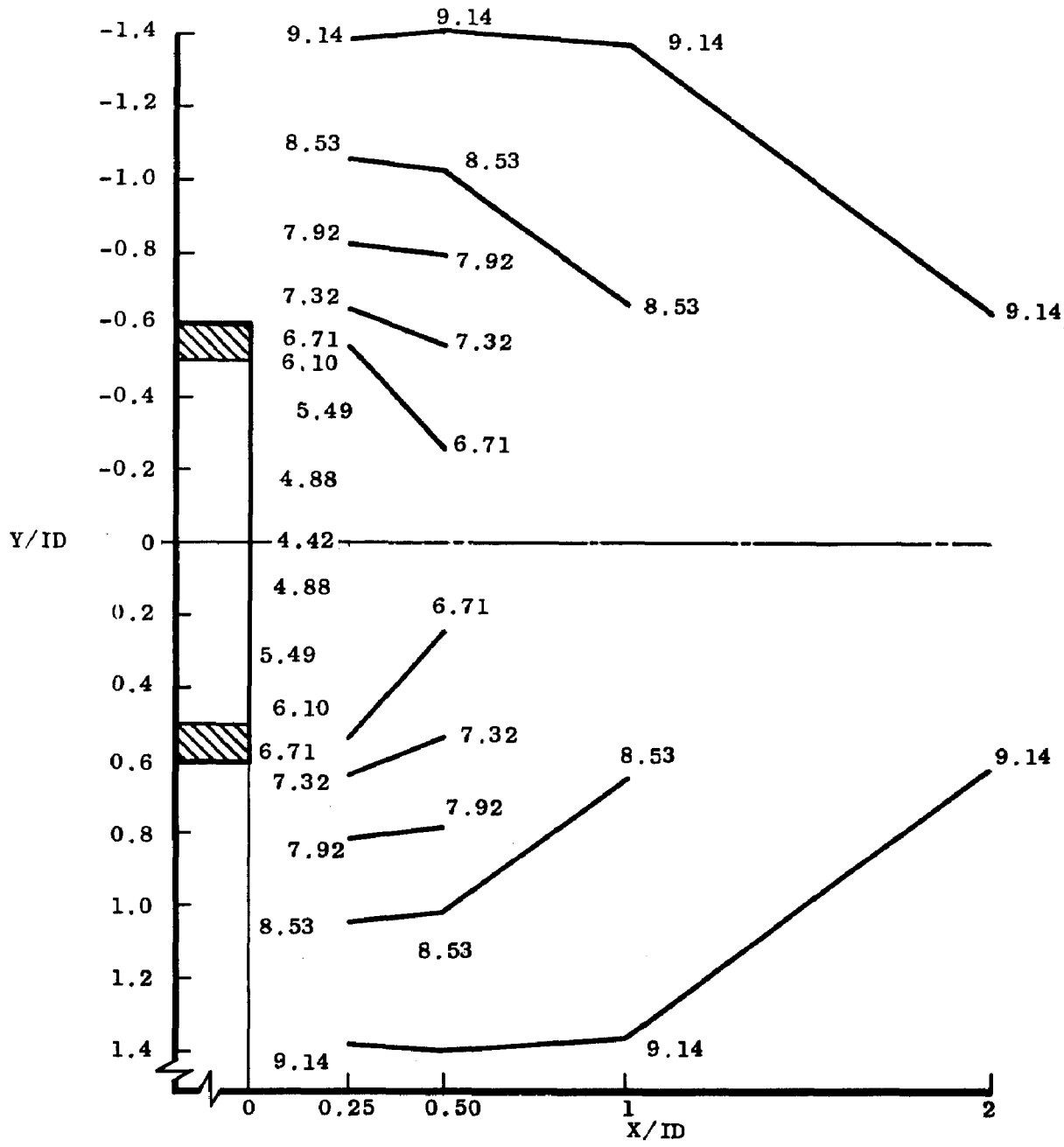

Figure 30. Constant velocity lines, 1.27-cm square-edge probe, $\Delta P = 7.11$ mm H_2O, $P_{in} > P_{out}$.

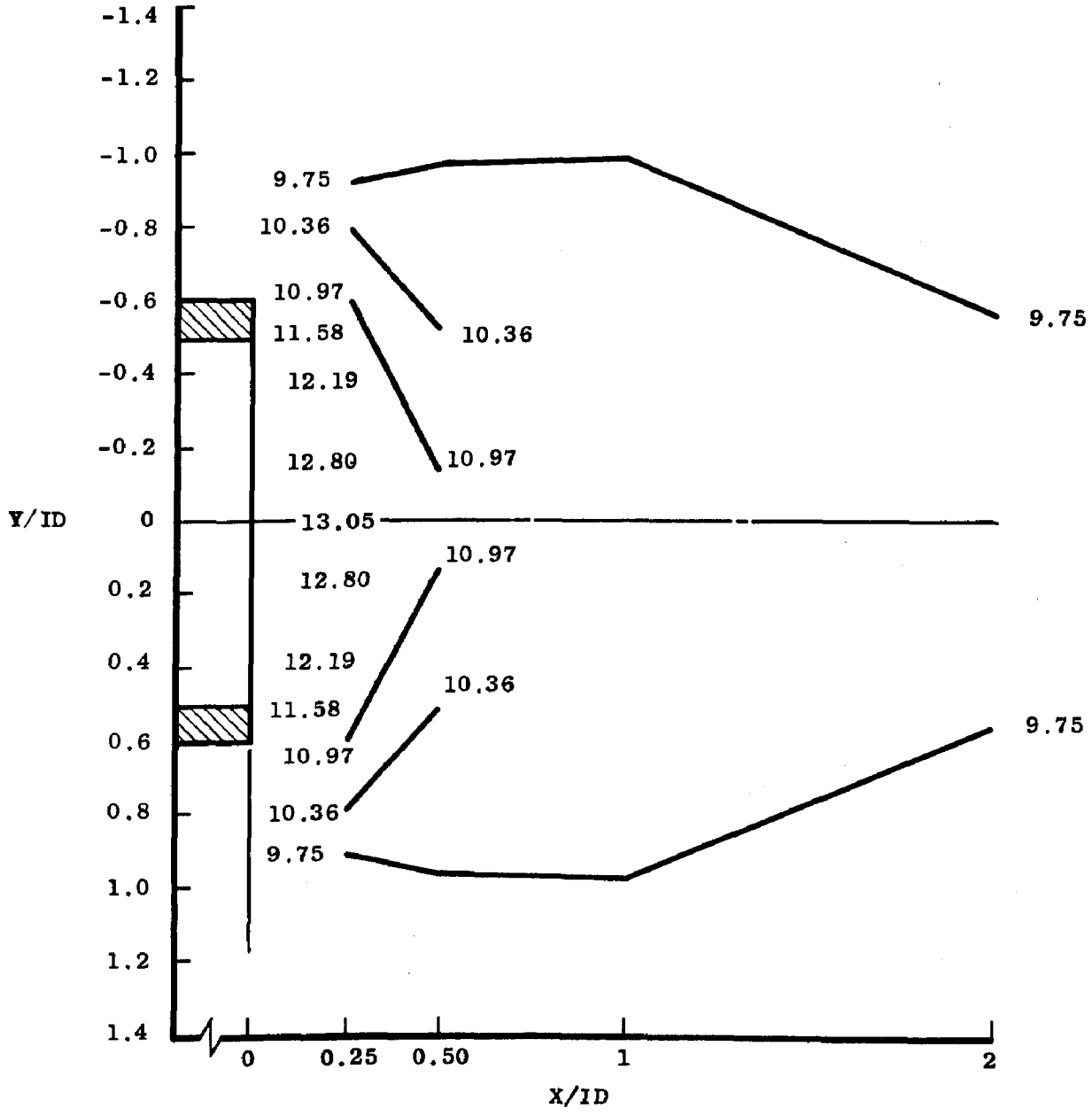

Figure 31. Constant velocity lines, 1.27-cm square-edge probe, ΔP = 25.4 mm H_2O, $P_{in} < P_{out}$.

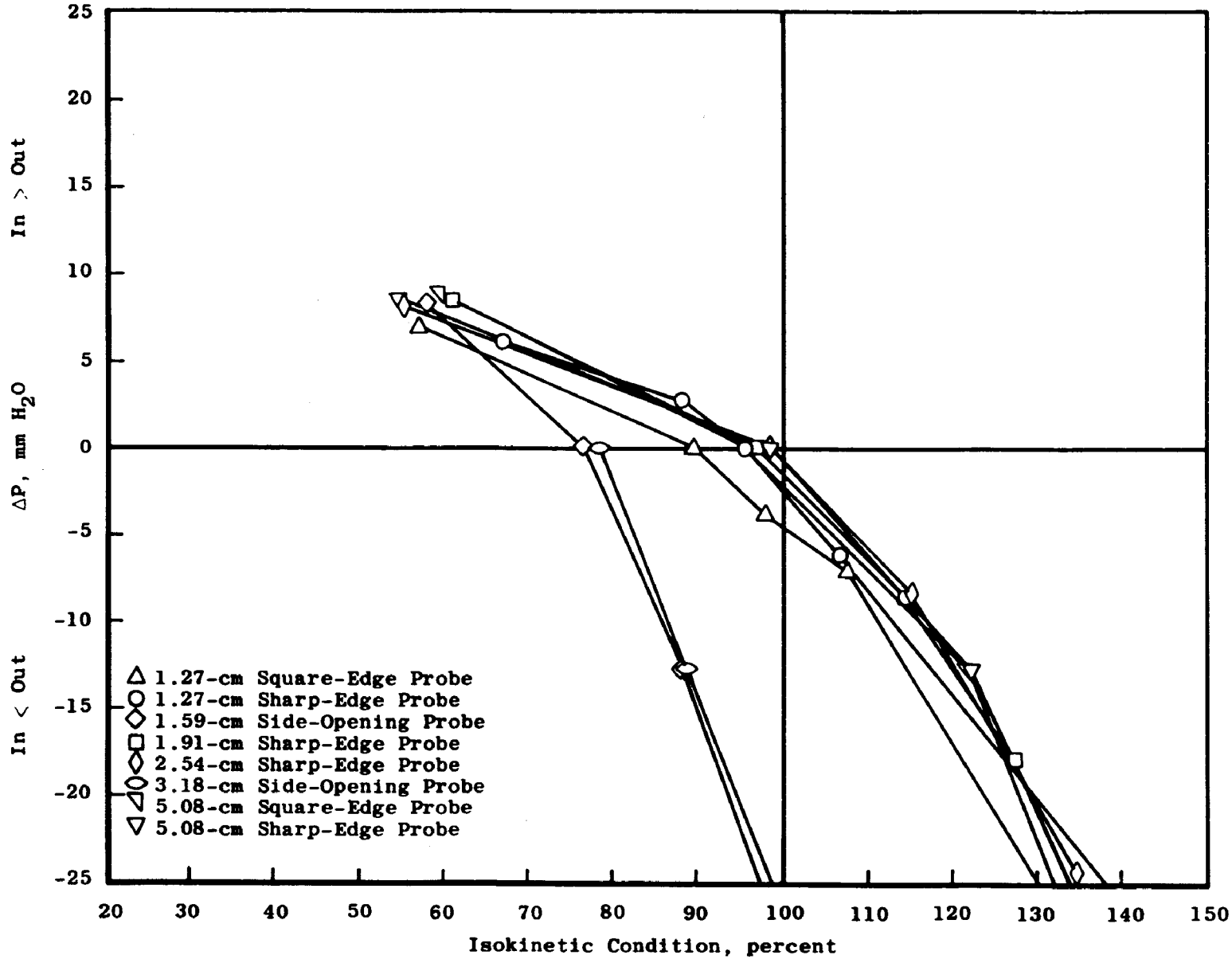

Figure 32. Probe performance at 9.14 m/sec and zero angle of attack.

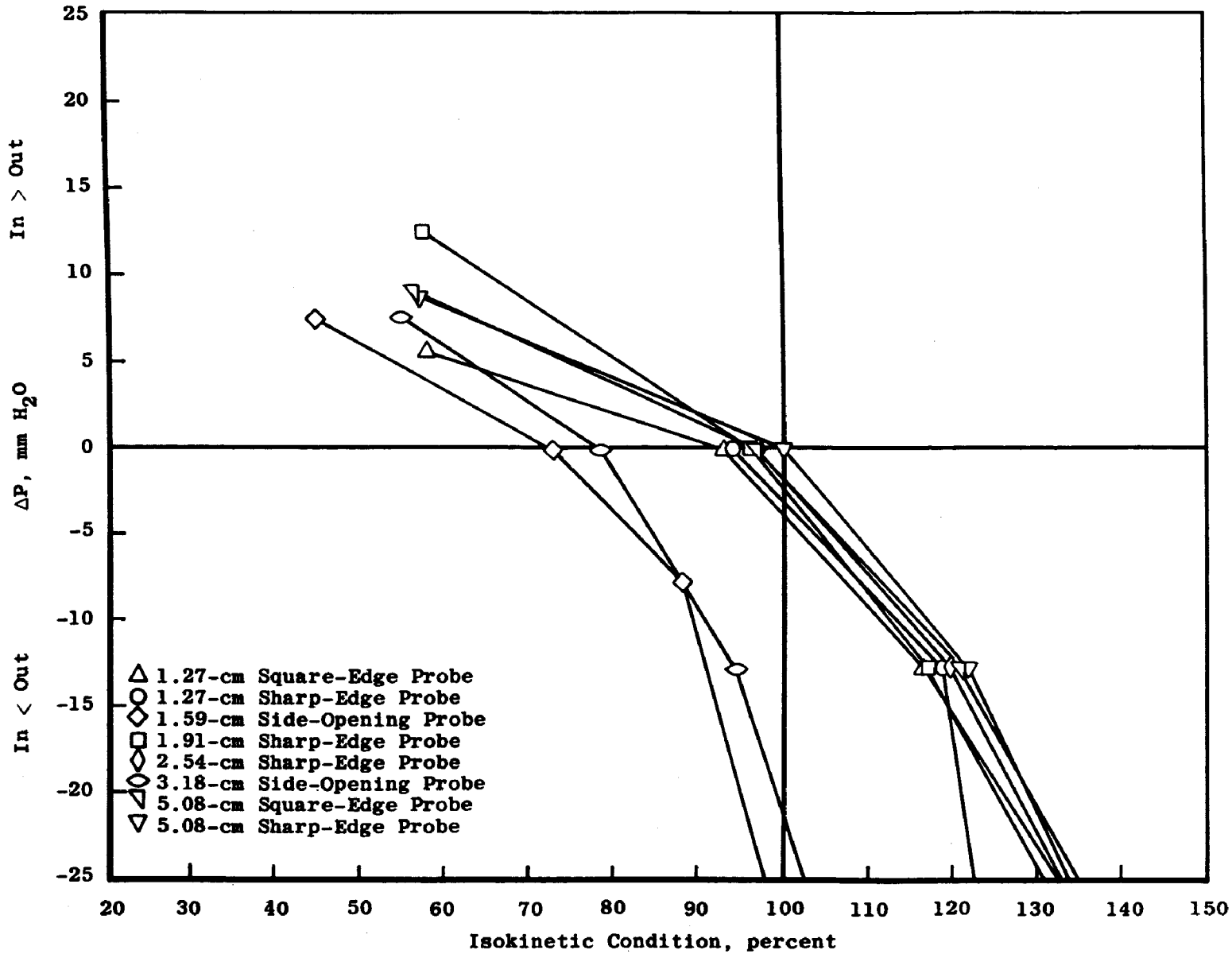

Figure 33. Probe performance at 9.14 m/sec and 7.5 deg angle of attack.

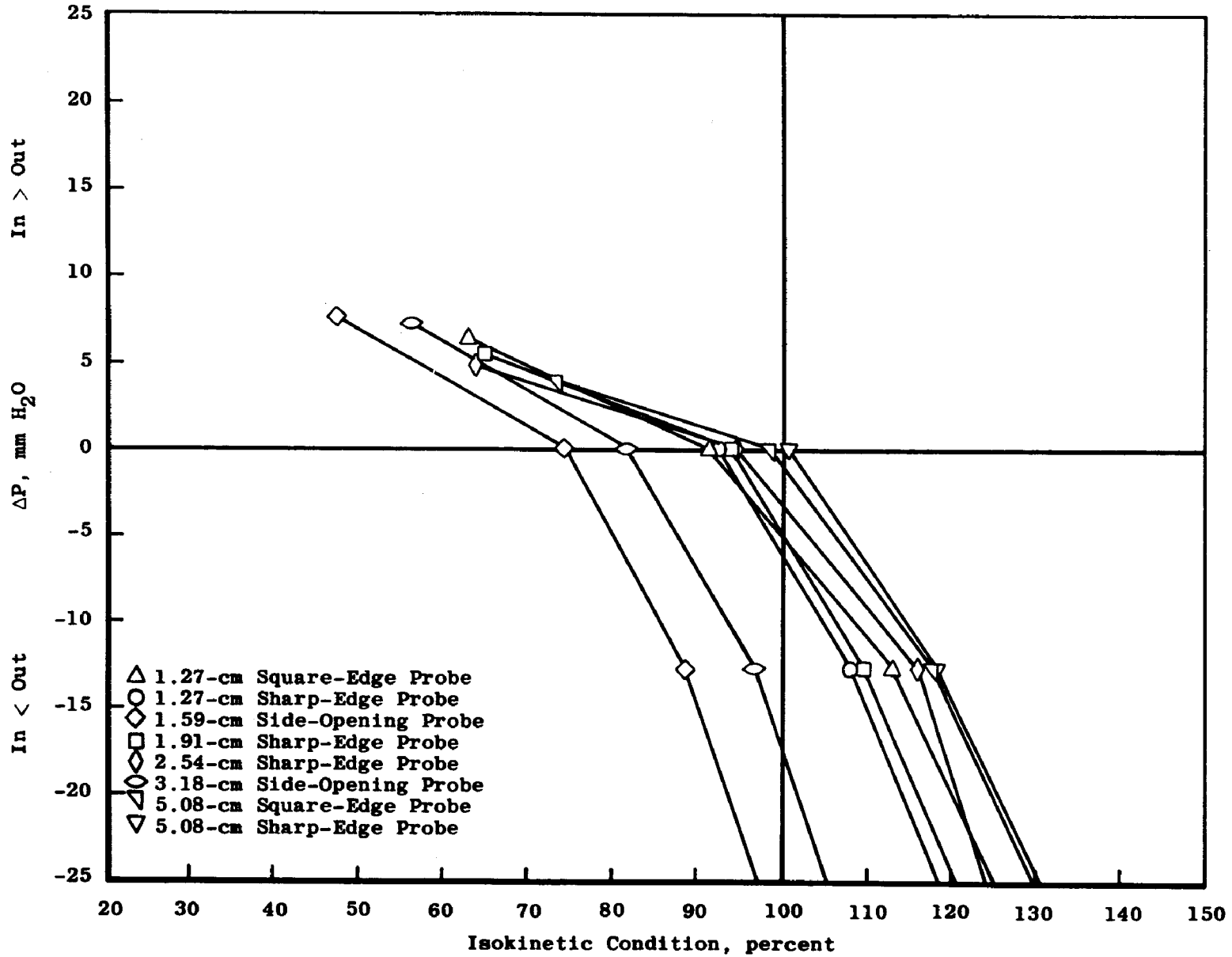

Figure 34. Probe performance at 9.14 m/sec and 15 deg angle of attack.

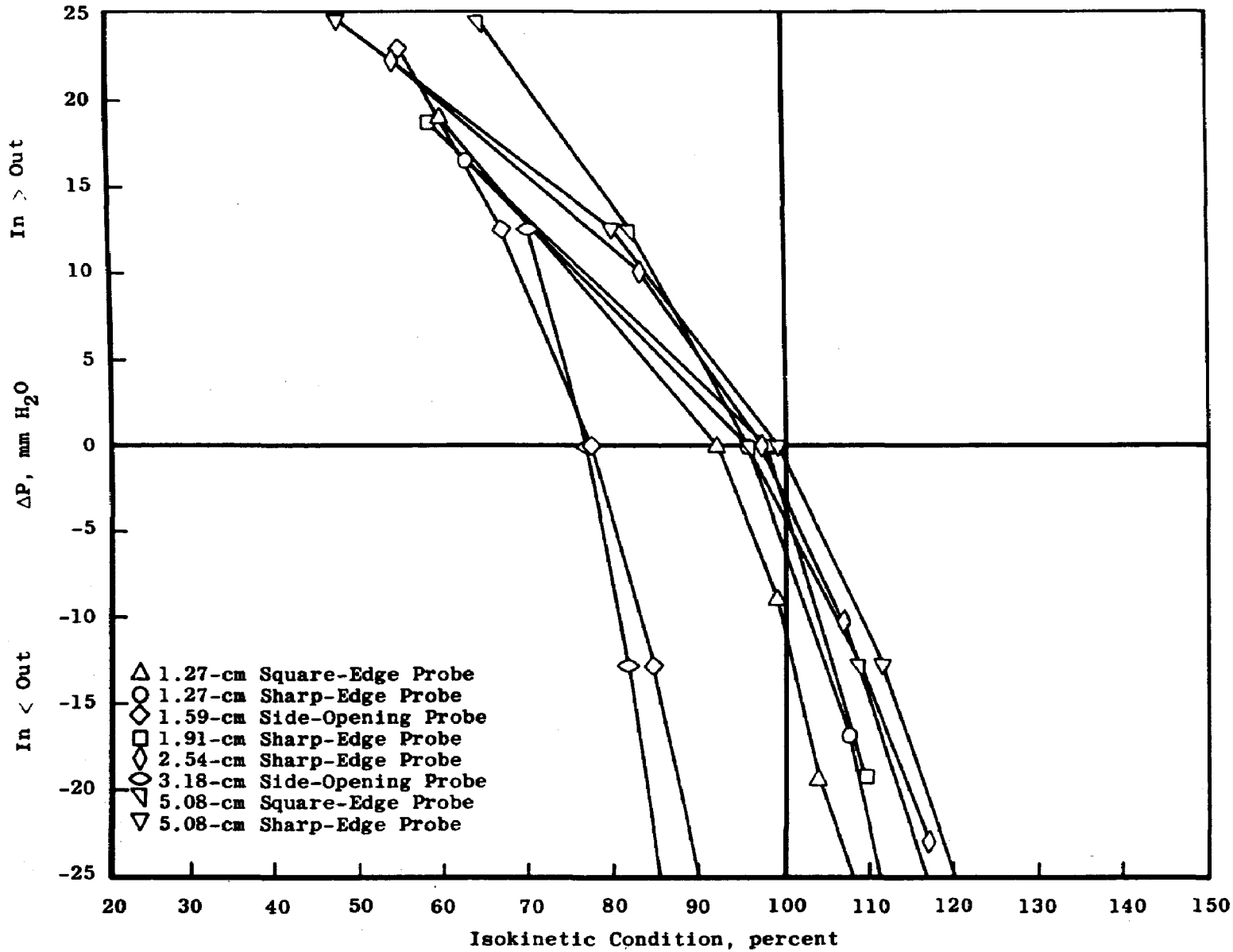

Figure 35. Probe performance at 15.24 m/sec and zero angle of attack.

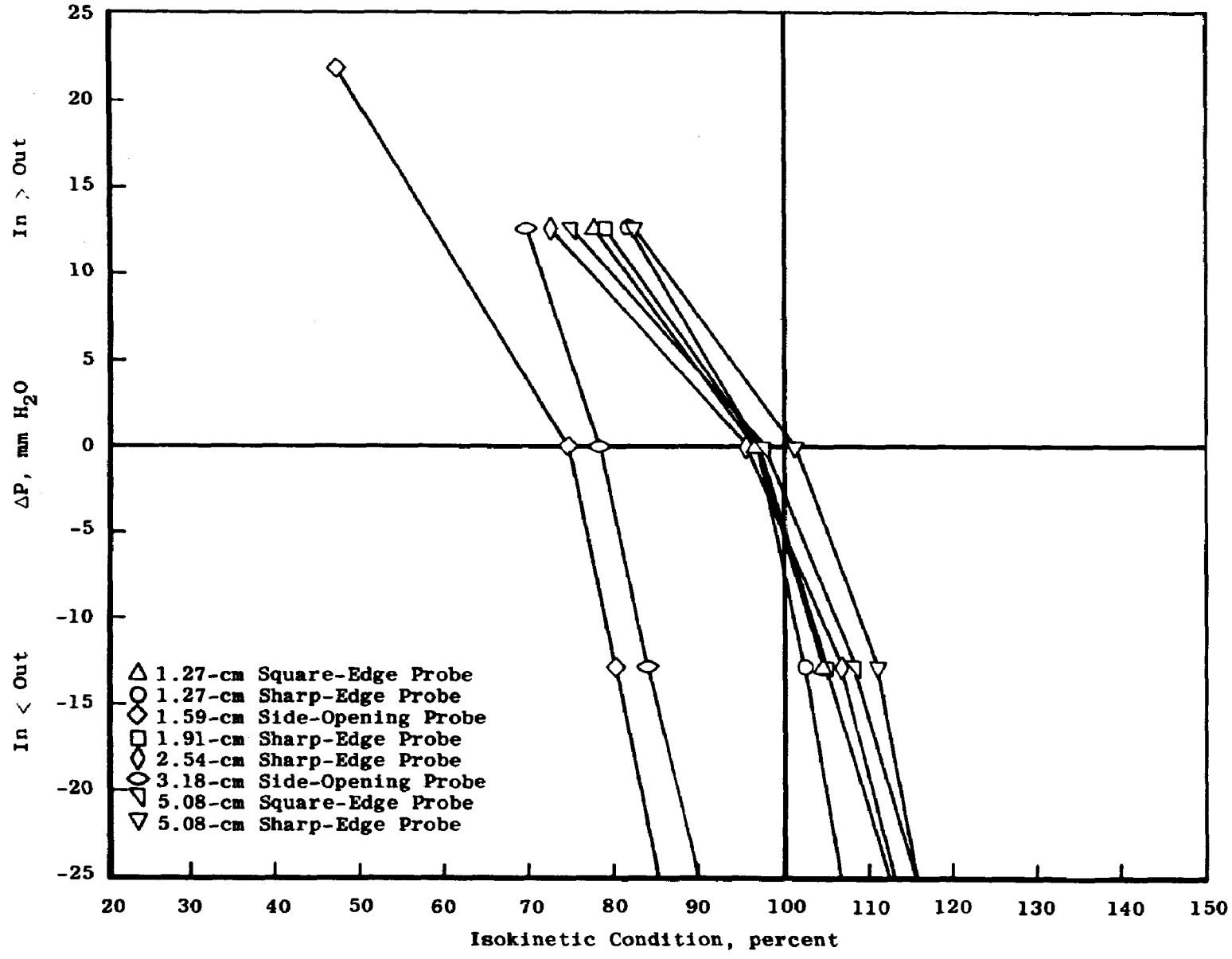

Figure 36. Probe performance at 15.24 m/sec and 7.5 deg angle of attack.

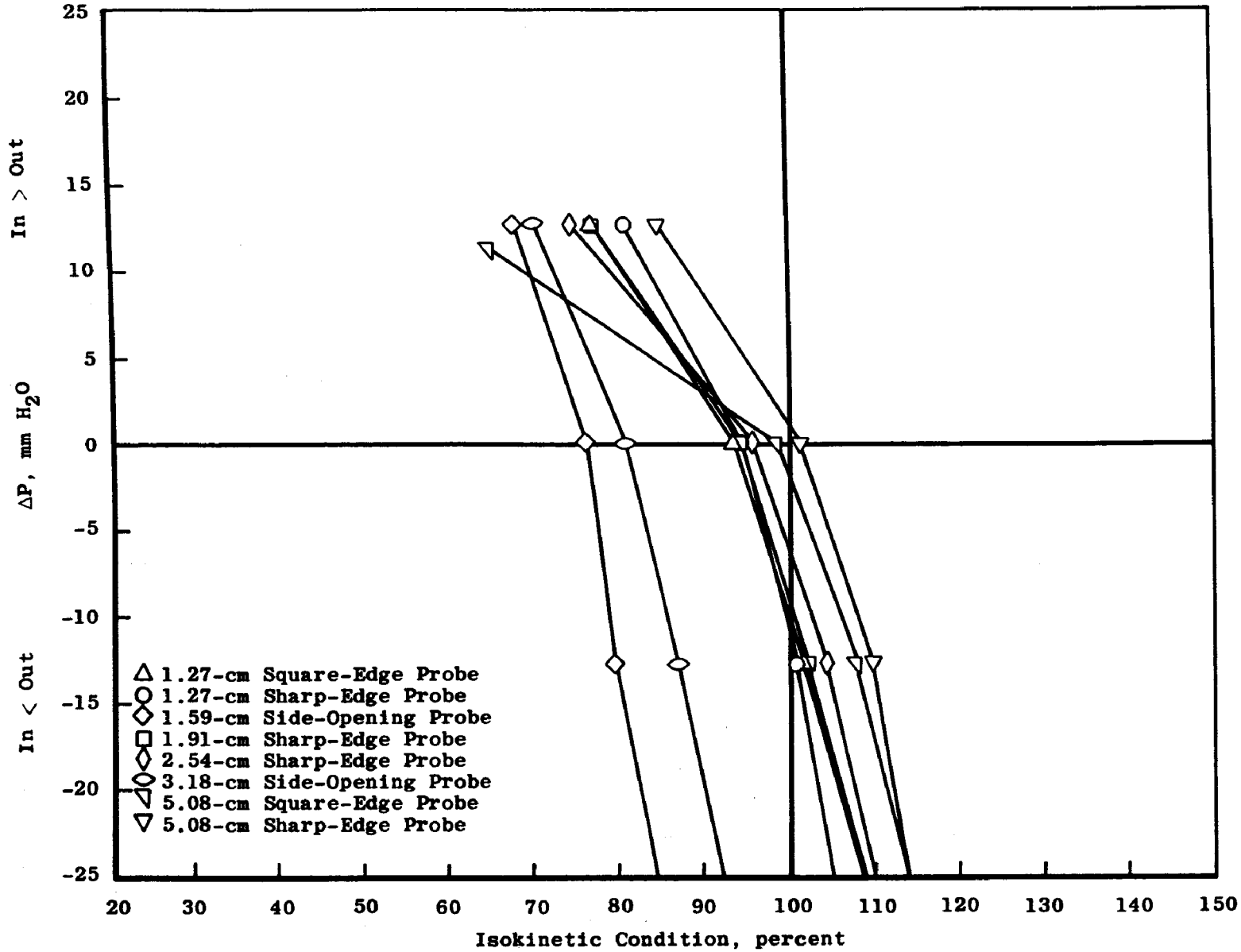

Figure 37. Probe performance at 15.24 m/sec and 15 deg angle of attack.

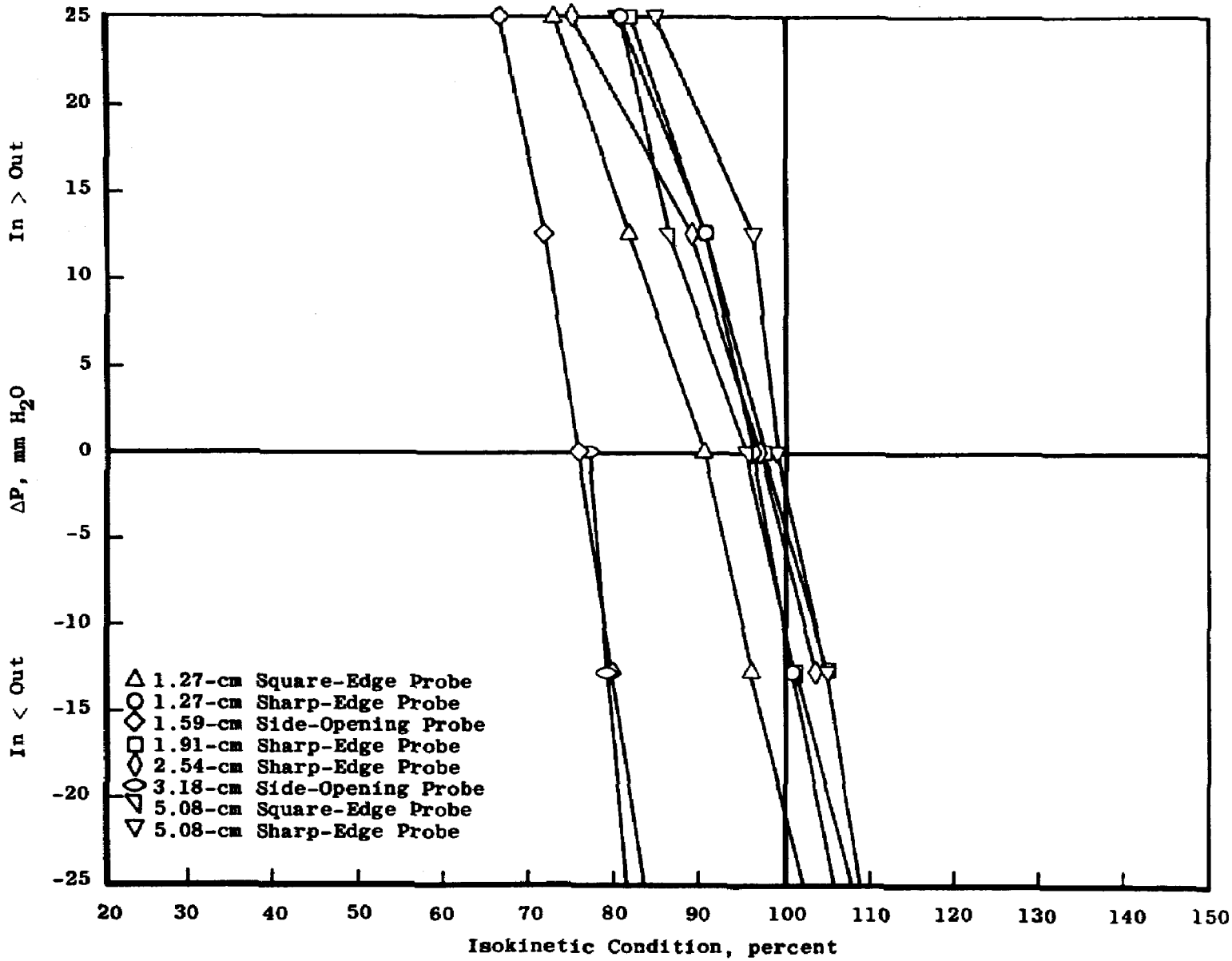

Figure 38. Probe performance at 21.34 m/sec and zero angle of attack.

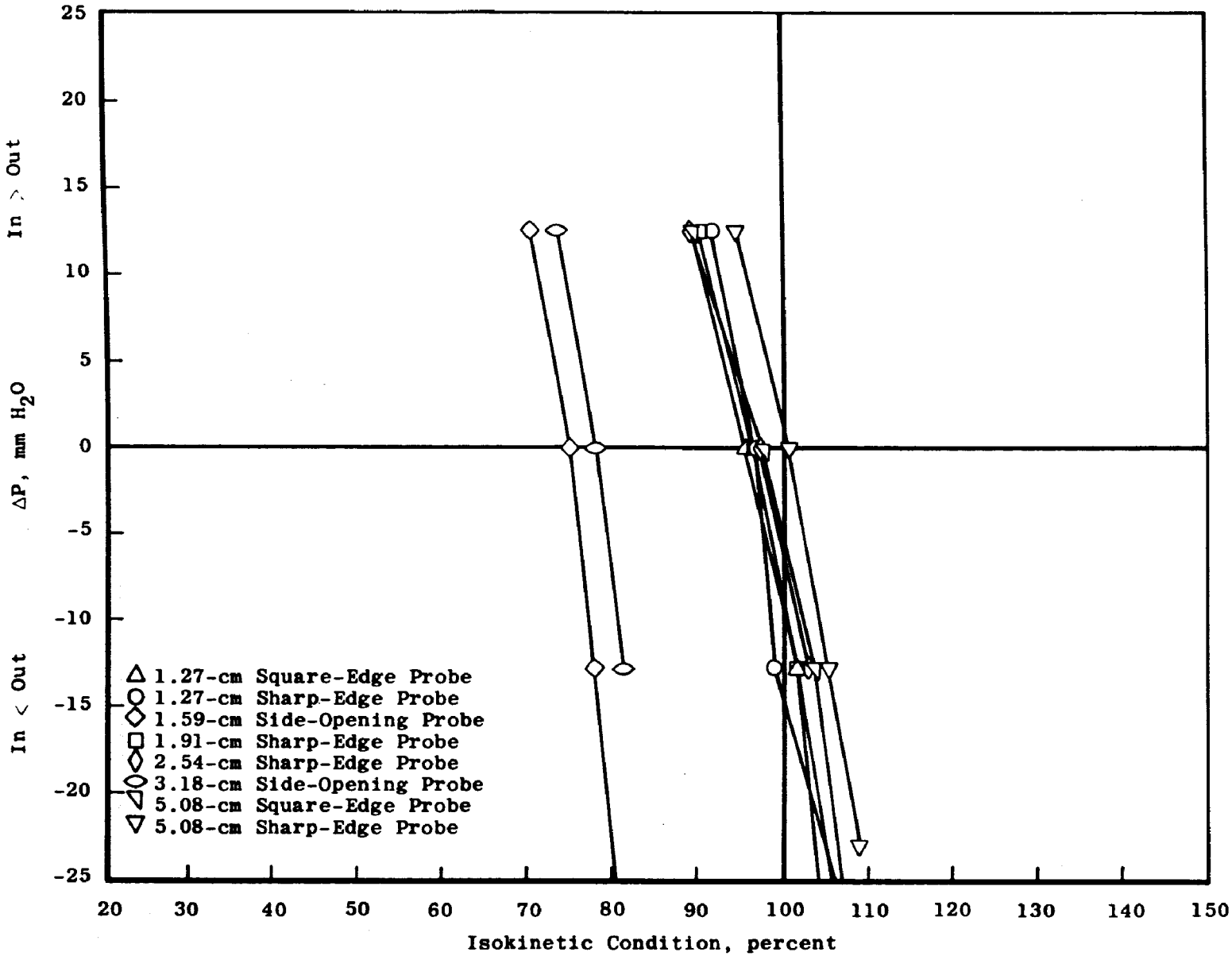

Figure 39. Probe performance at 21.34 m/sec and 7.5 deg angle of attack.

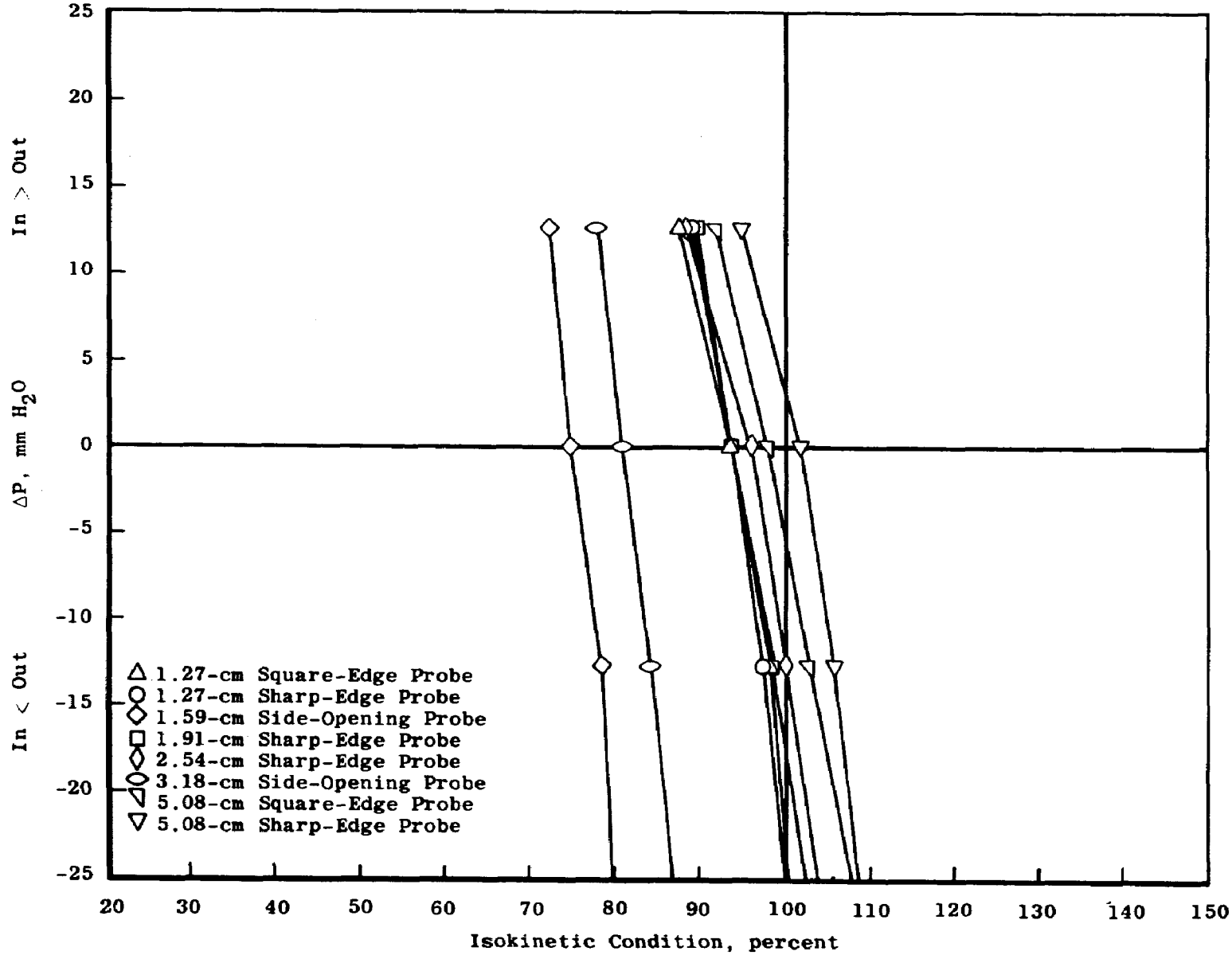

Figure 40. Probe performance at 21.34 m/sec and 15 deg angle of attack.

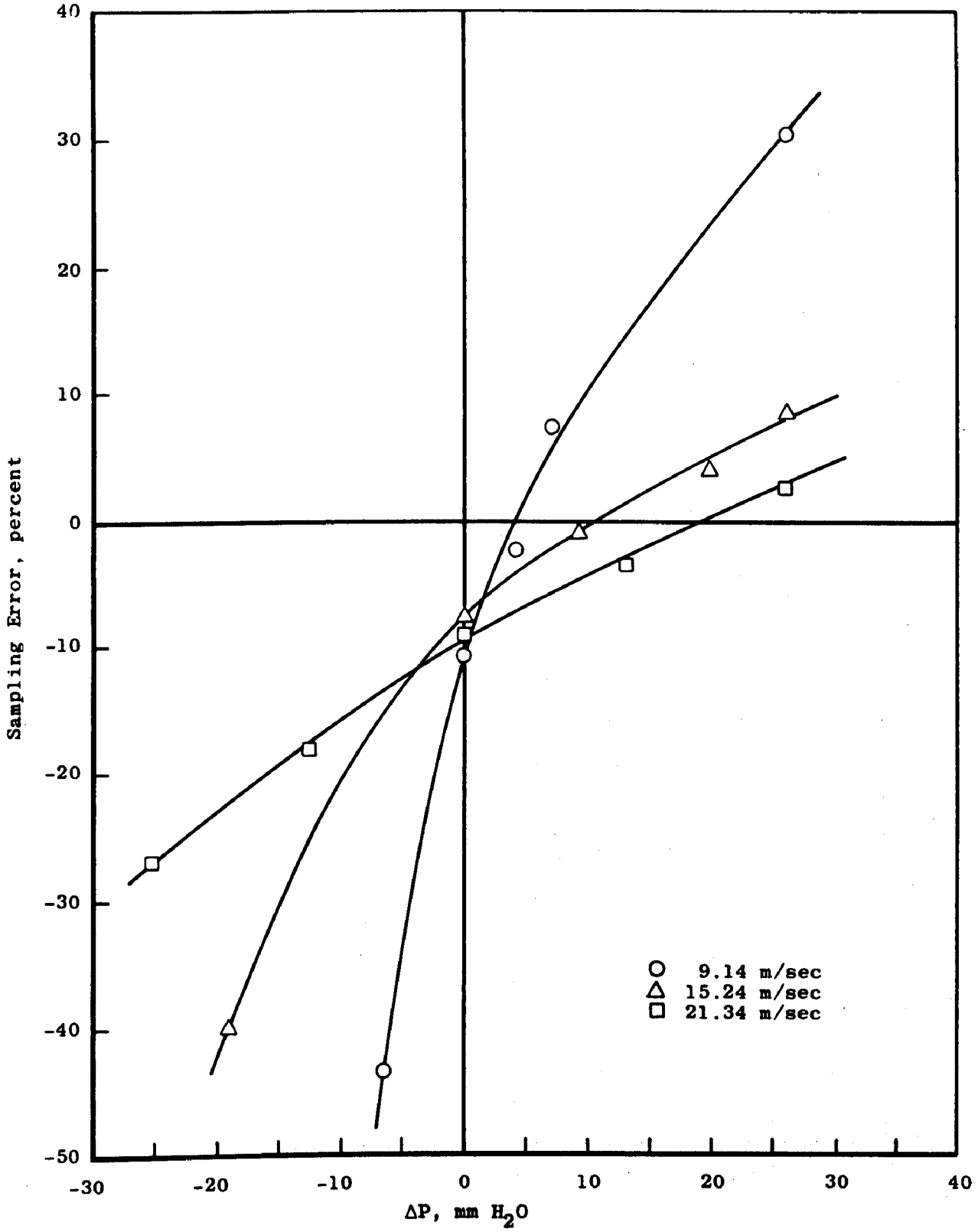

Figure 41. 1.27-cm square-edge probe.

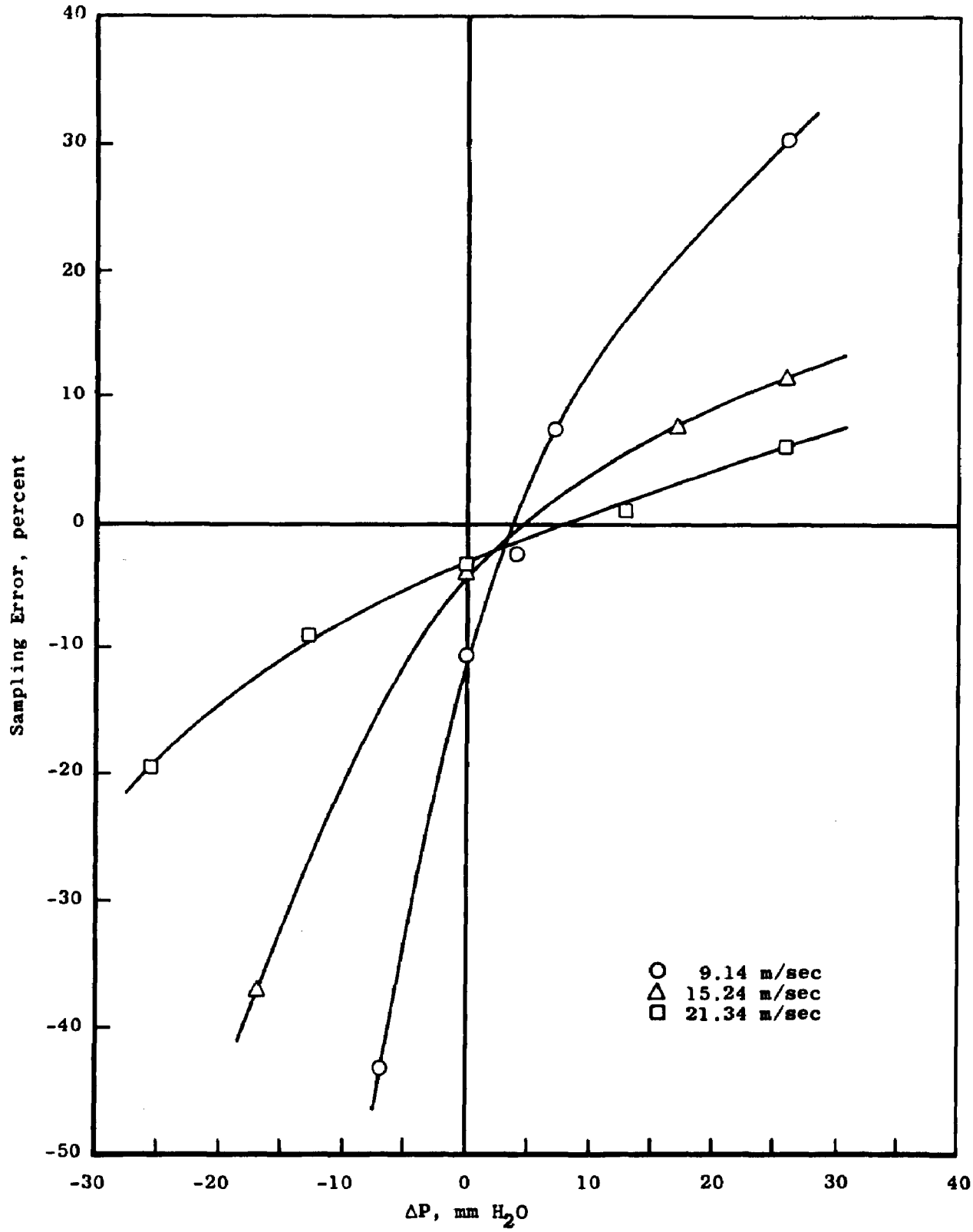

Figure 42. 1.27-cm sharp-edge probe.

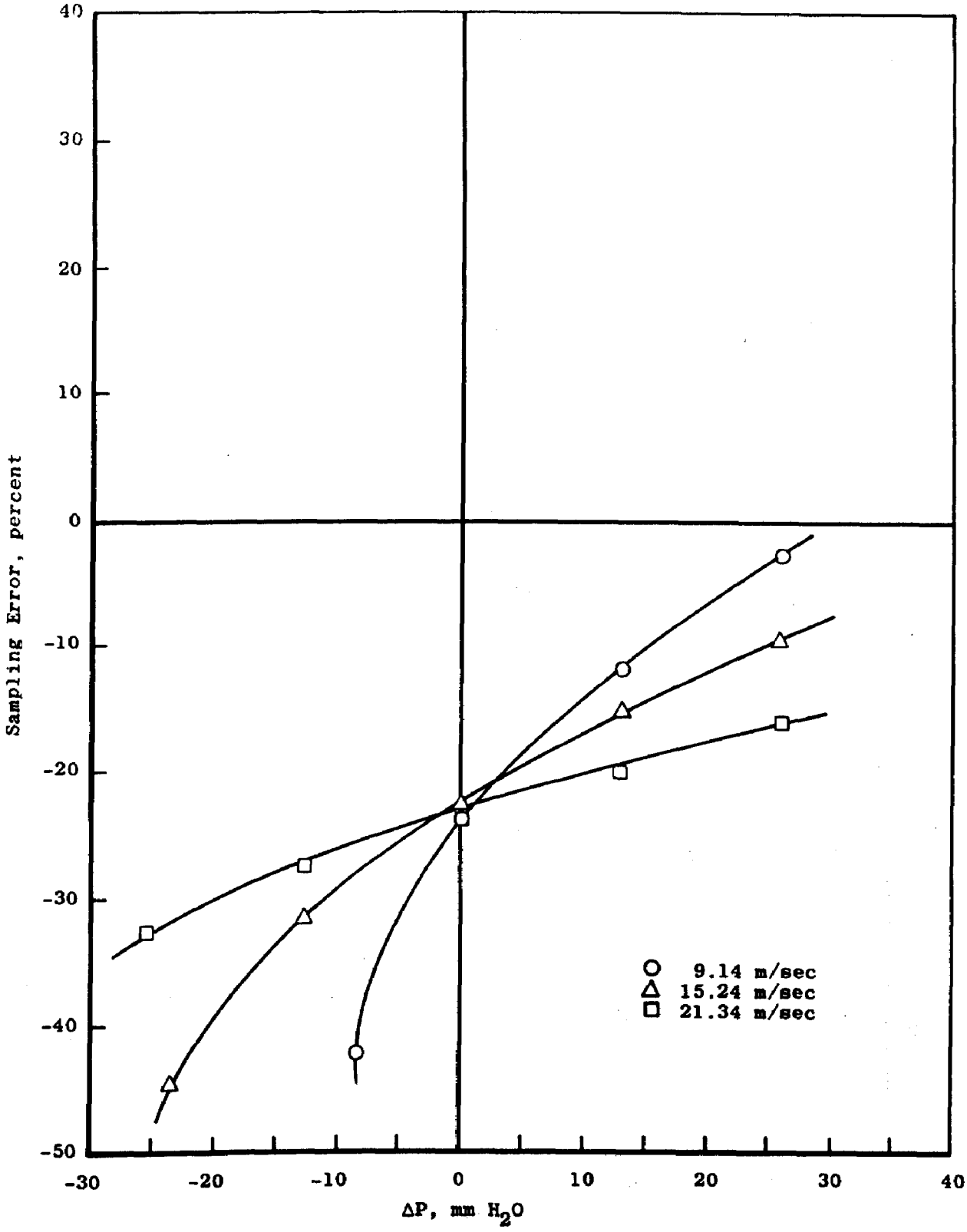

Figure 43. 1.59-cm side-opening probe.

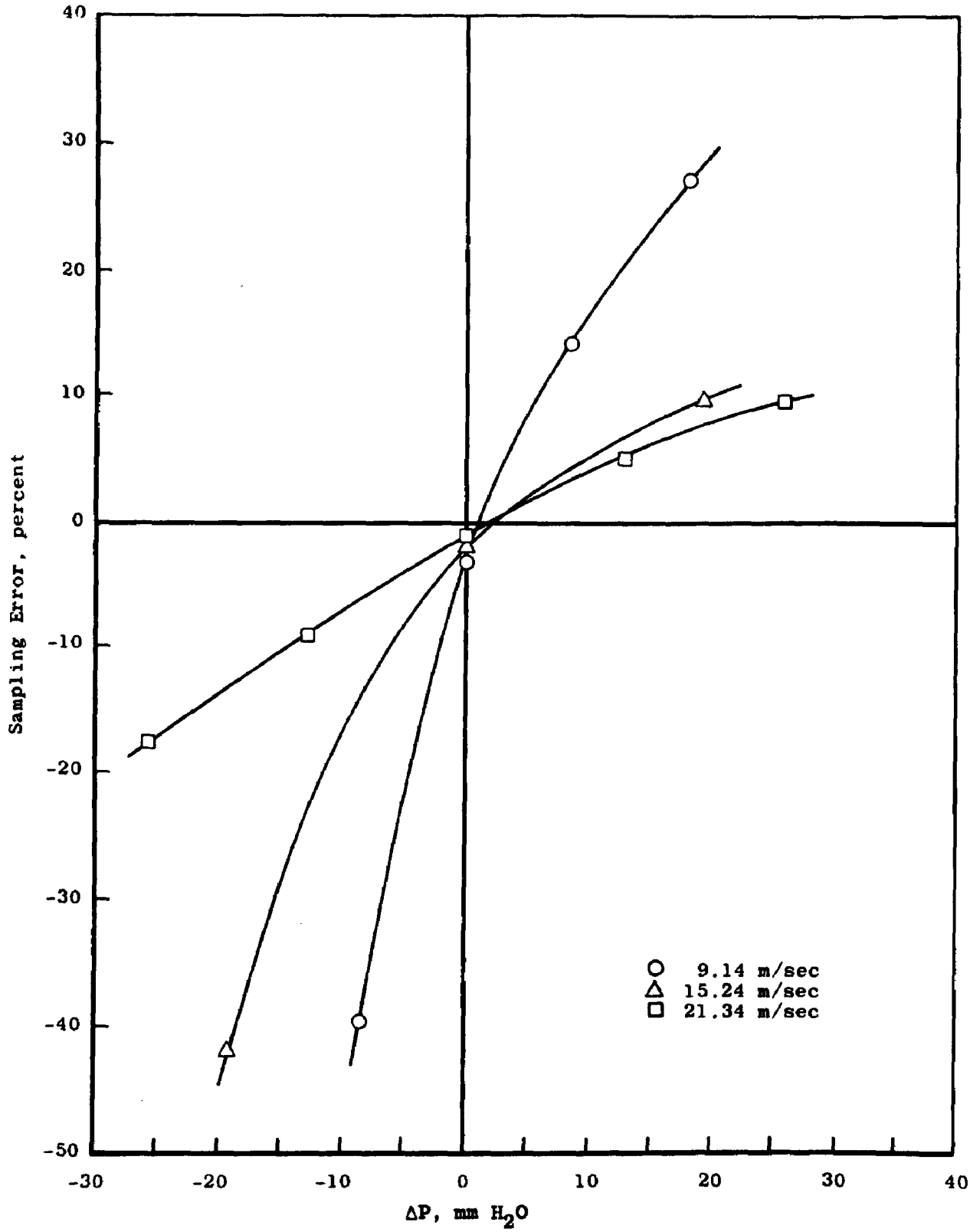

Figure 44. 1.91-cm sharp-edge probe.

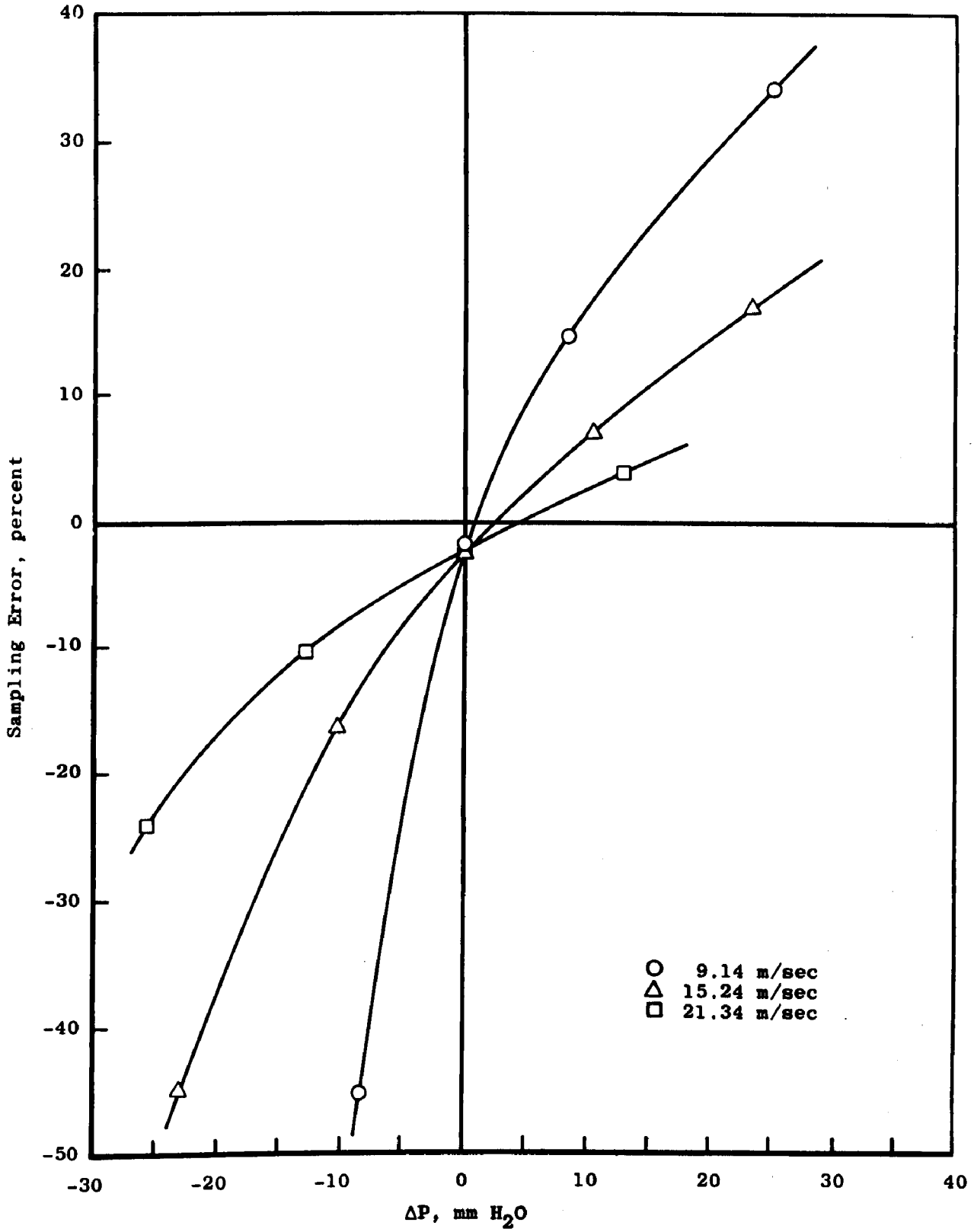

Figure 45. 2.54-cm sharp-edge probe.

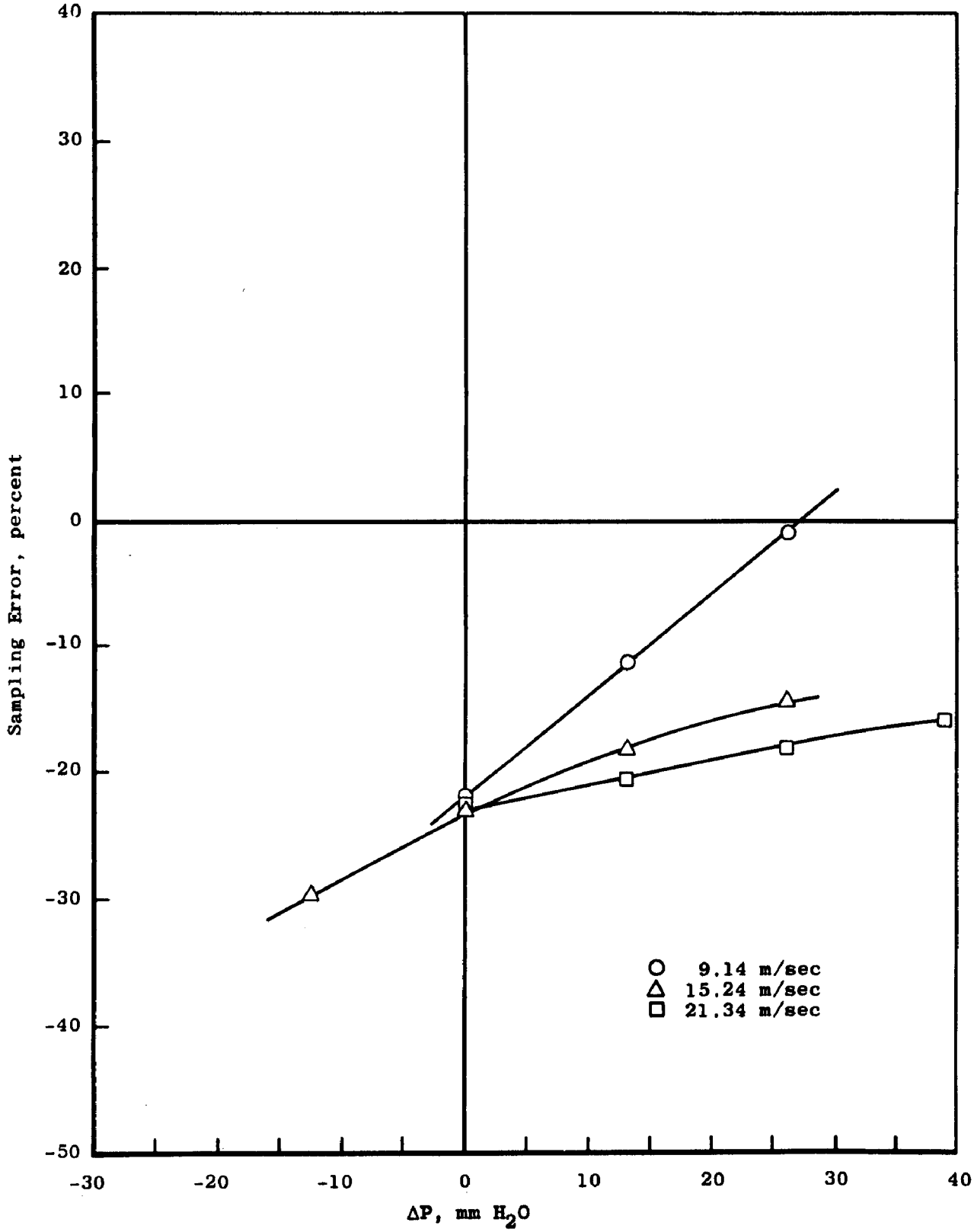

Figure 46. 3.18-cm side-opening probe.

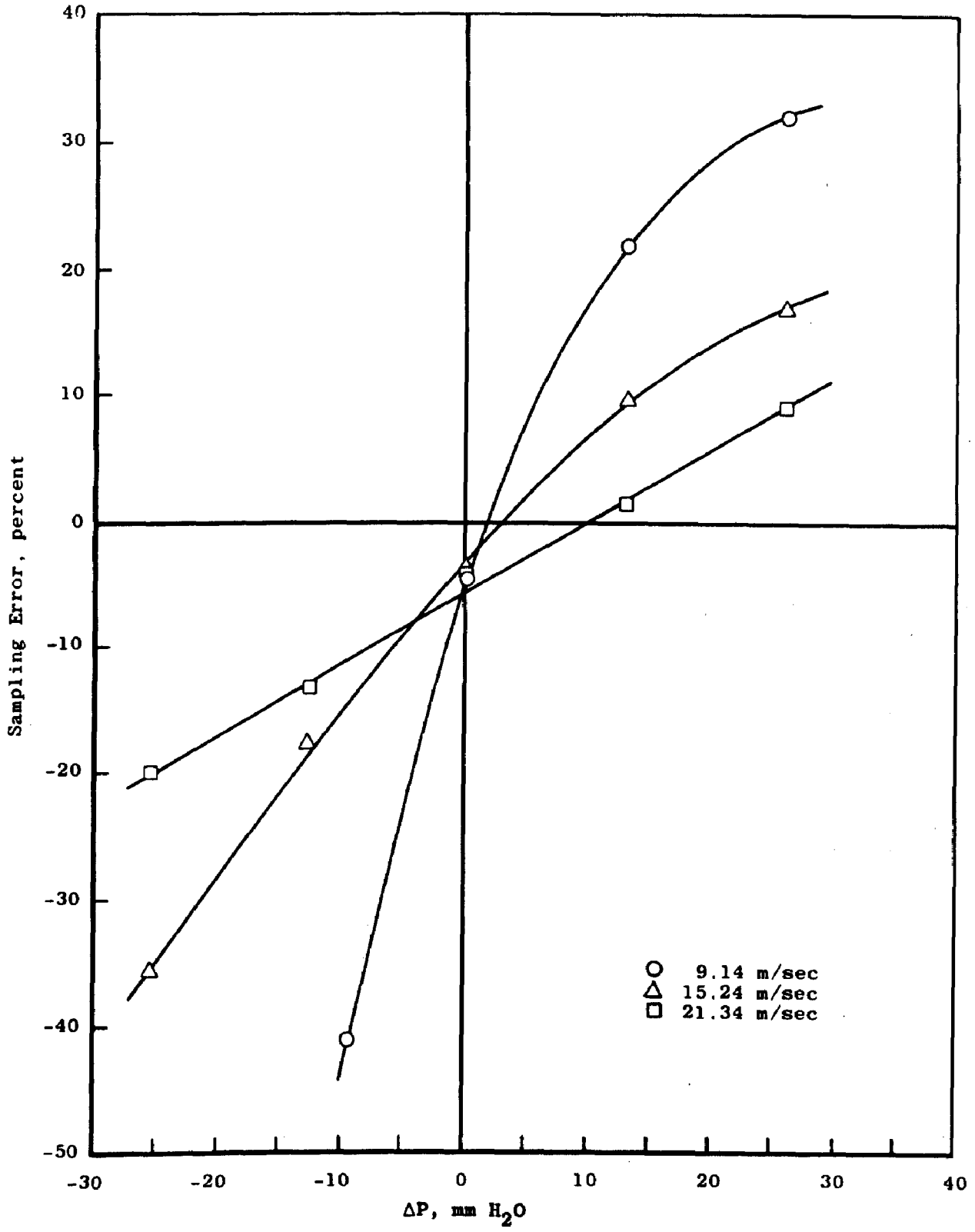

Figure 47. 5.08-cm square-edge probe.

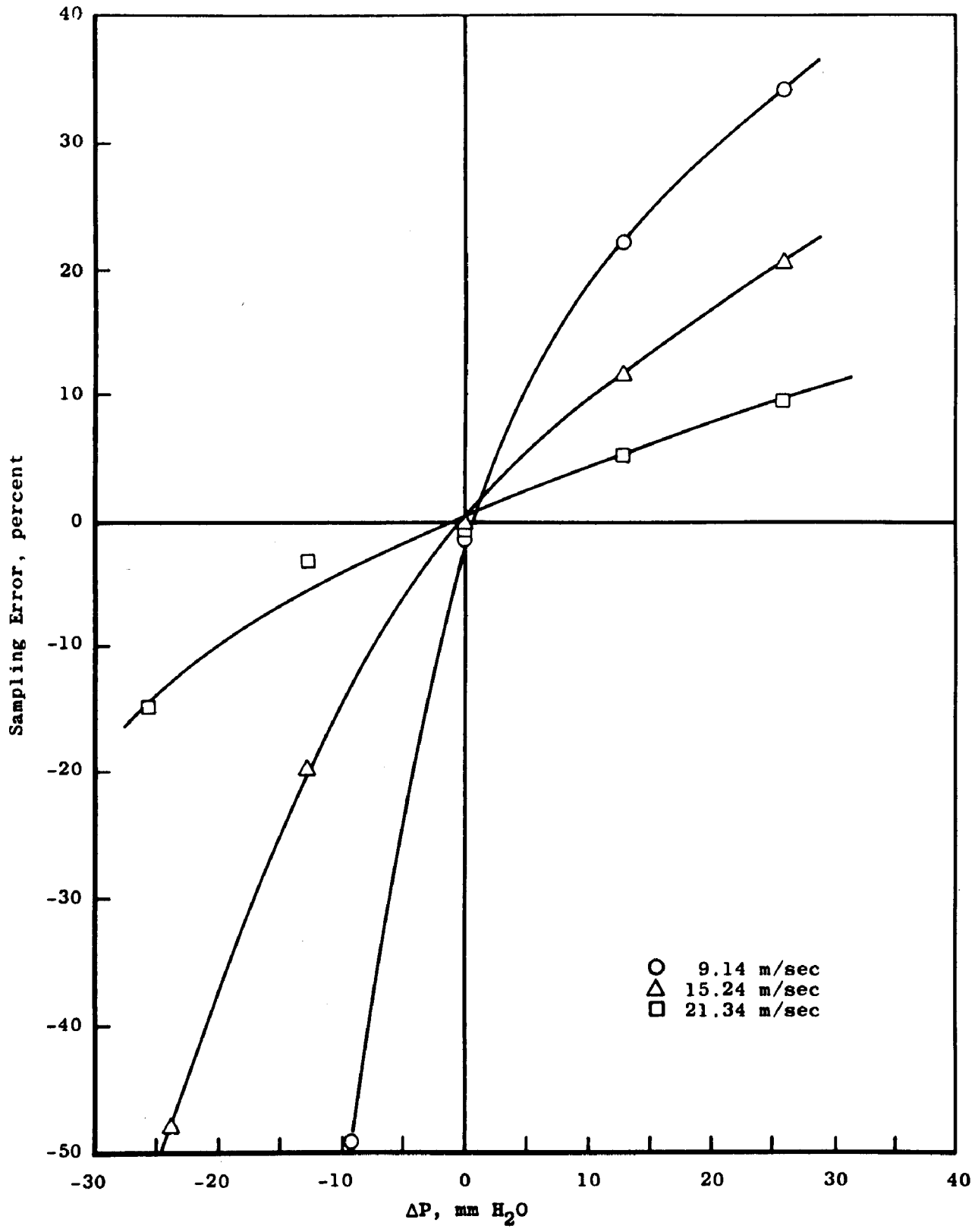

Figure 48. 5.08-cm sharp-edge probe.

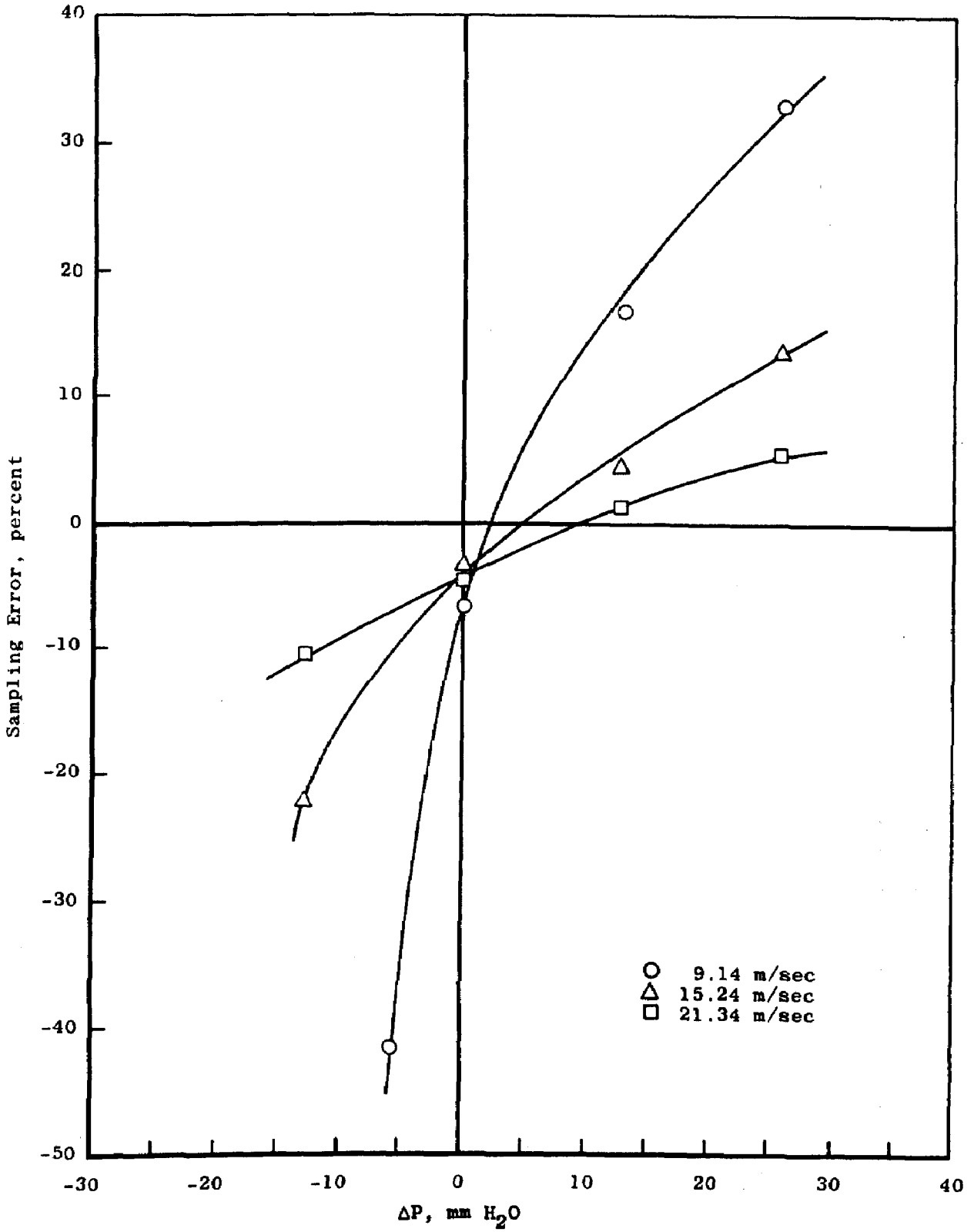

Figure 49. 1.27-cm square-edge probe at 7.5 deg angle of attack.

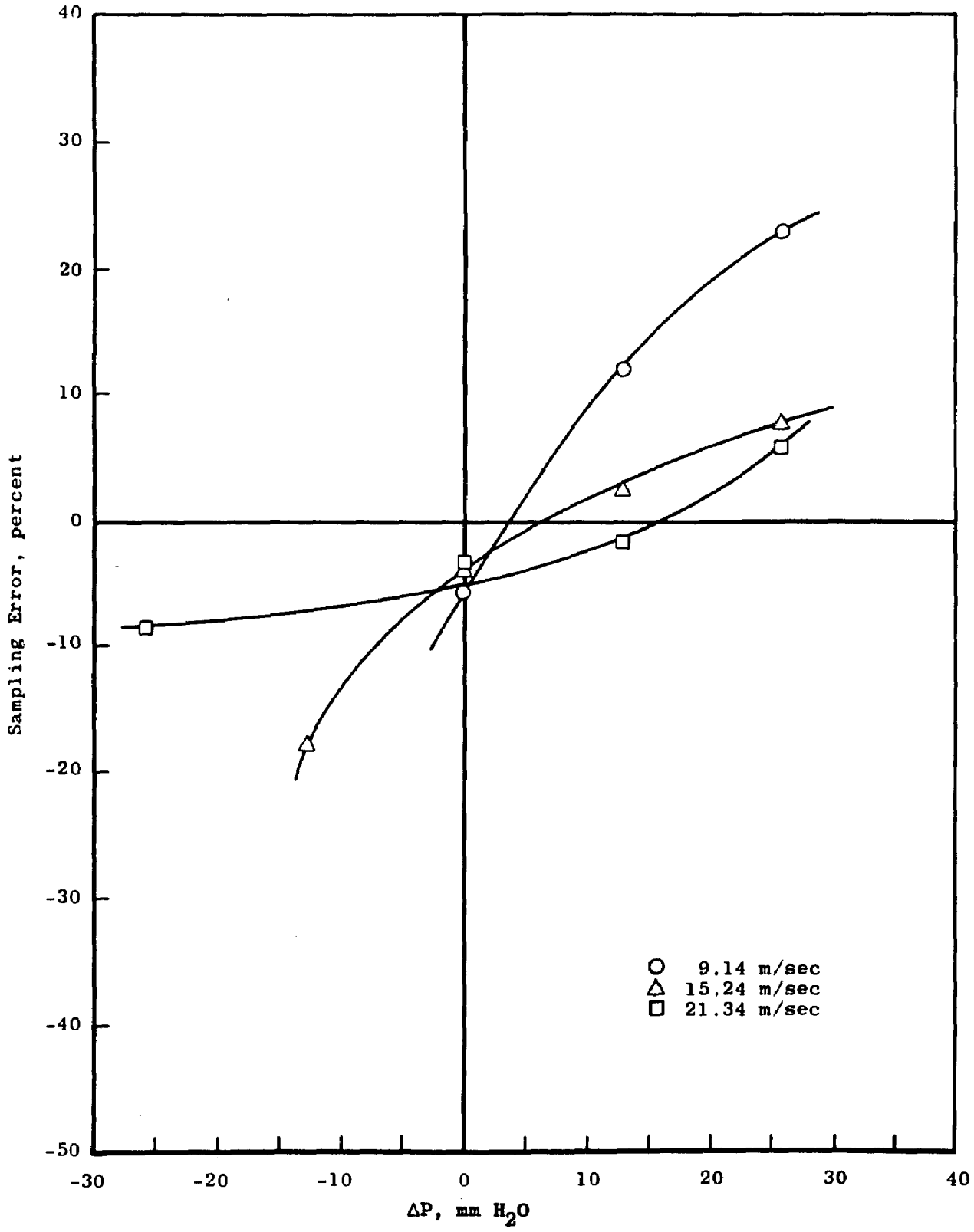

Figure 50. 1.27-cm sharp-edge probe at 7.5 deg angle of attack.

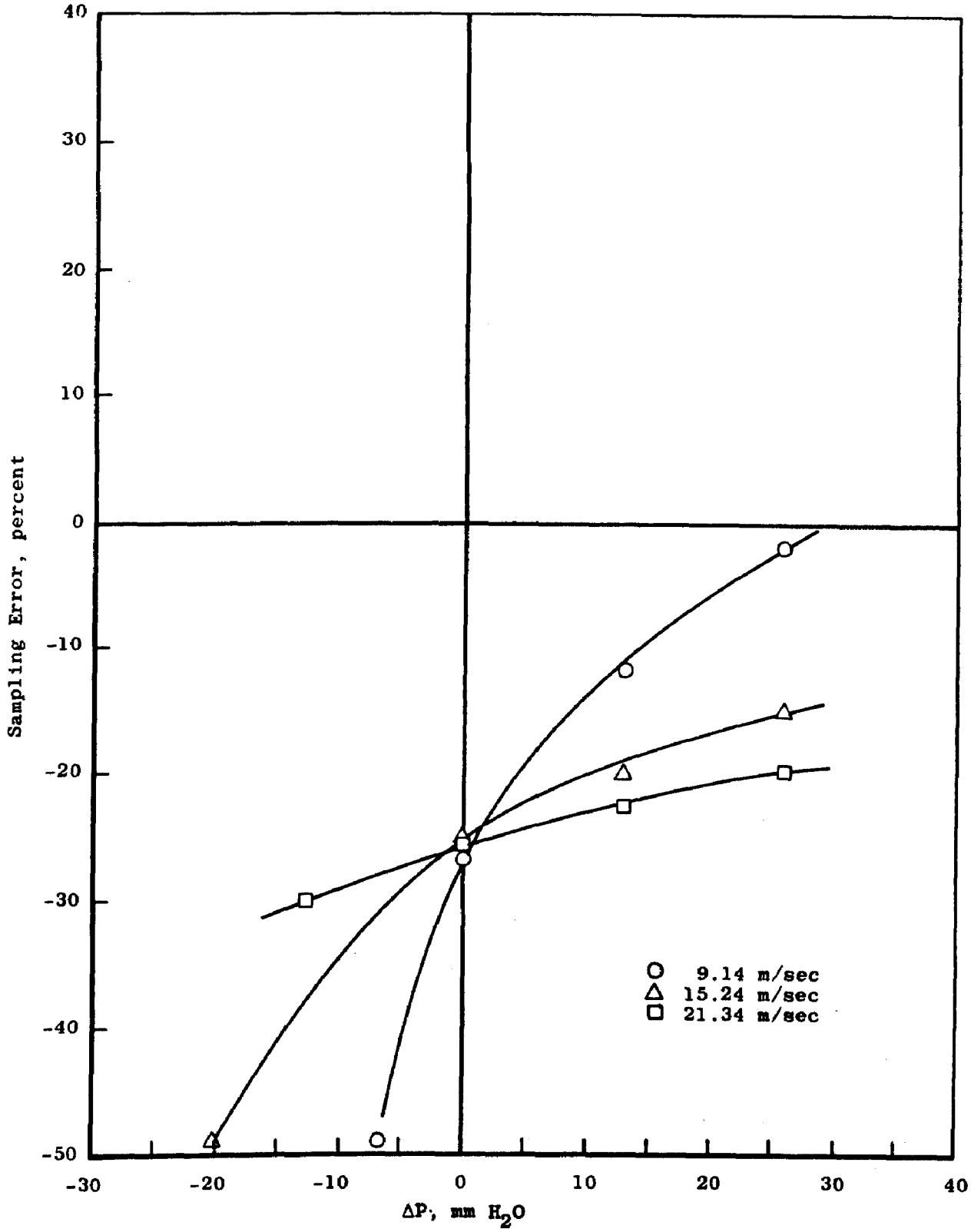

Figure 51. 1.59-cm side-opening probe at 7.5 deg angle of attack.

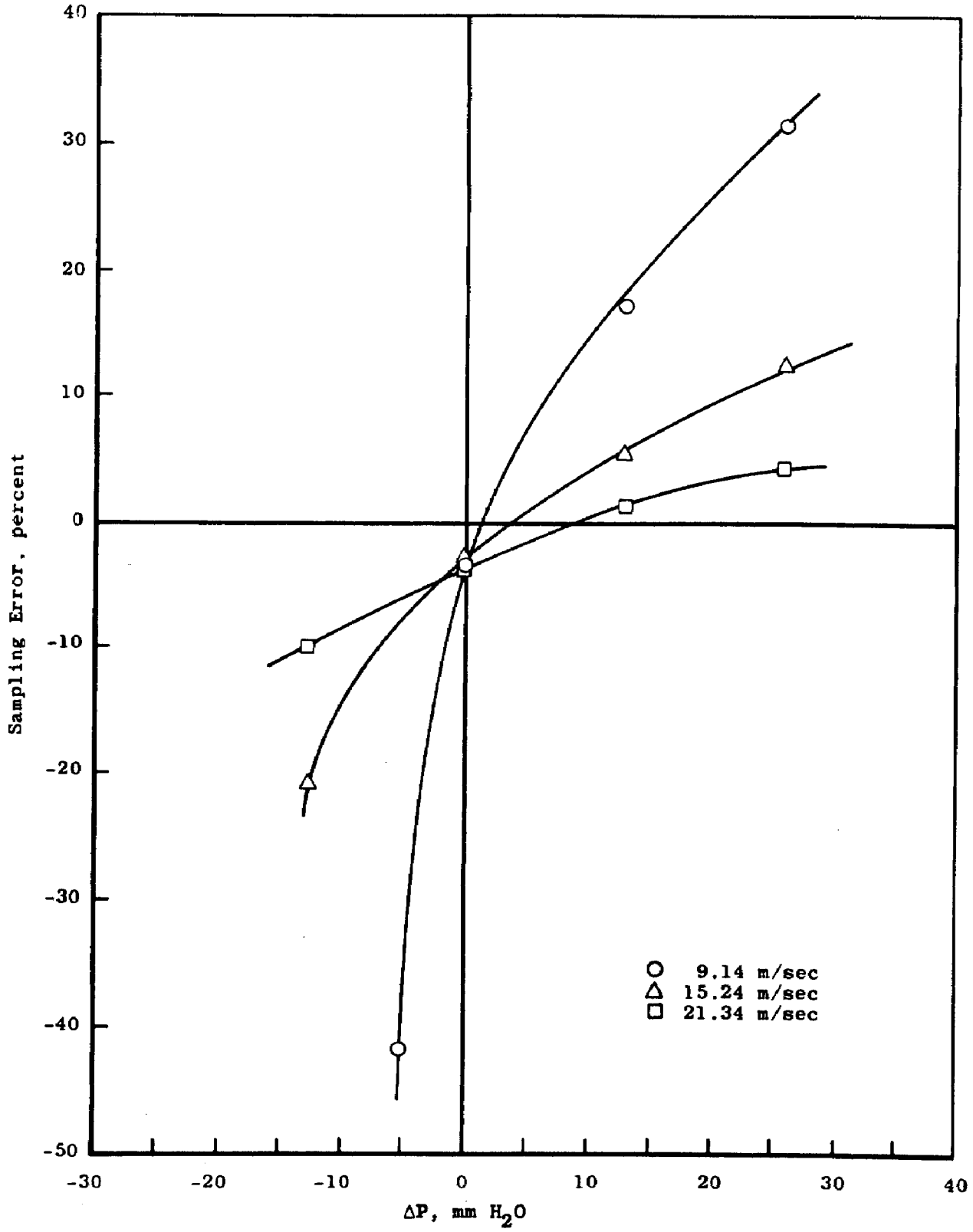

Figure 52. 1.91-cm sharp sharp-edge probe at 7.5 deg angle of attack.

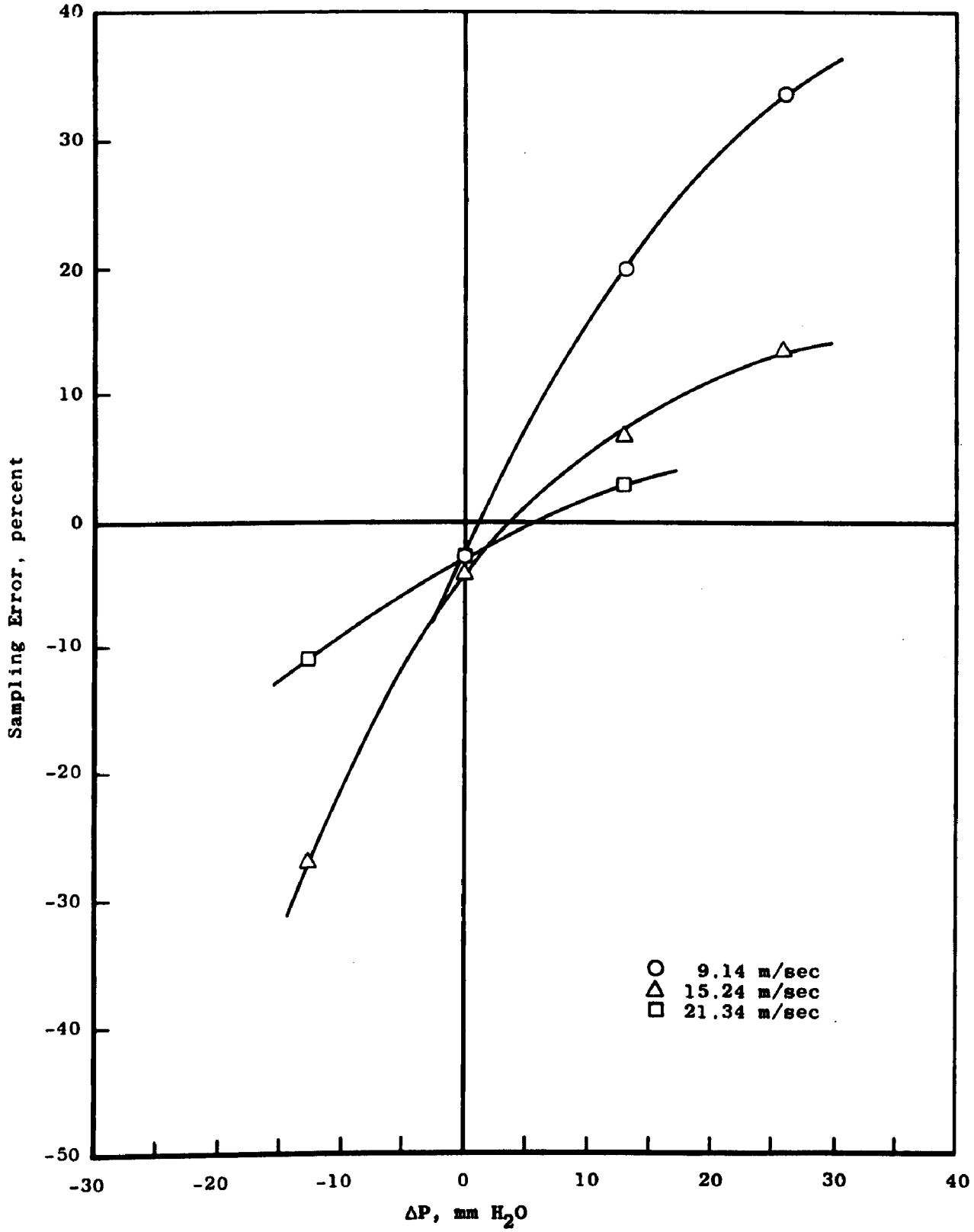

Figure 53. 2.54-cm sharp-edge probe at 7.5 deg angle of attack.

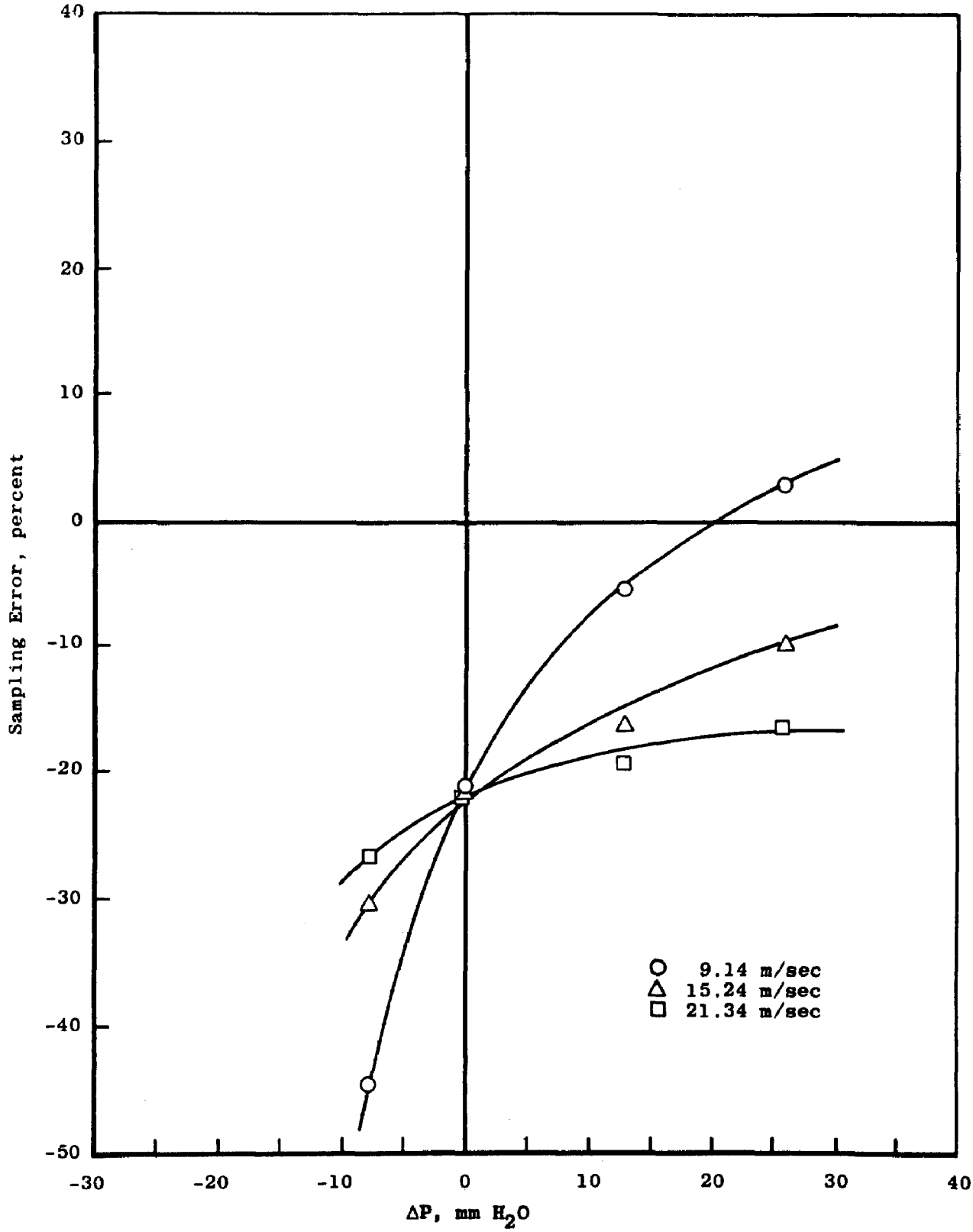

Figure 54. 3.18-cm side-opening probe at 7.5 deg angle of attack.

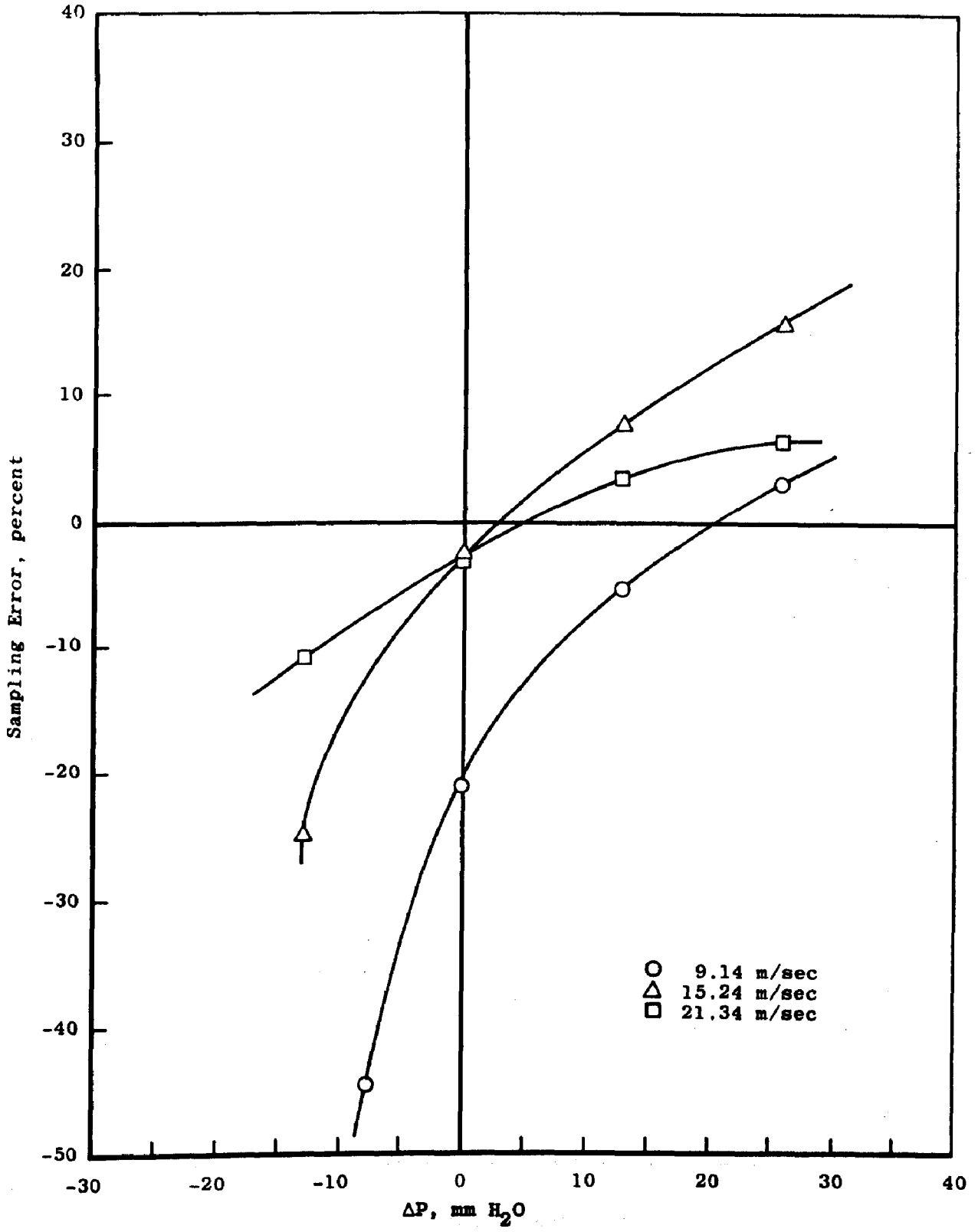

Figure 55. 5.08-cm square-edge probe at 7.5 deg angle of attack.

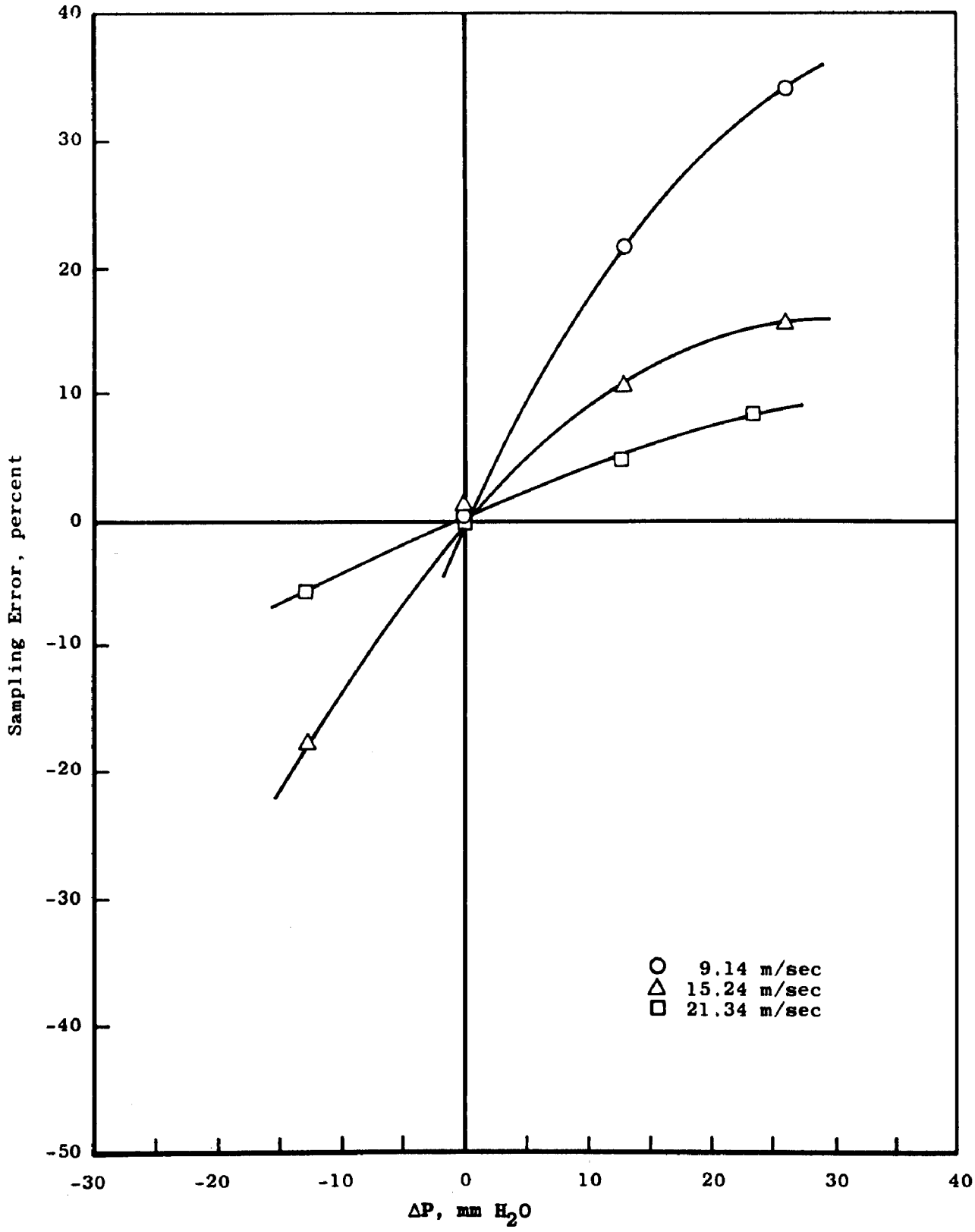

Figure 56. 5.08-cm sharp-edge probe at 7.5 deg angle of attack.

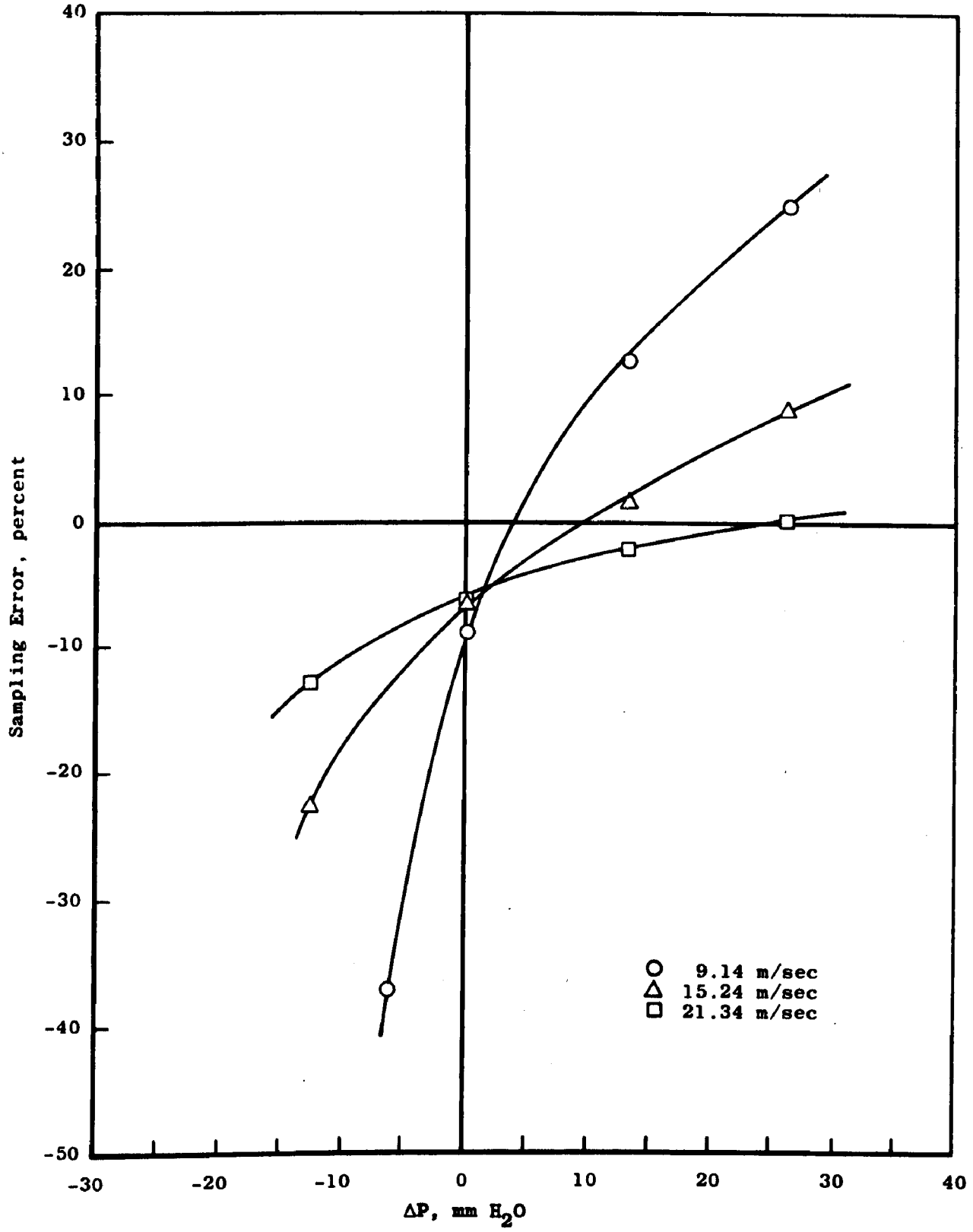

Figure 57. 1.27-cm square-edge probe at 15 deg angle of attack.

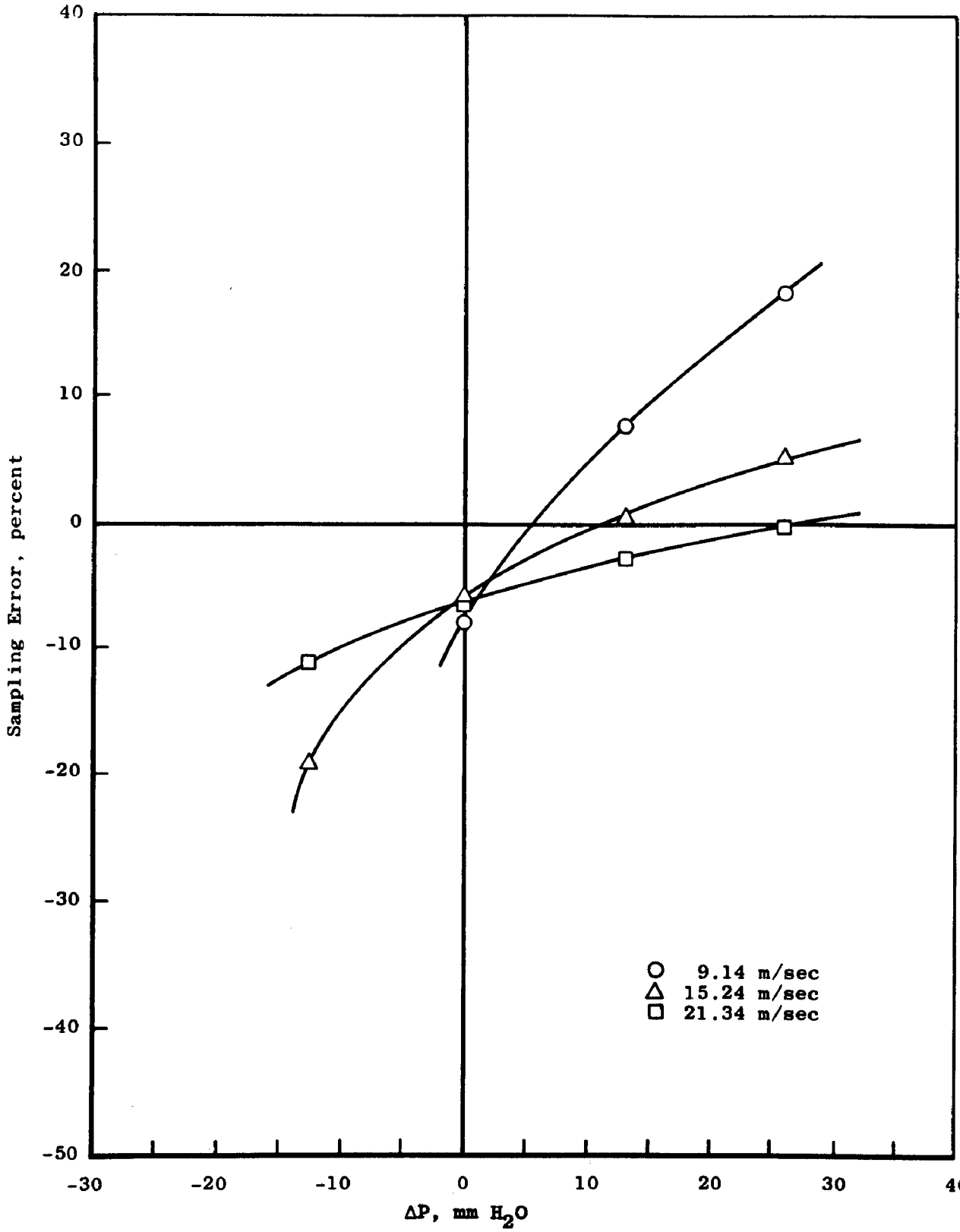

Figure 58. 1.27-cm sharp-edge probe at 15 deg angle of attack.

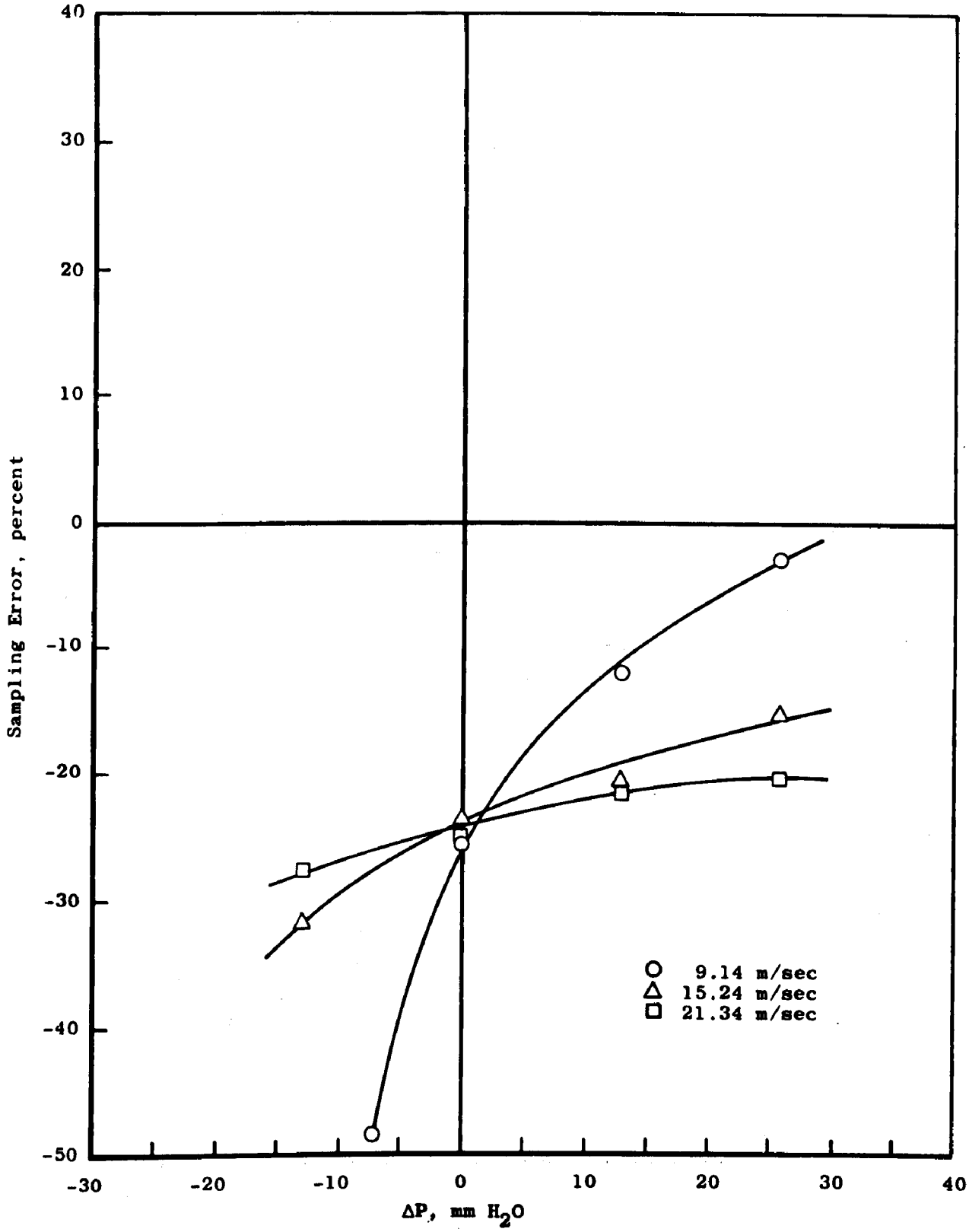

Figure 59. 1.59-cm side-opening probe at 15 deg angle of attack.

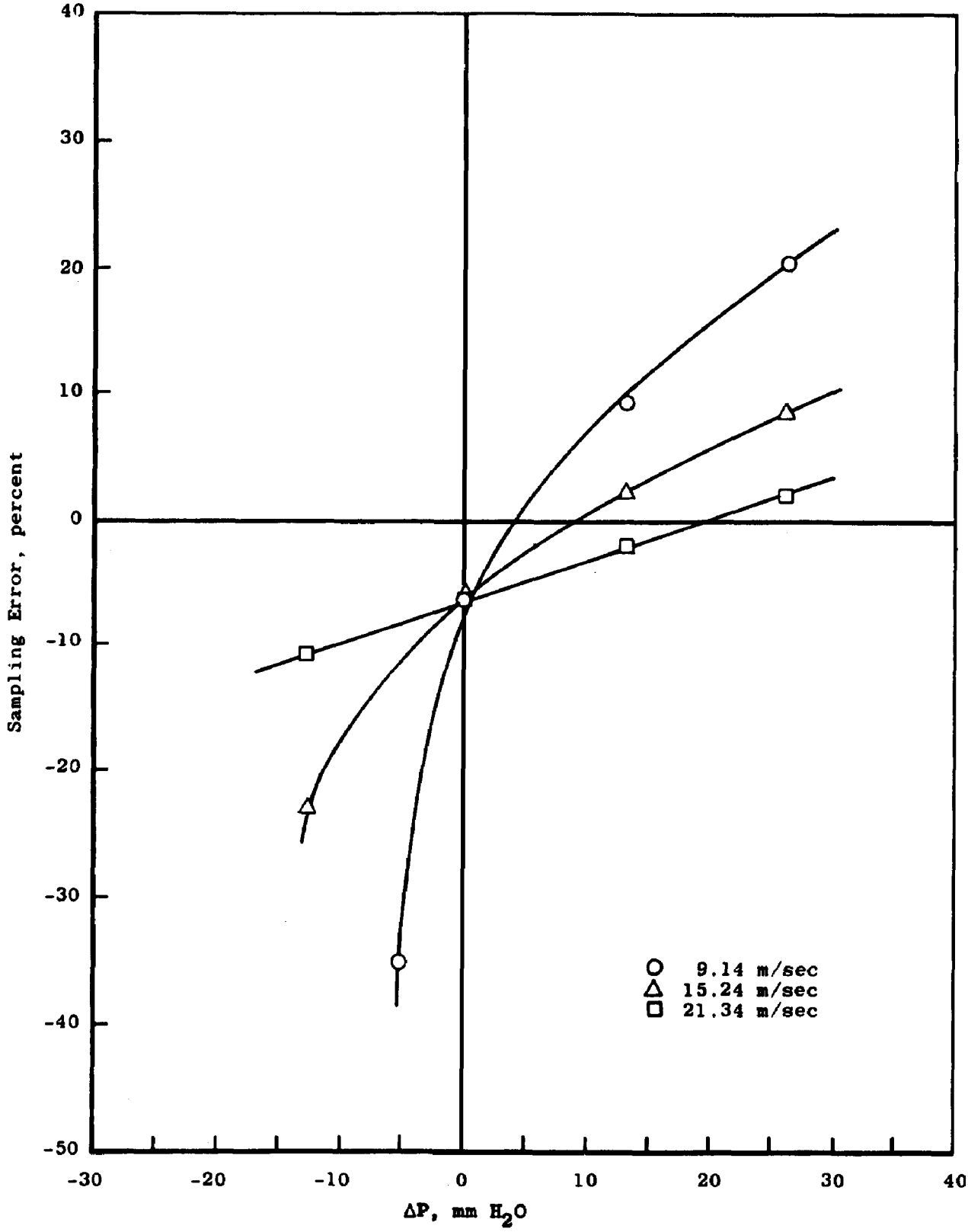

Figure 60. 1.91-cm sharp-edge probe at 15 deg angle of attack.

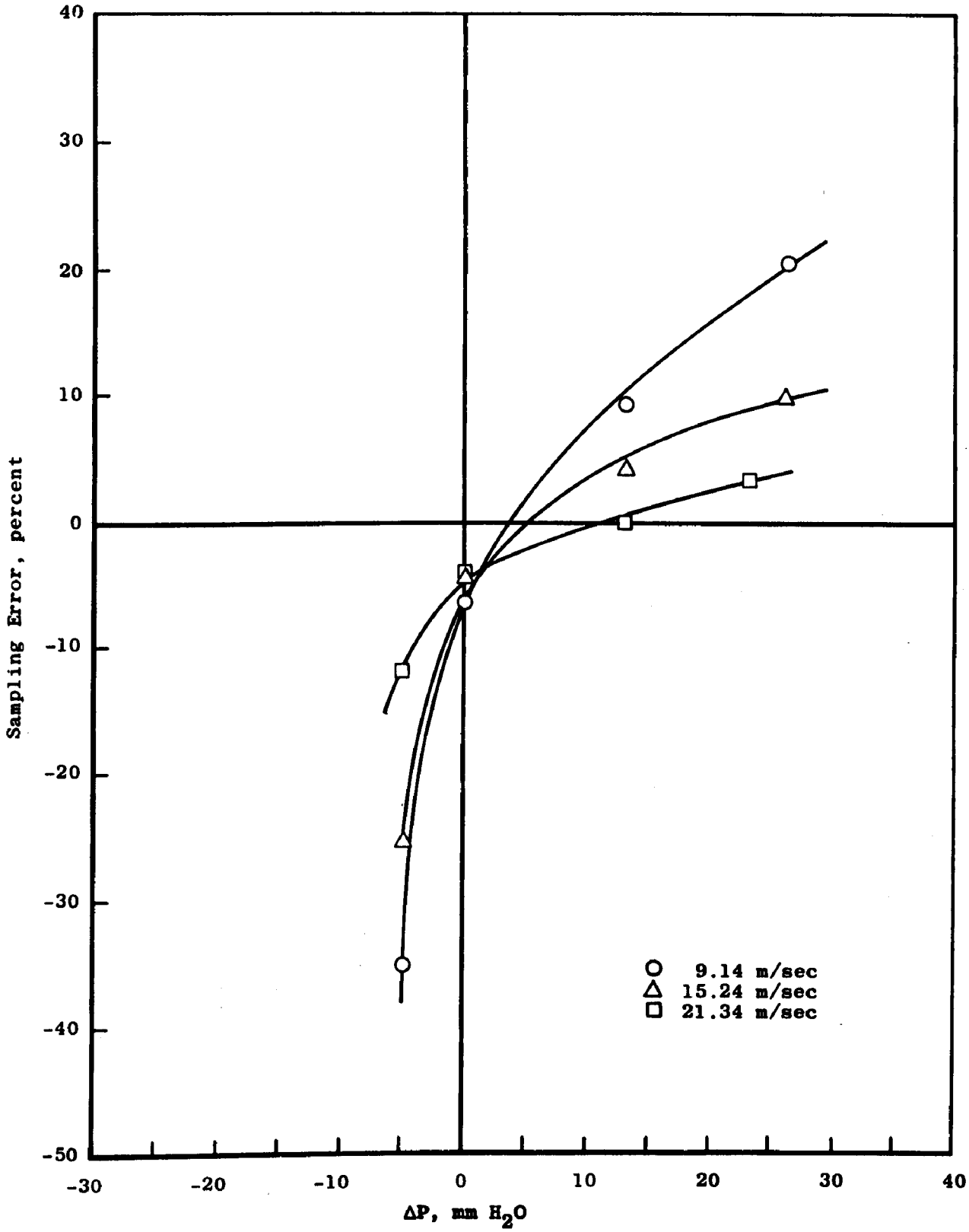

Figure 61. 2.54-cm sharp-edge probe at 15 deg angle of attack.

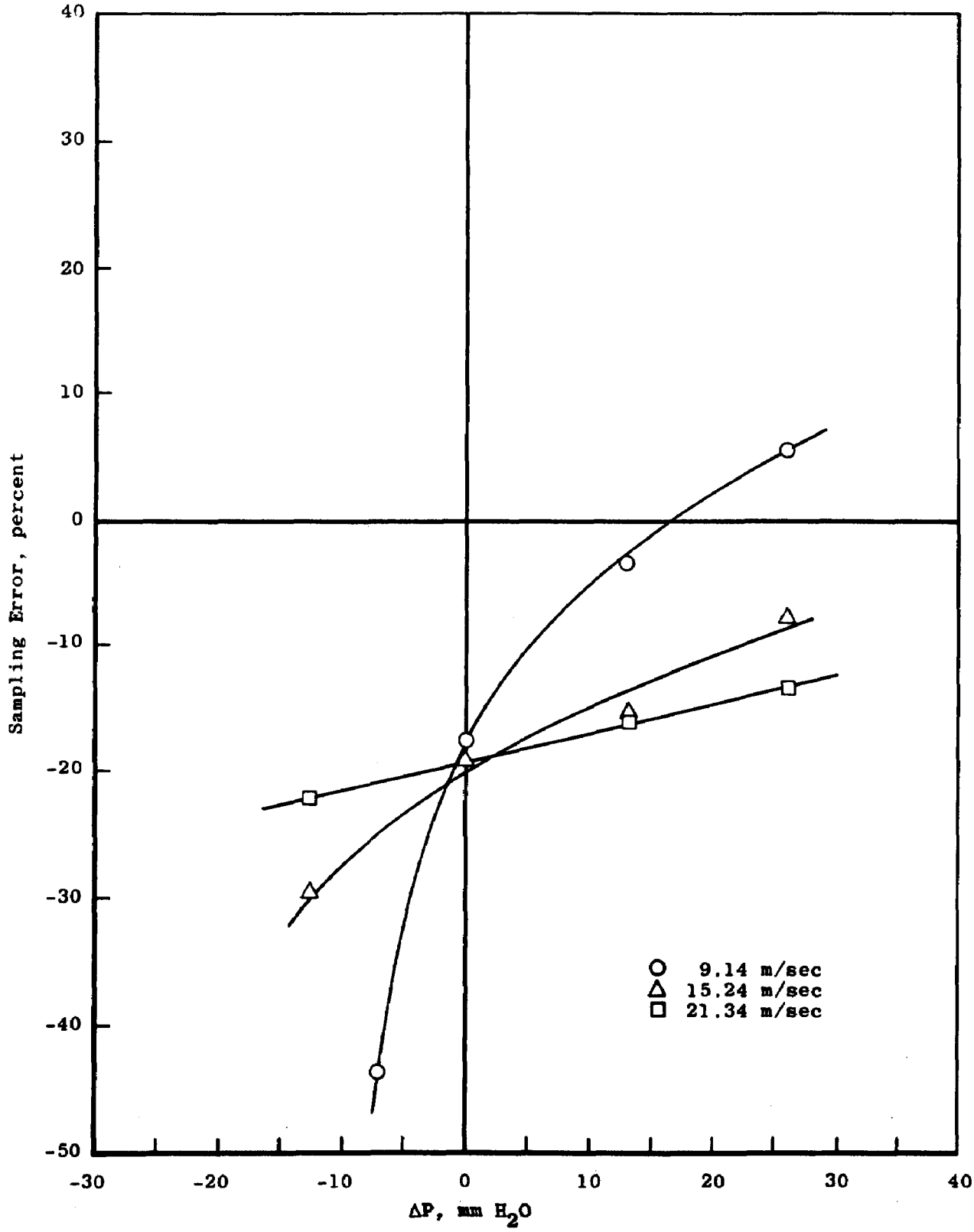

Figure 62. 3.18-cm side-opening probe at 15 deg angle of attack.

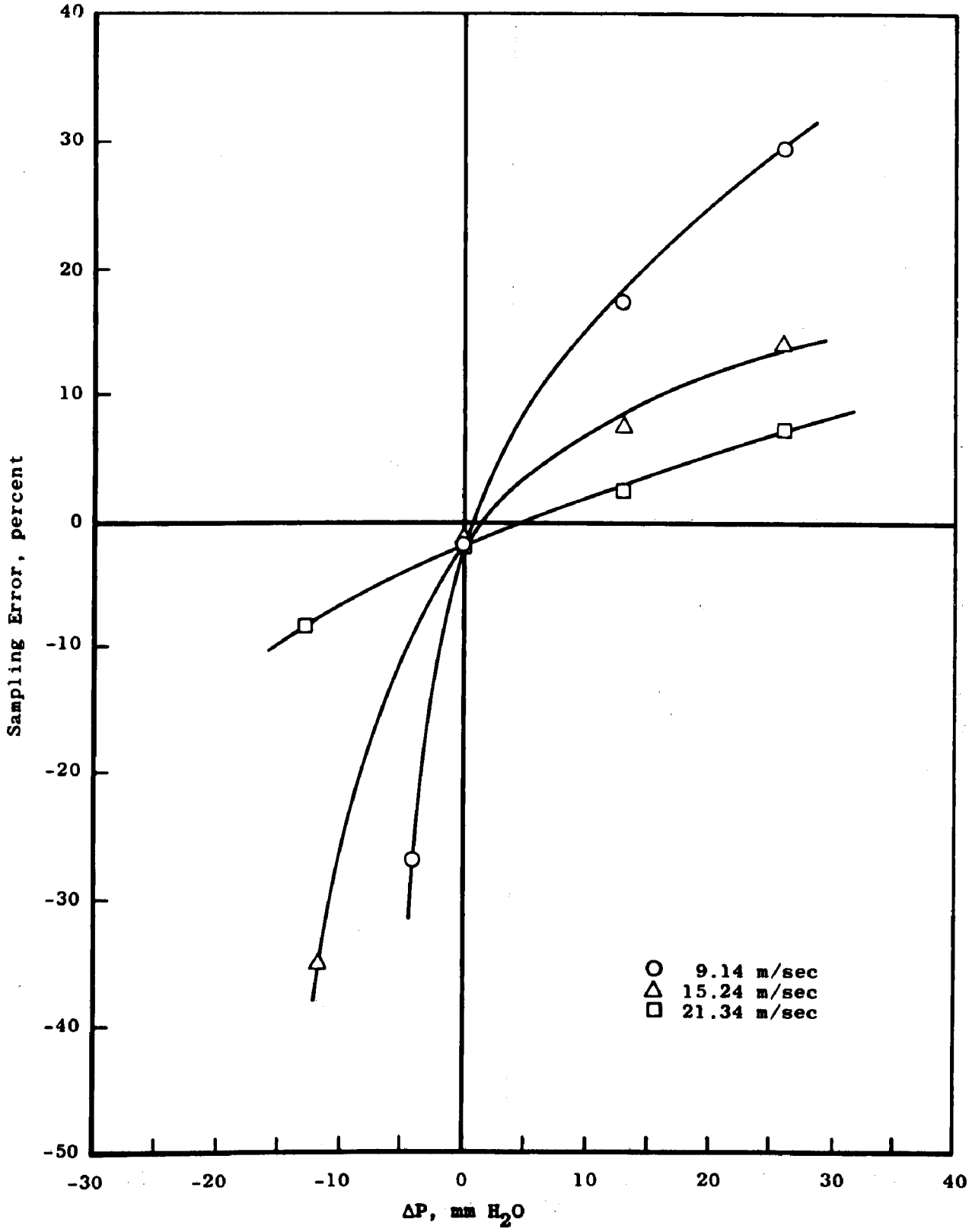

Figure 63. 5.08-cm square-edge probe at 15 deg angle of attack.

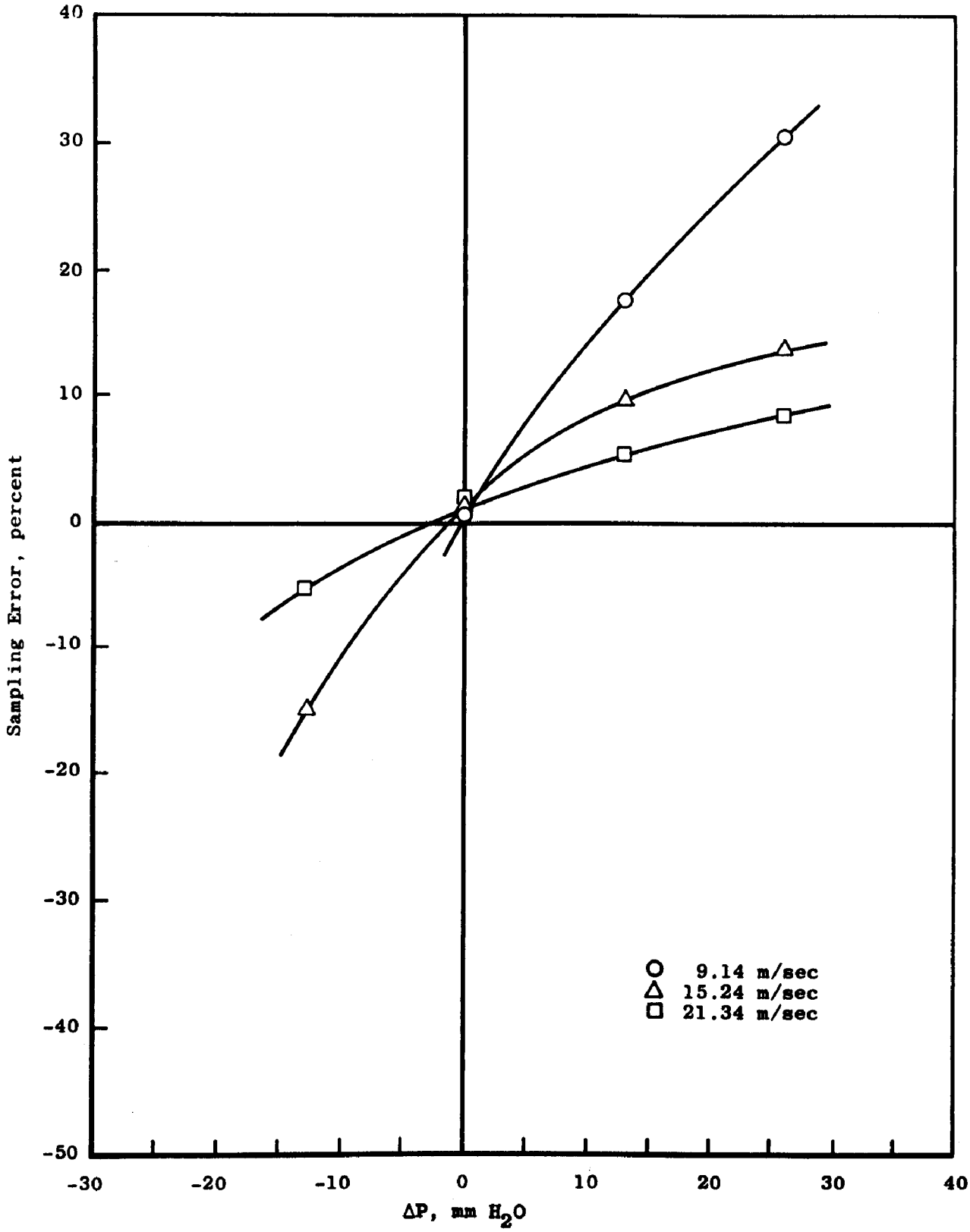

Figure 64. 5.08-cm sharp-edge probe at 15 deg angle of attack.

NOMENCLATURE

b_o	Laser beam radius
f	Rate at which fringes are cut in probe volume
p	Probe static pressure
t	Period of a-c component of PM tube signal
V	Velocity
δ	Interference fringe spacing
θ	Angle formed by intersecting beams
λ_o	Wavelength of laser